Okinawa Institute of Science and Technology
Graduate University

Thesis submitted for the degree

Doctor of Philosophy

Serotonergic Control of Brain-Wide Dynamics

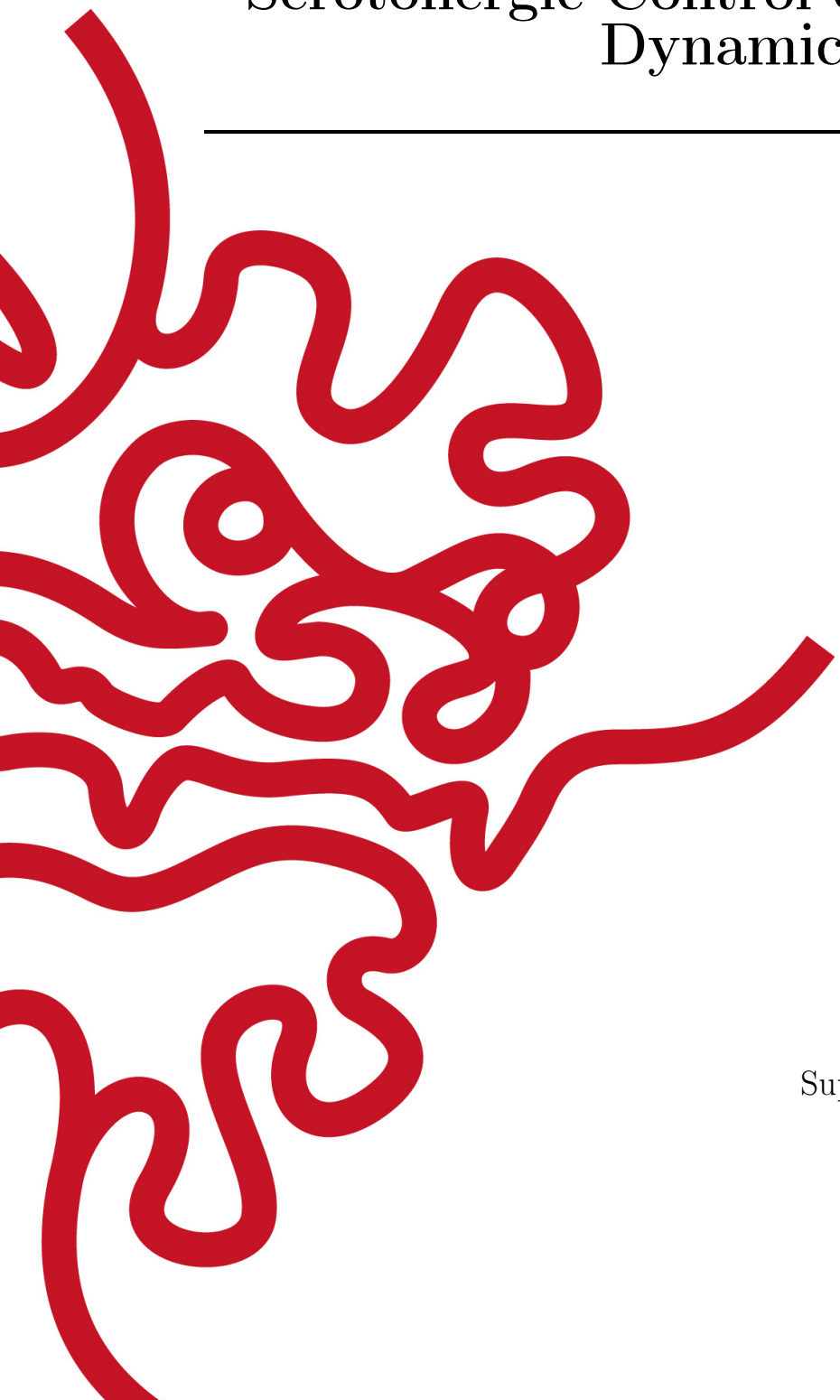

by

Hiroaki Hamada

Supervisor: **Prof. Kenji Doya**

Semptember, 2018

Declaration of Original and Sole Authorship

I, Hiroaki Hamada, declare that this thesis entitled *Serotonergic Control of Brain-Wide Dynamics* and the data presented in it are original and my own work.

I confirm that:

- No part of this work has previously been submitted for a degree at this or any other university.
- References to the work of others have been clearly acknowledged. Quotations from the work of others have been clearly indicated, and attributed to them.
- In cases where others have contributed to part of this work, such contribution has been clearly acknowledged and distinguished from my own work.
- None of this work has been previously published elsewhere.

Date: Semptember, 2018
Signature:

Abstract

Serotonergic Control of Brain-Wide Dynamics

Serotonin, one of the neuromodulators, is associated with multiple functions, such as the wake-sleep cycle, decision making, and mood. Serotonin is also the primary target of medication for major depression (MD), notably by selective serotonin re-uptake inhibitors (SSRIs). However, it is widely known that serotonergic antidepressants require long-term administration, and acute medication sometimes worsens symptoms. Serotonergic regulation of brain-wide dynamics remains crucial for understanding its roles in behavioral and cognitive functions as well as the mechanism of antidepressant medication. First, I studied the influences of a serotonergic antidepressant on brain dynamics with functional magnetic resonance imaging in rodents. I found that the functional connectivity between the bed nucleus of steria terminalis (BST) and the ventral retrosplenial cortex (vRSC) distinctively responded to acute serotonergic antidepressant treatment, escitalopram. Additionally, long-term serotonergic antidepressant treatment promoted spontaneous locomotion and influenced anxiety-like behaviors only in context-dependent and individually variable ways. The results imply that long-term serotonergic antidepressant treatment enhances intrinsic motivation, but not anxiety. Additionally, I analyzed large-scale brain dynamics with functional connectivity analysis and energy landscape analysis (ELA). My ELA analysis revealed that chronic administration of serotonergic antidepressants maintained dynamic brain states linking major attractor states, while conventional functional connectivity (FC) analysis did not show any difference caused by serotonergic antidepressants. The intermediate brain states, which are supported by modular integration, are associated with active exploration. My findings suggest that serotonergic antidepressants induce resilience by stabilizing brain state dynamics as a result of shaping functional network architecture. In the second study, I conducted a pilot experiment to assess serotonergic modulation of brain dynamics by optogenetic stimulation of serotonin neurons in the dorsal raphe nucleus (DRN). In the first animal test, I found brain responses in the frontal cortical regions (the anterior cingulate cortex, the medial prefrontal cortex, and the insular cortex), the striatum, and the ventral tegmental area (VTA). In a reward delay task, optogenetic activation of DRN serotonin neurons enhanced waiting for delayed rewards, which confirmed the effectivenss of optogenetic stimulation. The result suggested the feasibility of studying serotonergic modulation with opto-fMRI. My thesis delineates how the serotonergic system regulates brain-wide dynamics at short- and long-term scales.

Acknowledgment

First, I would like to acknowledge Prof. Doya for his endurance and supervision. When I was 20 years old, I was so desperate to be a scientist. I could not believe that I can join in a graduate school after I quit my high school. I found Prof. Doya, belonging to Nara Institute of Science and Technology at that time. I dreamed to be a part of his members, and I could not imagine that I ended up working with him. There are multiple research explorations, which will not be published forever, but some of them are working as joint projects. I also made multiple social connections not only in neuroscientific communities but also other communities including philosophy and computer science. It is noteworthy that me and my colleagues, Dr. Miyahara, Dr. Nishida, and Dr. Niikawa, started neurophenomenological projects after we joined in ISSA summer school in Kobe. We won funds and are about to complete the projects. I would hope to continue projects together. I also work with Dr. Tsukada for our studies in Doya lab for computational projects. It is certain for me that my asset of social connections came from social asset of Prof. Doya. I hope that we keep working as collaborators, and I can keep exploring new academic/non-academic frontiers. I learned a lot of things from him especially about patience and self-management. Furthermore, in someday, as he is an 'Ironman', I would like to be an 'Ultra trail runner'.

Second, I must acknowledge my great friends, Chris Reinke and Nino Espinas. Without them, it was impossible for me to improve my English and enhance my passion to continue my research. Having lunch and dinner with you was one of my best memories at OIST. We went to Germany to see Chris' family. We went to Kyoto to feel Japanese culture together. These memories are my precious memories, which will not fade forever. I can't thank them more.

Third, I acknowledge my collaborators, Associate Prof. Stephens for his theoretical comments, DMD. Cheng for elaborate supports for SSRI experiments, Dr. Shimizu for data analyses and fMRI preprocessing, Dr. Hikishima for MRI knowledge, Dr. Takata for surgery for mouse fMRI, and Associate Prof. Tanaka for educational mind, Mr. Ohba, who made almost all equipment for habituation, Dr. Sakai, who gave me clinical comments, and Dr. Abe, who gave me advice of fMRI imaging. Additionally, I would like to thank Dr. Tsukada for our fMRI analysis and warm kindness, Dr. Steven for his editing of the thessi, and Dr. Miyahara, Dr. Nishida, and Dr. Niikawa for their friendliness. Without any one of them, I could not reach here, and write up my thesis. I found that each project that people are working has a great story.

Next, I also write acknowledgement to my graduate school, Okinawa Institute of Science and Technology (OIST). When I found OIST, OIST was not even a school yet. Taking me as a student should be a risk due to my ability at that time. It is not

sure for me whether I did well or not, but I suspect I could do multiple good and bad examples to show. I would like to contribute to development of the OIST community by opening multiple frontiers. I hope that not only new students at OIST but also students in Japan feel something new from me and our first-year students.

Finally, I would like to thank my family for patient supports. Since I dropped out my high school, there were a lot of fights between us. I am so sure that my parents were anxious about my future. Although I made a lot of efforts, I obtained plenty of chances because of the parents. In the end, I recognized any problem always lies inside of myself. A Ph.D course was learning myself and shaping process of myself. I suppose that my next step is to give chances to other people and work together with them. I swear I will keep doing them, and would like to say 'I love you'.

Abbreviations

All abbreviations used in the thesis should be listed here, with their definitions, in alphabetical order. This includes trivial and commonly used abbreviations (at your own discretion), but not words that have entered into general English usage (such as laser or DNA). In particular, non-standard abbreviations should be presented here. This is an aid to the reader who may not read all sections of the thesis.

ABA	Allen brain atlas
ACC	Anterior cingulate cortex
ANTs	advanced normalization tools
BST	Bed nucleus of steria terminalis
BOLD	Blood-oxygen-level dependent
BCT	Brain Connectivity Toolbox
Ce	central nucleus of amygdala
CNS	Central nervous system
Cpu	Caudate putamen
CNS	Central nervous system
dlPAG	dorsolateral periaqueductal gray
DMN	Default mode network
DRN	Dorsal raphe nucleus
DWI	diffusion-weighted magnetic resonance imaging
dmDR	dorsomedial part of dorsal raphe nucleus
vlDR	ventro-lateral part of dorsal raphe nucleus
vmDR	ventro-medial part of dorsal raphe nucleus
ELA	energy landscape analysis
FC	functional connectivity
dFC	dynamic functional connectivity
FDR	False discovery rate
ELA	Energy landscape analysis
EPM	Elevated-plus maze
fMRI	functional magnetic resonance imaging
rs-fMRI	resting-state functional magnetic resonance imaging
FC	functional connectivity
GIFT	Group ICA Of fMRI Toolbox
HPC	hippocampal complex
IC	Inferior colliculus
ICA	independent component analysis

sICA	spatial independent component analysis
LS	Lateral septum
LH	Lateral hypothalamus
LHb	Lateral habenula
MD	major depression
MRN	Median raphe nucleus
mPFC	medial prefrontal cortex
NAc	Nucleus of accumbens
OA	Orbital area
OF test	Open-field test
MEM	maximum entropy model
PCC	Posterior parietal cortex
PCC	Posterior parietal cortex
PMA	Primary Motor area
ROI	Regions of interest
REST	REsting State fMRI data analysis Toolkit
RT	Thalamic reticular nucleus
RSC	Retrosplenial cortex
dRSC	dorsal retrosplenial cortex
RVLM	rostral ventrolateral medulla
SERT	serotonin transporter
SSRI	Selective serotonin reuptake inhibitors
SC	structural connectivity
VTA	Ventral tegmental area

I dedicate my dissertation work to my family, many friends who encouraged me in various ways, and the old self who suffered in the high school period. I would like to give a special thank to my friend, Sadia Oumohand. I appreciate my beloved friend, Ami Akamine, for our long journey. In the end, I devote this work to all the people suffering from major depression and its treatment. With all my dedications, I aspire to help to create better treatment, better prevention of major depression in the near future, and promotion of happiness.

Contents

List of Figures

List of Tables

Chapter 1

Introduction

1.1 Motivation

The role of the serotonin in neural systems is one of the enigmas in neuroscience. How serotonin regulates neural dynamics? This is a central question that attracted attention of not only in basic scientists but also clinical researchers. Psychiatrists would ask how serotonin can produce its antidepressant effects, while neuroscientists would inquire how serotonin regulates brain dynamics through its wide-spreading innervation.

To address those questions, I utilize resting-state functional magnetic resonance imaging (rs-fMRI) for the rodent to clarify serotonergic control of brain-wide dynamics, in combination with behavioral tests, pharmacology and optogenetics. By doing so, I aim to characterize serotonergic control of the brian-wide dynamics from the standpoints of basic and pre-clinical researches.

1.2 Outline of the thesis

I organize this thesis with the following chapters.

In the first chapter, I review the current status of the research on serotonergic regulation of neural circuits and cognitive behaviors, especially positive and negative reward systems and motivation. I also explain the rs-fMRI literature in the human and other mammalian brains, its application in psychiatry, and analytic methods for functional network, temporal dynamics, and multi-modal data integration. I finally propose the two main projects combining rs-fMRI for the rodent brain with pharmacology and optogenetics to decipher its control of brain-wide dynamics.

In the second chapter, I describe the first project about accute and chronic effects of serotonergic antidepressant on brain-wide dynamics. Serotonin is deemed as the critical target for medication for psychiatric disorders. I utilize serotonergic antidepressant treatment over two weeks and rs-fMRI recording across multiple sessions to address the question of where and how serotonergic antidepressants influence brain-wide dynamics

after acute and chronic administrations and how they are related with behaviors.

The chapter 3 presents the project to clarify the role of a serotonergic sub-system originating from the dorsal raphe nucleus (DRN). The serotonin system is composed of nine sub-systems. Conventional systemic manipulation by pharmacology can obscure the regulation by each sub-system. A recent advancement, so-called optogenetics, enables us to manipulate serotonergic activity of a selcted sub-system in a temporarily precise manner. Combining optogenetics and rs-fMRI, I address the question of where and how the serotonergic sub-system regulate functional brain dynamics.

Finally, in the chapter 4, I summarize methodological limitation of the projects, and discuss how we can take advantage of the findings and data for future serotonin research.

Chapter 2

Modulation of neural dynamics and cognition by the serotonin system

Serotonin is involved in various behavioral and cognitive functions, such as locomotion, awake-sleep cycle, reward and punishment, decision making, and mood [65, 73, 156, 173]. Many researchers have attempted to study the relationship between serotonin and reward/punishment systems, not only from a theoretical viewpoint, but also from a clinical perspective [45, 57, 61]. Since serotonin is the major target for medications to treat psychiatric disorders, it is also deemed an important factor for anxiety and depressive mood [45, 99, 159, 160]. Despite abundant studies, serotonergic control of cognitive functions and neural mechanisms of serotonergic medications remain enigmatic.

In this chapter, I review the current understanding of neural circuits and of cognitive functions of the serotonin system. I then introduce recent promising advances in functional brain imaging and its combination with pharmacological and ontogenetic manipulations.

Finally, I propose two experimental projects to elucidate serotonergic control of brain-wide dynamics: rodent resting-state fMRI experiments under chronic serotonergic medication and optogenetic stimulation of dorsal raphe serotonergic neurons. These projects would contribute to understanding complex regulation of the serotonin system.

2.1 The neural circuit of the serotonin system

The serotonin system in the mammalian central nervous system (CNS) originates from nine nuclei on the midline of the hindbrain and projects widely to diverse brain areas and the spinal cord (Figure. 2.1).

Serotonin has at least 14 receptor subtypes, including ionotropic and metabolic

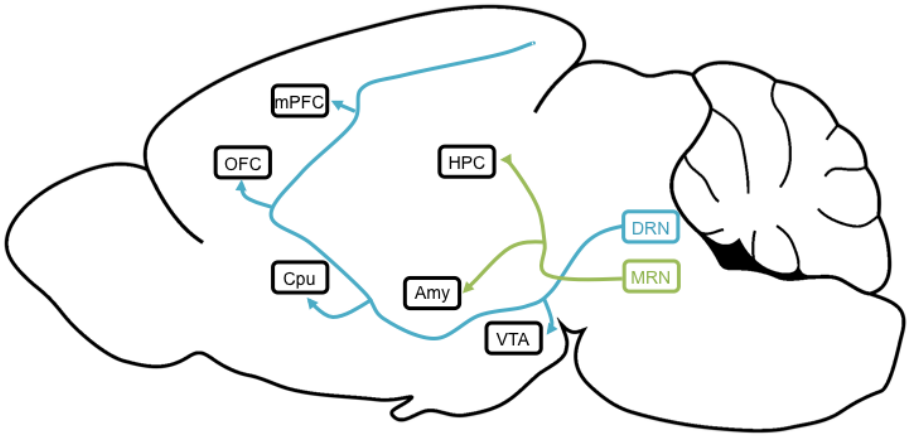

Figure 2.1: The representative figure of serotonergic projections. DRN serotonergic neurons mainly project to prefrontal regions, including the mPFC and the OFC, the caudate putament (Cpu), and the ventral tegmental area (VTA). Meanwhile, MRN serotonergic neurons innervate the hippocampal complex (HPC) and the amygdala complex (Amy) [193, 199].

receptors, expressed pre- and post-synaptically and its extracellular concentration is regulated by serotonin transporters (SERT) [91, 163, 177].

2.1.1 Afferents and efferents of the serotonergic nuclei

Most studies of the serotonergic system have focused on the two major nuclei, the dorsal raphe nucleus (DRN) and the median raphe nucleus (MRN). DRN serotonergic neurons have wide projections to the forebrain, such as prefrontal regions and the striatum, while MRN serotonergic neurons have projections to the hippocampus and the midbrain, including the habenula complexes [193, 199].

Serotonergic neurons in the DRN and MRN also receive multiple inputs from many brain regions [148, 150, 204]. Although outputs for the serotonergic system are nucleus-dependent, synaptic inputs to DRN and MRN serotonin neurons are from similar sources, such as the amygdala, the inferior colliculus (IC), the ventral striatum, the prefrontal regions, including the anterior cingulate cortex (ACC) and prelimibic area, the somato-motor areas, the pallidal regions, the lateral habenula (LHb), and the lateral hypothalmic area (LH) [148]. Although there is no distinguishing difference between input regions of the DRN and MRN, it revealed that DRN serotonin neurons have seven-fold larger connection inputs than MRN serotonin neurons [148].

The heterogeneity of DRN serotonin neurons has recently been featured [1, 41, 70, 190]. The DRN has been divided into three subareas, ventro-medial (vmDR), ventro-lateral (lateral wings, lwDR), and dorsomedial DR (dmDR) [28, 121, 189, 190]. Serotonergic projections of the vmDR mainly target a portion of the somatosensory cortex and the barrel cortex. Output projections of dmDR serotonin neurons were found in prefrontal regions, such as the mPFC and nucleus accumbens (NAc). Serotonergic innervations from the dlDR mainly project to subcortical regions, such as the dorsolateral periaqueductal gray (dlPAG) and the rostral ventrolateral medulla (RVLM). The dlPAG is especially known as stress-related circuitry [13]. Compared to the vmDR, serotonergic neurons in the lwDR exhibit different physiological properties of spontaneous activity, not only in a healthy state, but also after repeated social defeat stress [41, 42]. GABAergic neurons in the DRN are thought to participate in regulating neuronal dynamics in the DRN [6, 150, 192]. Interestingly, GABAergic neurons in the lwDR are predominantly interneurons. One study revealed that glutamatergic neurons from the vmPFC selectively innervate GABAergic neurons in lwDR, and the glutamatergic population to the DRN from the vmPFC augmented social avoidance [31]. Top-down control of serotonergic modulation might be driven by GABAergic innervation. However, another study [198] showed an antidepressant effect in the forced swim test by stimulating the $Glu^{vmPFC-DRN}$ circuitry in a similar manner to that reported by Challis et al. [31]. The basis for the discrepancy remains unknown.

2.1.2 Serotonin receptors and transporters

Heterogeneous expression of serotonin receptors also ambiguates understanding of the serotonergic system. There are seven categories (5-HT_{1-7}R) and over 14 subtypes [40, 145]. Almost all receptors have metabotropic G-coupled proteins except for iontropic 5-HT_3 receptors. Inhibitory metabotropic 5-HT_{1A} receptors coupled to G_i proteins are expressed in somata of DRN serotonin neurons [39]. Extracellular serotonin suppresses neuronal firing of DRN serotonergic neurons by activating 5-HT_{1A} receptors. This inhibitory mechanism is believed to prevent excessive release of serotonin [3, 17]. While there is evidence of the involvement of other receptors in the aforementioned functions, their explicit roles are still unknown [208].

Serotonin transporter (SERT) blockers have been used to understand serotonin regulation in the brain. Selective serotonin re-uptake inhibitors (SSRIs) are routinely prescribed as SERT blockers for patients with major depression (MD). Although multiple studies have attempted to reveal how SSRIs affect cognitive functions, few studies have attempted to show how SSRIs regulate brain-wide dynamics[131, 132, 164]. McCabe et al. hypothesized that SSRI medication normalizes abnormal brain regulation in MD subjects, targeting the dorso-medial PFC (dmPFC) [131, 132]. Consistent with this hypothesis, they found that SSRIs reduced functional connectivity between the dmPFC and the amygdala. Schaefer et al. found that a single dose of SSRIs globally reduces centrality in cortical regions, but increases centrality in the thalamus and cerebellum [164]. Furthermore, it is also known that acute SSRI administration sometimes worsens the symptoms of MD patients, and more than two weeks of medication are required before they begin to impact symptoms. On the other hand, some studies suggested that SERT subytpes determine antidepressant responses based on their structures [151, 184].

Nonetheless, how SSRI regulates brain-wide dynamics along a medication time course remains unknown [29, 208].

2.2 Serotonergic control and cognitive behaviors

Serotonergic function has been classically studied in the context of aversive signaling. In early studies, serotonin was thought to regulate behavioral inhibition [173]. However, it has been also suggested that behavioral inhibition reflects encoding of negative outcomes [178]. Therefore, it is hard to distinguish serotonergic encoding of negative values from mere physical behavioral inhibition. In 2002, Daw et al. proposed that serotonin regulates a negative system, including punishment and negative consequence prediction [45]. This hypothesis was inspired by the dopamine hypothesis of reward prediction error, and attempted to capture regulation in a negative system by the serotonin system, in apposition to the dopamine system [89, 166]. The theory was driven by serotonin involvement in negative value or prediction coding underlying behavioral

inhibition with respect to fight-or-flight responses. Some evidence supported the theory [43, 44]. This theory is also consonant with serotonin roles in stress control. A series of studies indicated that uncontrollable stress induces increased extracellular serotonin in the DRN to cause learned helplessness [2, 16, 125]. Amat et al. showed that venteromedial PFC (vmPFC) prevents stress-induced activation of DRN neurons[2]. Nonetheless, it is challenging for the theory to reconcile inconsistencies with effects of serotonergic antidepressant treatment.

On the other hand, in 2002, Doya proposed that serotonin regulates temporal discounting for delayed positive rewards. This can be interpreted as serotonin modulation in a positive reward and temporal system. The theory is consonant with behavioral symptoms of depressed subjects. This hypothesis led researchers to implement various serotonin studies [47, 136, 138, 139, 168, 182, 183], although some results revealed different serotonin roles, such as positive-value coding, but not reward discounting [23, 114, 141, 170]. Recent studies have demonstrated serotonin regulation in negative and positive systems [36, 85, 130]. These theories highlight the complexity of serotonin's roles in cognitive functions [20, 46]. Reflecting its complexity, Luo's group concluded that the function of serotonin is to evaluate and balance net benefit, considering positive and negative reward systems [123].

Furthermore, recent studies have shown that the serotonin system controls effort-related behaviors and vigor for exploration and rewards. In human studies, two groups showed that serotonin modulates effort-related behaviors and brain regions such as the ACC [135, 165], while serotonin involvement is rather controversial in rodent studies [55, 98, 161, 209]. Meanwhile, some evidence has revealed a relationship between serotonin system and vigor [38, 120]. Although transient serotonin activation caused behavioral inhibition in spontaneous locomotion, long-term stimulation of DRN serotonin systems promoted spontaneous locomotion [38]. Lottem et al. showed that serotonin activation with optogenetics promotes active exploitation of a reward site prior to giving up [120]. Distinguishing between effort-related behaviors and vigor is challenging, since reduction of cost to act and enhancement of intrinsic motivation are hard to discriminate.

In summary, we can interpret serotonin involvement in four categories, negative/positive reward systems and extrinsic and intrinsic motivational behaviors (Figure.2.2). Its involvement in miscellaneous functions reflects its broad projections and dynamics in the brain. Nonetheless, there is no integrative consensus regarding serotonin regulation.

2.3 Resting-state functional magnetic resonance imaging (rs-fMRI)

Functional magnetic resonance imaging (fMRI) is perhaps the most common tool to measure brain-wide activities in the human brain. Since its invention, it has mainly

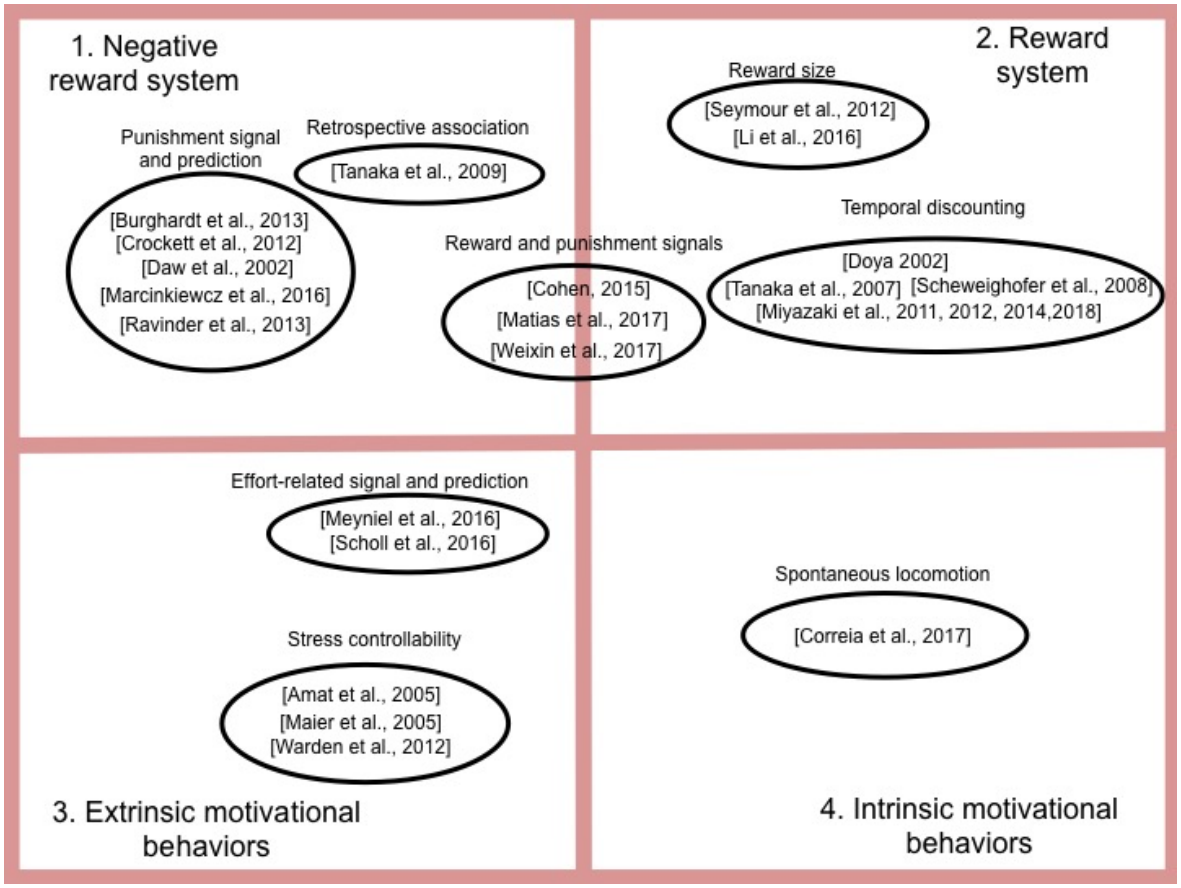

Figure 2.2: There are multiple aspects of serotonin studies. There are four categories of studies about serotonergic roles of cognitive behaviors. 1. Negative reward system such as coding of negative signals and prediction. 2. Reward system coding positive signals, prediction, and temporal discounting. 3. Extrinsic motivational behaviors such as cost sensitivity and stress responses. 4. Intrinsic motivational behaviors in spontaneous exploration. Each circle includes related-studies.

been used to study brain activities evoked during cognitive tasks. However, many researchers found that some brain areas are more active at rest or during a task-free state during fMRI runs. FMRI detects hemodynamic blood-oxygen-level dependent (BOLD) signals reflecting neuro-physiological states [117]. Rs-fMRI especially captures low-frequency hemo-dynamic signals ranging from 0.01 to 0.1(Hz). Previous studies defined five frequency band (1) slow-5 (0.01-0.027 Hz), (2) slow-4 (0.027-0.073 Hz), (3) slow-3 (0.073-0.198 Hz), (4) slow-2 (0.198–0.5 Hz), and (5) slow-1 (0.5–0.75 Hz) [215] based on electrophysiological studies[25, 149]. The slow-5 and slow-4 frequency bands are robust and covers the standard frequency range 0.01-0.08Hz[215].

Those brain regions include the angular gyrus, the medial prefrontal cortex (mPFC) and the posterior cingulate cortex (PCC) and they are recognized as the default mode network (DMN) [77, 78, 155]. FMRI measurement of subjects instructed not to engage in any particular thought is called resting-state fMRI (rs-fMRI) or task-free fMRI [15, 68, 111].

Follow-up rs-fMRI studies identified other reproducible brain activity components that are linked to specific cognitive functions, which are called functional brain networks [69, 113, 152, 186]. Functional brain networks reflect multiple states and features of subjects, such as emotion [124], cognitive demand [63], cognitive flexibility[191], intelligence level [86], and aging [185].

Recent studies have shown that functional connectivities measured by rs-fMRI are robustly reproduced in multiple imaging sessions on different days, and can be simulated by neural networks models based on the anatomical connections measured by diffusion-weighted MRI [51, 64, 75, 78, 90].

Another analysis of low-frequency oscillations (LFO) by rs-fMRI was amplitude of low-frequency fluctuations (ALFF), which detects regional spontaneous neuronal activity [211, 214]. ALFF measures amplitude of power spectrum at the standard low-frequency range (0.01-0.08 Hz), and has been applied to abnormal activity in subjects with mental disorders such as major depression [207] and autism spectrum disorders[180].

These observations suggest that rs-fMRI enables us to capture not only spontaneous mental processes but also individual personality, and group categories, including psychiatric disorders.

2.3.1 rs-fMRI for psychiatry

Due to its simple procedure and applicability to a wide range of subjects, rs-fMRI has attracted attention from neuro-psychiatrists [68, 113]. Multiple studies have exploited rs-fMRI to find brain markers for diagnosis of psychiatric disorders [76, 92, 162, 171, 172, 181]. For example, depressed patients showed abnormal functional connectivity and unstable synchronization in DMN-related areas [54, 76]. Since DMN is active

during task-free states, DMN may have some roles in imagination or self-referential processing. From this perspective, rs-fMRI study of DMN has become the major method to elucidate spontaneous mind processes, such as imagination, day dreaming, and rumination [34, 35, 67, 79].

Rs-fMRI has also been utilized in model animals in pre-clinical, translational studies since we can combine multiple invasive approaches. It has been shown that mammalian brains, including those of monkeys, rats, and mice retain a common functional organization, including the DMN-like structure [116, 122, 176, 197] despite the anatomical differences across species, such as in the prefrontal cortex [14].

Rs-fMRI with rodents can provide information about brain-wide activity with the same methodology used in human studies to facilitate translational studies of animal models [93, 102]. Current validities of animal models of psychiatric disorders, such as construct validity, face validity, and predictive validity, have been based on behavioral assessments [205]. New validities also have been proposed, based on neurological criteria [10, 142]. Rs-fMRI with model animals allows us to build a translational map between human and animal brains satisfying such criteria.

Recent advancement in high-magnetic field functional magnetic resonance imaging (fMRI), enables us to access brain-wide dynamics in the rodent brain. Thus, fMRI for rodents may provide a framework to establish a pre-clinical translational map underlying neural circuits across species.

2.3.2 Analysis and modeling methods for rs-fMRI

Rs-fMRI enables us to observe spontaneous brain-wide dynamics without external stimuli. A series of studies revealed linkage with cognition and personality, implying that such spontaneous dynamics underlie internal thinking processes. Multiple methods such as network analysis, temporal analysis, and integrative modeling have been suggested to explore such spontaneous dynamics. These approaches have potential for simulation of brain-wide dynamics under multiple conditions, including diseases and drug manipulation.

Network analysis

As a conventional approach, network analysis has been used in rsfMRI studies[157, 174, 175]. Temporal correlation of BOLD signals among brain regions has been called "functional connectivity" (FC). Multiple studies have exploited FC analysis to reveal linkage between brain dynamics and behaviors. Some studies have also utilized network analysis, such as centrality[119] and rich club coefficient[187] to study multiple FC structure, often called "functional networks." In addition, network analysis has also exploited graph clustering methods, such as the Louvain algorithm, to investigate

underlying activation patterns in functional networks [8, 116, 175]. Structural connections, similarly called "structural connectivity" (SC), have been studied by diffusion-weighted magnetic resonance imaging (DWI)[81, 107]. Association between FCs and SCs indicates a topological advantage to control brain dynamics[50, 78, 133].

Analysis for temporal dynamics

Multiple studies have offered analytical methods to inspect temporal functional brain dynamics. Those have been formalized with terms such as dynamic functional connectome, chromatonome, or dynome [27, 109, 154]. Human functional imaging studies also revealed an abnormality possibly associated with a depressive symptoms in temporal functional brain dynamics [54, 103, 206].

There are some methods for detecting temporal dynamics, such as dynamic functional connectivity (dFC) analysis [95, 154], energy landscape analysis (ELA) [60, 200], and a hidden Markov model [194–196]. ELA, an especially promising method for analyzing temporal dynamics, enables us to determine brain states in an ***a priori*** manner. Previous ELA studies revealed individual differences in brain dynamics in perceptual switching [202], abnormal brain state dynamics in subjects with autistic spectrum disorders (ASD) [203], and age-dependent brain state dynamics [59]. Furthermore, some evidence implies neuro-anatomical and neurophysiological links with state dynamics [4, 80].

Network simulation

Integrative approaches to understand underlying mechanisms of spontaneous brain dynamics has been used in human rs-fMRI studies. Multiple researchers combine neuronal firing models with empirical data from rs-fMRI and anatomical connection to emulate brain activities [51, 52, 83, 133]. The field aims to investigate the relationship between anatomical connections and functional dynamics from a dynamic perspective [50, 52]. This integrative approach has further potential to understand detailed neuronal modulation by integrating precise neural manipulations, such as immuno-chemistry, chemogenetics, and optogenetics in rodent studies [62, 71, 82, 118].

2.4 Pharmacological and optogenetic approaches

A major advantage of animal models in pre-clinical studies is that we can apply pharmacological or optogenetic manipulations that are technically or ethically impossible in human studies. Although many studies have been done to associate such manipulations with behaviors, their combination with rs-fMRI has enabled new opportunities to assess their effects on brain-wide dynamics. Integration of such brain-wide dynamics

and multi-modal data with evolving integrative approaches (Section.2.3.2) should contribute to understanding complex regulation of the serotonin system on brain dynamics and cognitive behaviors for future research 2.3.2.

Pharmacological fMRI

Pre-clinical studies leverage rodents to probe antidepressant drug effects on behavioral assessment. Serotonergic antidepressant treatments are hypothesized to normalize abnormal brain activities in MDD-related brain regions, including default mode network and limbic network, which are the key regions for controlling motivation and mood.

Consistent with this hypothesis, acute and sub-chronic serotonergic antidepressants in humans reduced brain-wide cortical centrality and functional connectivity between the amygdala and medial prefrontal cortex, respectively [131, 132, 164]. It is clinically well known that serotonergic antidepressants alter their influence along a time course of about two weeks. Acute medication tends to promote anxiety in some cases [24]. However, there have been no human brain imaging studies that addressed how serotonergic antidepressant medication alters brain-wide dynamics during a treatment time course.

Pharmacological fMRI has been used for rodents [7, 102]. Multiple studies aimed to characterize brain-wide mapping of pharmacological manipulations on the brain [19, 106, 167]. Some studies revealed brain-wide activation patterns in affective regions including the Amygdala, the Cpu, and the prefrontal cortex, and the ventral tegmental area (VTA) by SSRI administration [106, 167]. Nonetheless, association of SSRI influence on the human brain and the rodent brain has not been well characterized.

Furthermore, serotonin is the major target of medication for MD. Since one of the major symptoms in MD patients is characterized by rumination, which is repetitive negative spontaneous thoughts [37, 126, 146], the serotonin system may influence brain-wide, time-varying dynamics and even subjective state. However, little is known about serotonin modulation of brain-wide dynamics.

Chemogenetic and optogenetic fMRI

There is a novel trend to capture causality of brain dynamics by combining brain-wide imaging with chemogenetics and optogenetics[22, 53, 62, 71, 112, 118]. Consistent with implications from structural studies, one chemogenetic study showed that the serotonin system activates affective regions, such as the amygdala, the mPFC, and the striatum [71]. To be more temporally precise, a combination of fMRI and opogenetics, so-called optogenetic fMRI (ofMRI) has been used to study dopaminergic modulation in neural circuits [22, 53, 62, 118]. Their application to the serotonergic system may help to reveal serotonergic modulation.

Previous optogenetics studies to address the effect of serotonin stimulation on motivational behaviors [38, 66, 97, 120, 137, 139]. Two research groups independently showed that optogenetic stimulation induced waiting behaviors for delayed rewards [66, 137, 139]. In addition, different cognitive roles such as spontaneous locomotion [38], learning [97], and punishment [129]. It is interesting to combine ofMRI and these cognitive tasks to identify neural circuits associated with cognitive behaviors.

2.5 Experimental plan

In order to clarify serotonergic influence on brain-wide dynamics and how it changes during a time course of SSRI medication, I employ a combination of pharmacology, optogenetics, rs-fMRI, and behavioral tests in rodents. Specifically, I performed the following two experiments, which are detailed in the following chapters.

- Pharmacological rs-fMRI experiments to assess the short-term and long-term effects of serotonergic antidepressant medication on whole-brain dynamics
- Optogenetic rs-fMRI experiments to identify phasic modulation of dorsal raphe serotonergic neuronal activation.

Chapter 3

Pharmacological fMRI study of acute and chronic effects of SSRI

3.1 Aims

In this chapter, I report procedures and results of a pharmacological fMRI experiment aimed at answering the following questions.

1. How does serotonergic antidepressant administration for two weeks affect behavioural performance?

2. How do whole-brain network dynamics change over two weeks of serotonergic antidepressant administration?

3. Is there any correlation between behavioral performance and brain network dynamics?

To answer these questions, we conducted experiments with rs-fMRI and two behavioural tests (Figure. 3.1). First, we compared behavioural parameters between SSRI and control groups. Second, we extracted significantly different functional connectivity between the two groups. We then checked whether there is an association between functional connectivity and behavioural parameters. Finally, we asked whether temporal dynamics exhibit differences using large-scale components. The project was done as a part of the collaborative work with Dr. Abe, Dr. Takata, and Dr. Tanaka for awake resting-state fMRI setups. I conceived and performed the all experiments and all analyses.

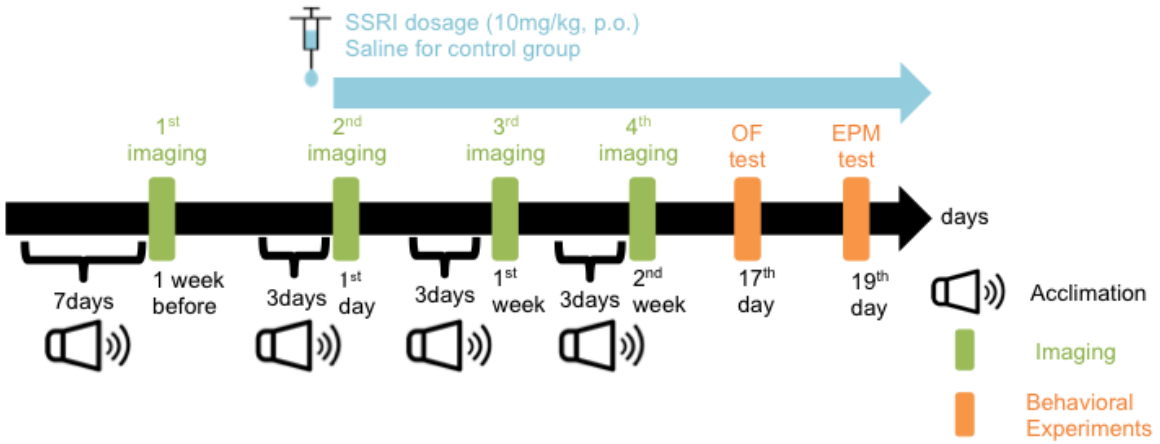

Figure 3.1: Subject underwent four imaging sessions, and two behavioral tests. After 7 days of acclimation training, the first session was performed without any intervention. From the 1^{st} day of SSRI administration, we started injecting SSRIs to subjects (10mg/kg, p.o., saline to the control group). Two behavioral experiments, open-field and elevated-plus maze tests, were done after imaging sessions.

3.2 Methods

3.2.1 Experimental paradigm

The experiment was composed of four resting-state fMRI (rs-fMRI) sessions and two subsequent behavioral tests after imaging sessions, as shown in Figure 3.1. In the week before a session, there were no injections to subjects. SSRI was administrated to a group one hour prior to the 1^{st} day imaging sessions. We administered SSRI to a group for 19 days including the day of the 1^{st} day imaging session while saline was administered to a control group.

3.2.2 Subject and acclimation

We introduced wild-type C57BL6J male mice (n=64, over 12-19) to our SSRI experiments. We completed all experiments for 48 subjects (SSRI:n=28, Cont:n=20). We divided subjects into two groups, and there were no statistical differences in age ($P = 0.9$, U-test) or body weight change during SSRI administration between the two groups (Table 3.2). An acrylic bar (3x3x27 (mm)) was attached to each mouse skull prior to rs-fMRI sessions. All mice were bred in the reversed day/dark cycle, and mice underwent all experiments during the dark period (10 am - 10 pm, GMT+9). In order to perform awake imaging, we applied the head fixation and acclimation protocols reported in [210]. We initiated acclimation with subjects after a 7-10-day recovery period of the head fixation. All mice were acclimated to MRI sounds (2 hours, 80-113dB), which were recorded from a high-field 11.7 tesla MRI scanner with a cryoprobe and an

optical microphone (Opto MIC model 1140, KOBATEL Co., Japan), combined with a noise meter (TYPE 6236; Aco Co., LTD, Japan) and a linear PCM recorder (TASCAM DR-40, TEAC, Co., Japan). We performed the acclimation protocol at least for seven days before the imaging session, and resumed training for 3 days prior to the other three imaging sessions (3.1).

Table 3.1: Demographic Table

Method	SSRI-treated group	Control group	p values with unpaired t-test
Sex	male	male	-
Age	15.33 (3.9641)	15.45 (3.804)	$P = 0.9062$
No. Subjects	28	20	-
Average No. one week before Sessions	2.19 (SD=0.69)	2.10 (SD=0.74)	$P = 0.69$
Average No. 1^{st} day Sessions	2.27 (SD=0.78)	2.21 (SD=0.63)	$P = 0.79$
Average No. 1^{st} week Sessions	2.35 (SD=0.79)	2.11 (SD=0.46)	$P = 0.24$
Average No. 2^{nd} week Sessions	2.23 (SD=0.71)	2.11 (SD=0.57)	$P = 0.53$

3.2.3 SSRI administration

Escitalopram, a SSRI, was mixed with saline. The mixed escitalopram (10 mg/kg, p.o.) was administered to the SSRI-treated group (n=28) while the saline-treated group (n=20) received only the same amount of saline. We performed administrations one hour before each session in 1^{st} day, 1^{st} week, and 2^{nd} week imaging sessions while administrations were executed in the dark period on other administration days.

3.2.4 Open-field test

The experiment with the open-field box test was performed in a sound proof box (50x50cm). The open-field box (O'Hara & Co., Tokyo) consisted of a grey box. We defined a center region (20x20cm) as the center arena. Each session was performed for 10 minutes with white illumination (15 lux). After each session, the open-field box was sterilized with 75 % ethanol.

Table 3.2: MANOVA of Body weights

Source	Sum Sq.	d.f.	Mean Sq.	F	Prob>F
group	0.033	1	0.0331	0.01	0.9104
period	7.512	3	2.50389	0.96	0.4124
group*period	6.574	3	2.19128	0.84	0.473

3.2.5 Elevated-plus maze

The experiment with the elevated-plus maze was performed in a sound proof room [108]. The elevated plus maze (O'Hara & Co., Tokyo) was composed of a center platform and four arms (two open and two closed arms with walls; 25 x 5 x 16 (cm) ($LxWxH$) for Closed arms, and 25 x 5 x 0.5cm for Open arms), and the maze was elevated 50 cm above a base [108]. X and Y positions of each mouse were continuously tracked with a video camera on the ceiling of the sound proof room (2 frame/second). Each session was performed for 15 minutes with white illumination (100 lux). After each session, the maze was sterilized with 75 % ethanol.

3.2.6 MRI imaging

Each mouse was placed in the MRI animal bed. After the body temperature of a mouse stabilized at 36 ± 1 (C°), T2-weighted structural imaging and T2* functional imaging were performed. MRI images were acquired with an 11.7 T MRI scanner for small animals (Biospec 117/11 system, Bruker Biospin, EmbH, Ettlingen, Germany) with a a cryogenic quadrature RF surface probe (Cryoprobe, Bruker BioSpin AG, Fällanden, Switzerland). T2-weighted structural imaging was performed with a fast spin echo sequence using the following parameters: 140 x 140 matrix, 13.5 x 13.5 mm^2 field-of-view, repetition time(TR)/effective echo time(TE) 4000/18.75 (ms), 32 coronal slices, slice thickness: 300 μm, and a total acquisition time of 2 min.

After T2-weighted structural imaging was performed. All T2* functional imaging was performed using a gradient-echo echo planar imaging (EG-EPI) sequence, which is a conventional functional MRI acquisition sequence. Interleaved slice acquisition was also applied to our EPI sequence in order to minimize the influence of cross-slice artifacts. Our EPI sequence was performed with the following parameters: a 90 x 90 matrix, flip angle, 13.5 x 13.5 mm^2 field-of-view, TR/TE 2000/14.2 (ms), flip angle: 50°, Bandwidth: 400k(Hz), 41 coronal slices and slice thickness: 300 μm, 300 repetitions, and a total acquisition time of 10 min.

3.2.7 Preprocessing and de-noising

The first five functional images in each run were deleted from analyses in order to prevent contamination of initial imaging artifacts due to motion and non-steady state image quality. Statistical Parametric Mapping (SPM12). 10-fold magnification of images was done to process images with Statistical Parametric Mapping (SPM12), which is designed to process human-size brain images. Therefore, the voxel size was 1.5x1.5x3mm in analytical steps. Pre-processing including motion correction, realignment, co-registration, normalization to a C57BL6/J template, and spatial smoothing (kernel with 3x3x6mm) were executed by Statistical Parametric Mapping (SPM12).

Since each slice of 3D brain image was taken at a different time, slice timing correction was applied to correct slice-timing differences by temporal interpolation. Next, realignment of 3D brain images was conducted to correct motion-related changes of brain position. Then, co-registration was executed to overlay functional T2* images onto structural T2 images and to save coordination changes of T2* images for normalization. During normalization, T2 structural images were first warped to fit the average C57BL6/J template [87]. Then T2* functional images were further warped to the template using the co-registered coordination change of the images. In spatial smoothing, voxel signals were spatially smoothed using a gaussian kernel (3x3x6mm). In the de-noising process, linear de-trend filtering, temporal filtering (0.01-0.08 Hz), 6 motion regressions, signal regression of grey matter(GM), white matter(WM), and cerebrospinal fluid (CSF) de-spiking and motion scrubbing were employed so as to reduce false-positive functional connectivity [153] with a MATLAB toolbox, functional connectivity toolbox (CONN17; Table.A.1). Linear de-trend filtering was applied to remove the linear accumulation of imaging noise. Temporal filtering was done over the standard 0.01-0.08 Hz frequency range, because the lower frequency of T2* signals reflects spontaneous brain signals [215]. Six motion-related artifacts in T2* signals, such as x, y, z coordinates and pitch, and raw, yaw rotations were regressed out for possible correlation. Average signals of GM, WM and CSF were further removed to reduce potential influence of non-physiological signals. Motion-related artifacts were further smoothed with a squashing function in the despiking step. Prior to these analyses, motion scrubbing was finally executed to remove signal outliers (z-score > 5).

3.2.8 Extraction of BOLD signals

A C57BLJ mouse atlas from the Allen Brain Atlas (ABA) was spatially warped to a C57BL6J mouse template [87] using Advanced Normalization Tools (ANTs;Figure. A.1). We extracted mean BOLD signals from the regions of interest (ROIs) based on the atlas (Supplementary Section. A.2). We further utilized ROIs from spatial independent component analysis (sICA) to examine how SSRIs regulate large-scale functional components understood as cognitive brain modules. We extracted a mean time-series from the large-scale ROIs for conventional functional connectivity analysis and energy landscape analysis (ELA;Supplementary section. A.4).

3.2.9 Seed-based FC analysis

We performed seed-based FC analysis with a subset of depression-related target regions including the caudate putamen (Cpu), the bed nucleus of the stria terminalis (BST), the dorsal raphe nucleus (DRN), the medial prefrontal cortex, the orbital area (OA), the ventral tegmental area (VTA) from ABA with functional connectivity toolbox (CONN; Figure. A.1). Using these regions of interest (ROI), seed-based functional connectivity (FC) analysis was applied to test the hypothesis that SSRIs influence signals in depression-related brain targets [131, 132]. Seed-based FC analysis was

composed of two steps. First, Pearsons' correlation between a time series of an average seed ROI and each voxel in images was calculated, and regional clusters were formed by thresholding (uncorrected $p<0.001$). In the second step, formed clusters were further statistically corrected with the positive false discovery rate (pFDR; $p < 0.05$). By comparing the SSRI-treated and control groups, it is possible to identify brain regions influenced by SSRIs. For a further validation with seed-based FC analysis, different frequency range (0.01-0.1 Hz) was applied in temporal filtering, and seed-based FC analysis was performed with liberal thresholding (uncorrected $p<0.01$) for regional clustering and corrected with pFDR ($p < 0.05$).

3.2.10 Analysis of amplitude of low-frequency fluctuations

Amplitude of low-frequency fluctuations (ALFF) was performed to detect difference in regional activity between SSRI and control groups. After preprocessing was executed, Fourier transformation was applied to each voxel, and sum of amplitudes of low fluctuations at multiple ranges of low-frequency dynamics (0.01-0.08, 0.01-0.1, and 0.01-0.15 Hz) was compared between the groups. The analysis was executed by MATLAB.

3.2.11 Large-scale component extraction with independent component analysis (ICA)

Spatially independent component analysis (sICA) is one of the common approaches to extract synchronously activated spatial components from fMRI data. Such components are known to correspond to functional organization of the brain and to exist both in human and animal brains[122, 176, 212]. The default mode network (DMN) is the major representative component that is active during a task-free state. Previous studies revealed that there are multiple functional modules in the mouse brain. Therefore, we used sICA to extract multiple functional components with Group ICA of the fMRI Toolbox(GIFT; Supplementary Table. A.1). We selected ten interpretable and previously known brain regions (Table. 3.3; [122, 176, 212]).

3.2.12 Energy Landscape analysis

We performed energy landscape analysis (ELA) using large-scale components extracted from sICA. ELA renders brain dynamics as a ball in the energy landscape, and enables us to define local minima as the state of dynamics (Supplementary Section. A.4). Energy in this case does not refer to any metabolic or biological senses, but the information-theoretical sense. First, we set regions of interest (ROIs) to extract brain signals. Then, extracted signals were binarized using the thresholding mean. Next, we fit the binarized signals to the pairwise maximum entropy model to define local minima. A disconnectivity graph was utilized to visualize local minima of the energy

ROI id	ROI name	Corresponding anatomical regions
1	DMN-like component	mPFC, dorsal RSC
2	Parietal component	parietal cortex, auditory cortex
3	Thalamic component	thalamic complex
5	Visual component	Primary visual cortex
6	Mid component	ventral RSC, Auditory cortex
7	Fronto-lateral component	Primary motor cortex
8	cerebellar component	Cerebellar complex
9	Ventral hippocampal complex	CA1, CA2, CA3, Denate gyrus
10	Striatal component	Caudate putamen, nucleus accumbens

Table 3.3: Extracted large-scale brain components

landscape. Energy in the disconnectivity represents the percent of time in the open field test that the test animal remained in the center region, encoded or recorded in brain activity patterns. By applying the results of local minima, ELA allows us to statistically test behaviors of brain dynamics.

3.3 Behavioral Results

We examined whether long-term medication influences behavioral performance. Subjects underwent two behavioral tests, the open-field test and the elevated-plus maze, subsequent to four imaging runs (Figure.3.1.).

3.3.1 Serotonergic antidepressants promote spontaneous locomotion

We first investigated whether long-term serotonergic antidepressants affect anxiety-like behaviors(Figure. 3.2.). We could find no statistical difference in the average of percent stay in the center region of the OF test and in the open arms of the EPM test, between SSRI and control groups(Figure.3.2.B,G.). Although there was no statistical difference in the variance in the OF test, we found significant difference in the variance in the EPM test($P < 0.001$, F-test; Figure.3.2.G).

Next, we examined whether spontaneous locomotion changed during chronic SSRI administration(Figure.3.2.C-E,H-J). The SSRI-treated group showed statistically longer total moving distance in both tests(Figure.3.2.C,H.). We decomposed total moving distance into two contributing factors, average speed during movement and immobility time. We verified whether either or both factors showed significant difference between SSRI-treated and vehicle-treated groups. We found that contributing factors were dependent on tasks. Average moving speed and percent immobility were signif-

icantly different in the OF test (moving speed: $P < 1e^{-10}$, U-test; immobile state: $P < 1e^{-8}$, U-test), while only percent immobility was significantly different in the EPM test($P < 0.0005$, U-test;Figure.3.2.E,E,I,J).

If long-term SSRIs promote general motor outputs, behavioral measures in the two tasks should be correlated. However, neither of the behavioral measures were significantly correlated in the two tests (Figure.3.3.A,B.). We then tested whether the difference between groups in average moving speed and percent immobility depended on the locations (Figure.3.4.). Both near the walls in the OF test and in the closed arm in the EPM test, the average moving speed was significantly higher(OF test: $P < 1e^{-9}$, EPM test: $P < 0.05$;Figure.3.4.A,E.), and percent immobility was significantly lower in the SSRI group compared to the control group(OF test: $P < 1e^{-9}$, EPM test: $P < 0.005$;Figure.3.4.C,H.). These measures were not significantly different in the center region in the OF test and the open arm in the EPM test, except for marginal significance of average moving speed in the center region of the open field ($P < 0.01$, U-test;Figure.3.4.B,D,F,G,I,J.).

Hence, we concluded that although influence on anxiety-like behaviors is context-dependent, serotonergic antidepressants promote spontaneous locomotion, especially in secure regions, but this enhancement may not be due to general motor output.

3.4 Anatomical seed-based functional connectivity analysis

3.4.1 SSRI influences functional connectivity from depression-related brain regions

Previous studies showed that neural circuits in motivation and mood are especially influenced by SSRI administration [24, 106, 129, 131, 132, 167]. Therefore, we hypothesized that the effects of short-term and long-term SSRI medication on the whole-brain dynamics, including the cortico-limbic regions, are different. To test this hypothesis, we first performed anatomical seed-based FC analysis with six seed regions selected in depression-related regions, namely, the caudate putamen (Cpu), the bed nucleus of stria terminalis (BST), the dorsal raphe nucleus (DRN), the medial prefrontal cortex (mPFC), the dorsal retrosplenial cortex (dRSC), and the ventral tegmental area (VTA). The DRN is the core of serotonin system. The Cpu and VTA are the main components of a neural circuit in motivation whereas the BST, mPFC, and dRSC are parts of a neural circuit controling mood. Their locations were based on the Allen rodent brain atlas (Supplementary Figure.A.1 and Table.A.1).

First, we compared regional spontaneous dynamics of the seed regions by fractional ALFF (fALFF) with multiple frequency ranges (0.01-0.08, 0.01-0.15, and 0.01-0.2 Hz) across imaging sessions. However, we could not observe any statistical difference of the

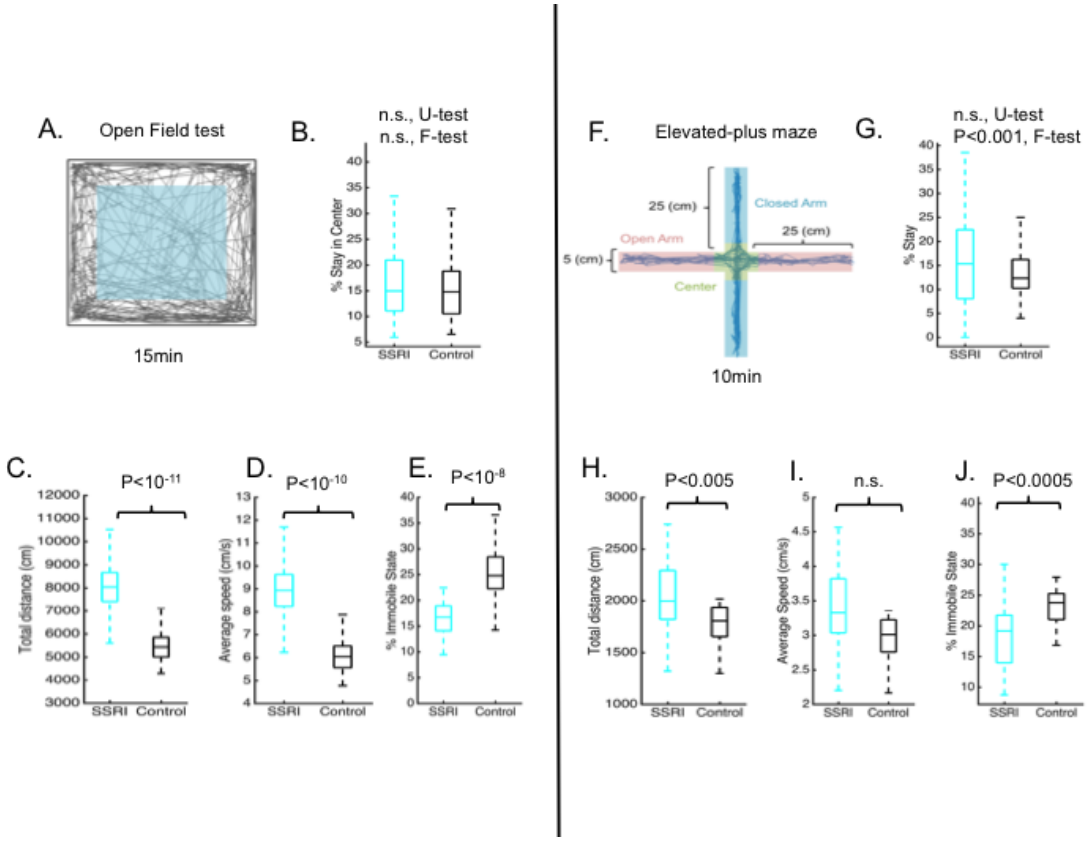

Figure 3.2: A. Open field box. Mice underwent the open-field (OF) test 17 days after SSRI/vehicle doses for 15 min (15 lux). B. There are no significant differences in the mean and variance of percent stay in the center region in the OF test. C. The SSRI-treated group showed significantly longer total distance than the control group in the OF test ($p < 1e^{-11}$, U-test). D, E We inferred that the significantly longer distance was influenced by average speed (cm/s) or percent immobility. Average speed ($P < 1e-10$, U-test) was significantly higher and immobility was significantly shorter ($P < 1e^{-8}$, U-test). F. Elevated-plus maze (EPM) test. Mice subsequently underwent the elevated-plus maze 19 days after SSRI/vehicle doses for 10 min (100lux). G. There are significant differences in the mean and variance of percent stay in the open arms in the EPM test. H. We confirmed significant longer total distance in the SSRI-treated group in the EPM test (p<0.05, U-test). I, J. We also checked influences of average speed (cm/s) and percent immobility in the EPM test. Although there was no significant difference in average speed (cm/s) between groups (p=0.076, U-test), the SSRI-treated group showed significantly less percent immobility ($p < 5e^{-4}$, U-test).

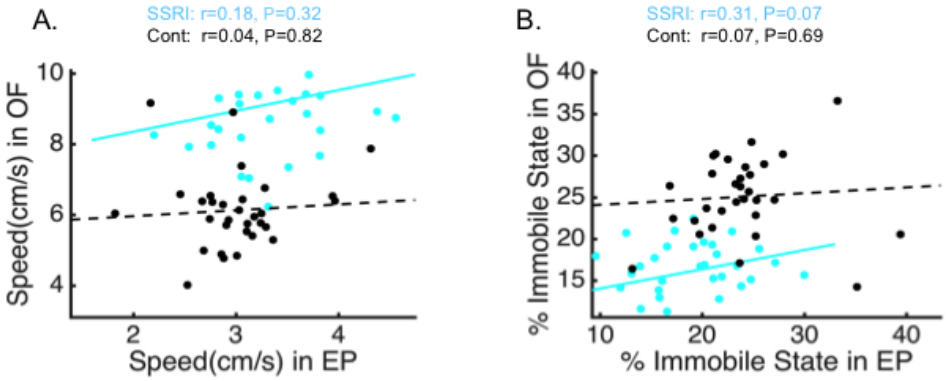

Figure 3.3: A. Correlation of behavioral parameters. Speed was compared between SSRI and control groups. There was no statistically significant correlation between the groups (SSRI: $r = 0.18$, $P = 0.32$; Cont: $r = 0.04$,$P = 0.82$). B. Correlation of behavioral parameters. Immobility was also examined between SSRI and control groups. There was no statistically significant correlation between the groups (SSRI: $r = 0.31$,$P = 0.07$;Cont: $r = 0.07$,$P = 0.69$).

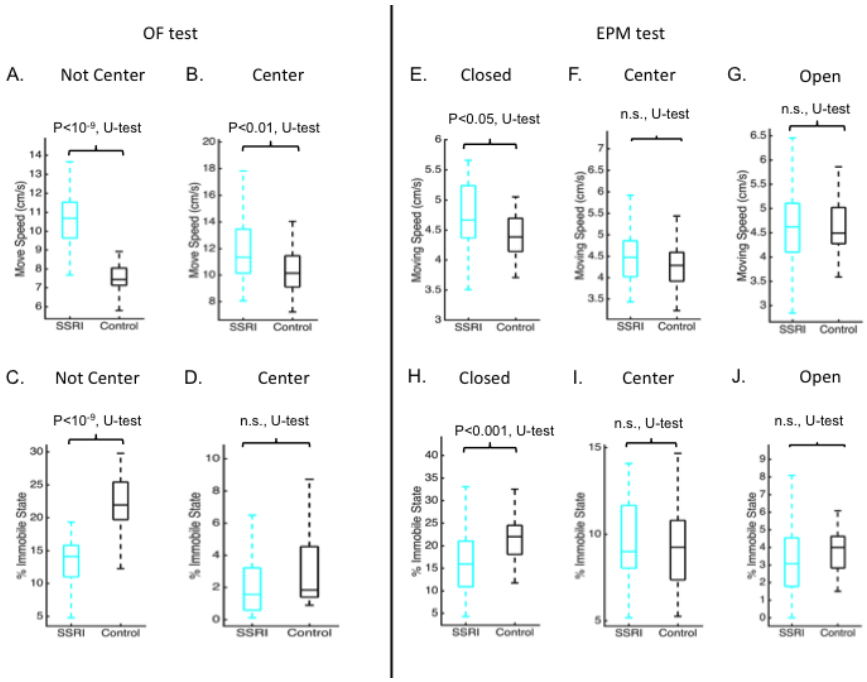

Figure 3.4: A, B. Average Speed in peripheral and center regions in the OF test. The SSRI-treated group showed significantly higher speed in both conditions (peripheral: $P < 1e^{-9}$, U-test; center: $P < 0.01$, U-test). C, D. Percent immobility in peripheral and center regions. Percent immobility was also significantly different in the two regions (peripheral: $P < 0.01$, U-test). E,F,G. Average speed in the EPM test. Although there were no significant differences in the center and open regions, we found statistically higher speed in SSRI-treated group in closed arms ($P < 0.05$, U-test). H,I,J. Percent immobility in the elevated-plus maze. There was a significant difference only in the closed arms ($P < 0.005$, U-test).

six selected ROIs in fALFF (see the detail in the section 3.2.10).

Next, we compared SSRI and control groups between acute and chronic SSRI administration. Our seed-based analysis revealed two significantly different FCs between BST and ventral RSC, and DRN and the thalatmic reticular nucleus (RT;Figure.3.5 and 3.6. We also observed FC differences across sessions using the FCs(Figure.3.8.A,B.). In the both FCs, there were statistically significant difference between one week before and 1^{st} day sessions (BST-vRSC: $P < 0.001$; DRN-RT: $P < 0.005$, unpaired t-test). However, we could not find a statistically significant difference between one week before and 2^{nd} week sessions (BST-vRSC: $P = 0.54$; DRN-RT: $P = 0.81$, unpaired t-test). Consistently, we found similar changes of FCs between BST and ventral RSC, and DRN and RT under different frequency range (0.01-0.1 Hz; Figure.3.7).

Our seed-based analyses suggest that the influence of acute SSRI administration is associated with reshaping neural circuits in the DMN-limbic and the mid-brain circuits.

3.5 Functional network-based analysis

We next investigated whether brain-wide functional components identified by sICA were altered by SSRI administration.

3.5.1 Ten functional networks identified by sICA

We employed spatial independent component analysis (sICA) to extract functional brain network components. From the joint data of all animals in all four scans, sICA extracted 30 spatial independent components. Among those, we identified 10 interpretable spatial components, including DMN-like, frontal, hippocampal, and striatal components (Figure. 3.9). Similar functional components were identified by sICA in previous studies [122, 176, 212].

3.5.2 SSRI administrations did not affect functional connectivity between functional brain networks

We calculated FCs among the ten functional networks along the time course of drug administration. However, no FCs showed statistically significant differences in the time course of administration (Figure. 3.10). This result may indicate that SSRI effects are limited within each functional module, but do not affect large-scale dynamics. Another possibility is that conventional FC analysis over the whole scanning session is insufficient to extract dynamic changes in the functional networks by SSRI administration.

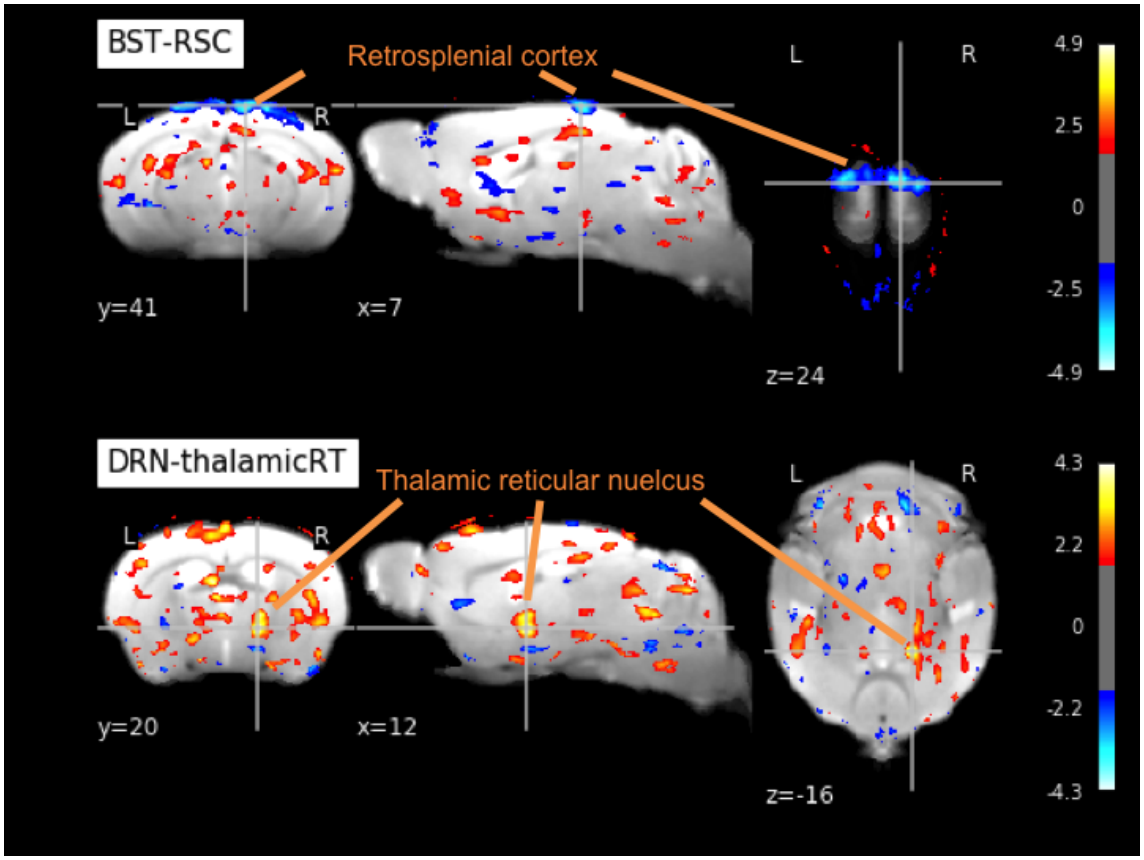

Figure 3.5: A. Seed-based analysis with the seed region, BST, revealed statistically significant contrast in the retrosplenial cortex (RSC), a homolog of the PCC in mouse brain (uncorrected $P < 0.01$ for cluster forming, and further correction with cluster size $P_{FDR} < 0.05$). B. The seed region, DRN, also revealed a statistical difference in the thalamic reticular nucleus(RT; uncorrected $P < 0.01$ for cluster forming, and further correction with cluster size $P_{FDR} < 0.05$).

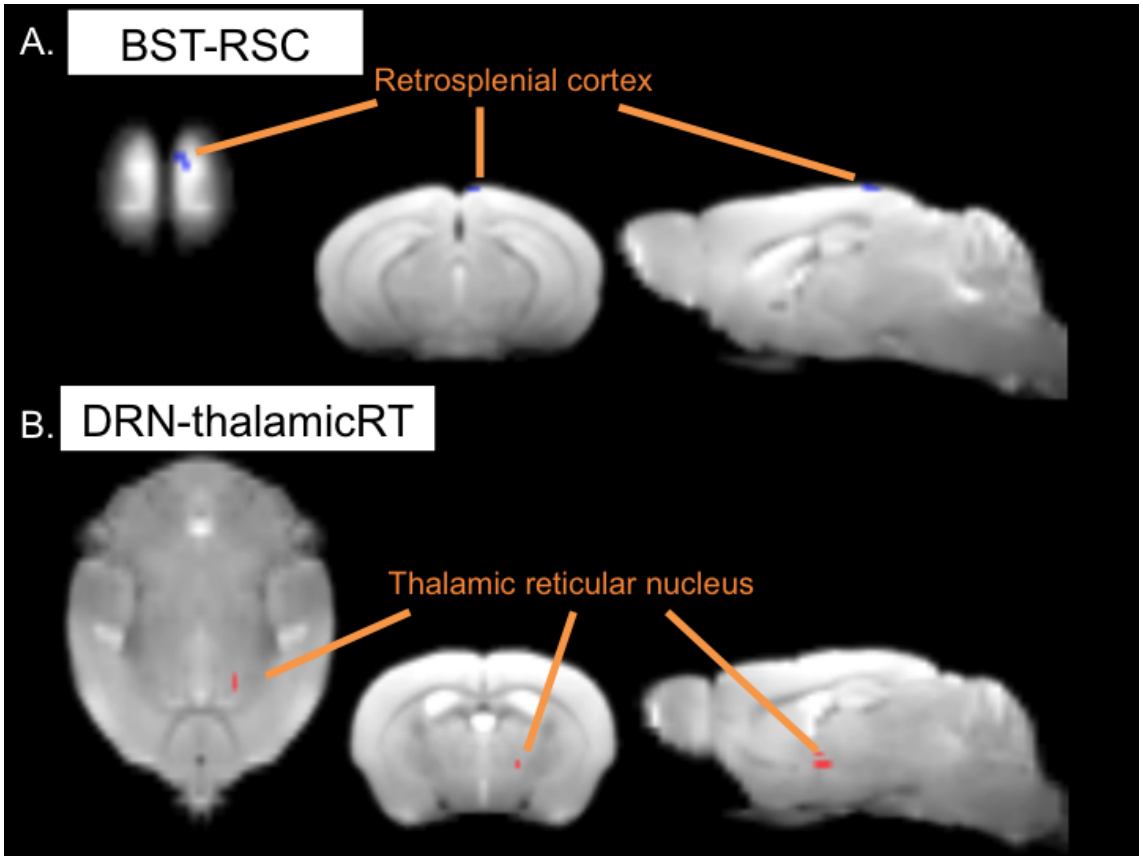

Figure 3.6: We confirmed that higher statistical threshold resulted in statistically significance of FCs between BST-RSC and DRN-thalamic RT A. Seed-based analysis with the seed region, BST, revealed statistically significant contrast in the retrosplenial cortex (RSC) with cluster forming (uncorrected $P < 0.001$) and further corrected about the number of voxels ($P_{FDRcorrected} < 0.05$). B. The seed region, DRN, also revealed a statistical difference in the thalamic reticular nucleus(RT; $P_{FDRcorrected} < 0.05$).

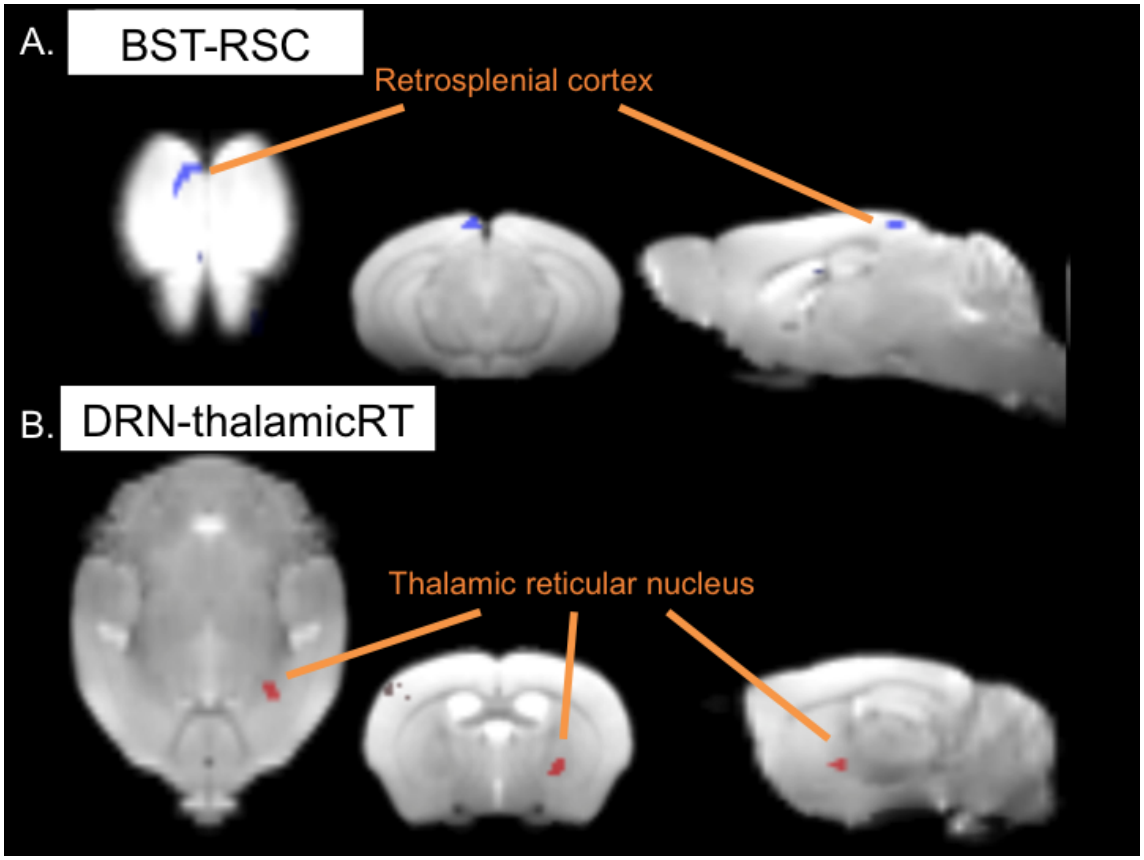

Figure 3.7: We further confirmed change of FCs between BST and RSC, and DRN and thalamic RT with different frequency range (0.01-0.1 Hz). A. Seed-based analysis with the seed region, BST, revealed statistically significant contrast in the RSC with cluster forming (uncorrected $P < 0.01$) and further corrected about the number of voxels ($P_{FDRcorrected} < 0.05$). B. The seed region, DRN, also revealed a statistical difference in the thalamic reticular nucleus(RT; $P_{FDRcorrected} < 0.05$).

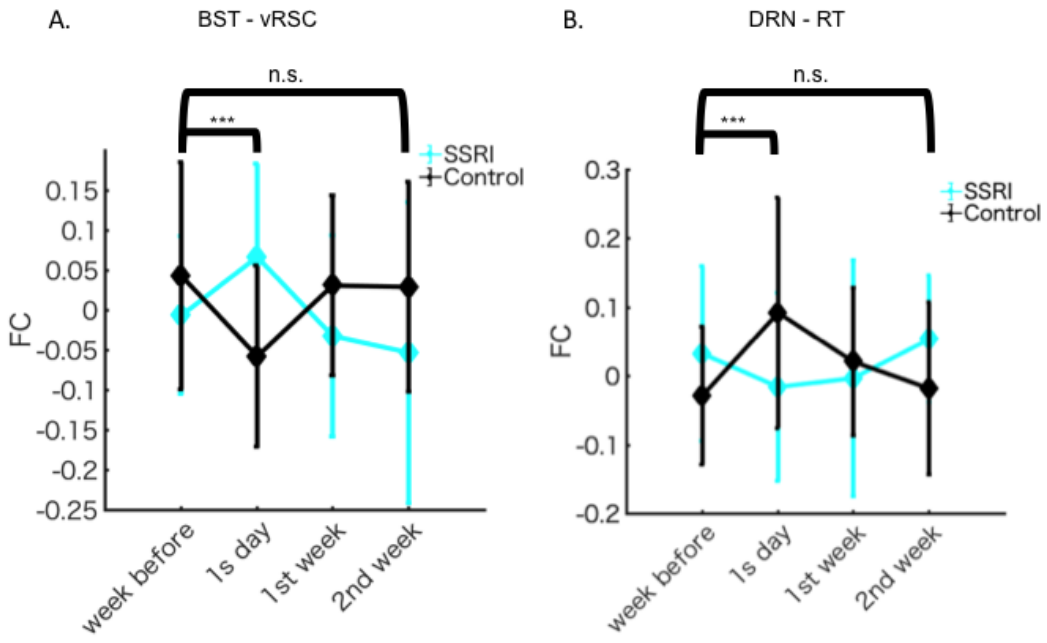

Figure 3.8: A. Change of FC between the BST and the vRSC across sessions. There was a statistically significant difference in the change from one week before to the 1^{st} day($P < 0.001$, unpaired t-test). However, we could not find statistically significant difference between one week before and 2^{nd} week sessions ($P = 0.54$, unparied t-test). B. Change of FC between the DRN and the RT across sessions. There was a statistically significant difference in the change from one week before to the 1^{st} day($P < 0.005$, unpaired t-test). However, we could not find a statistically significant difference between one week before and 2^{nd} week sessions ($P = 0.81$, unpaired t-test). *** means $P < 0.005$ with unpaired t-test.

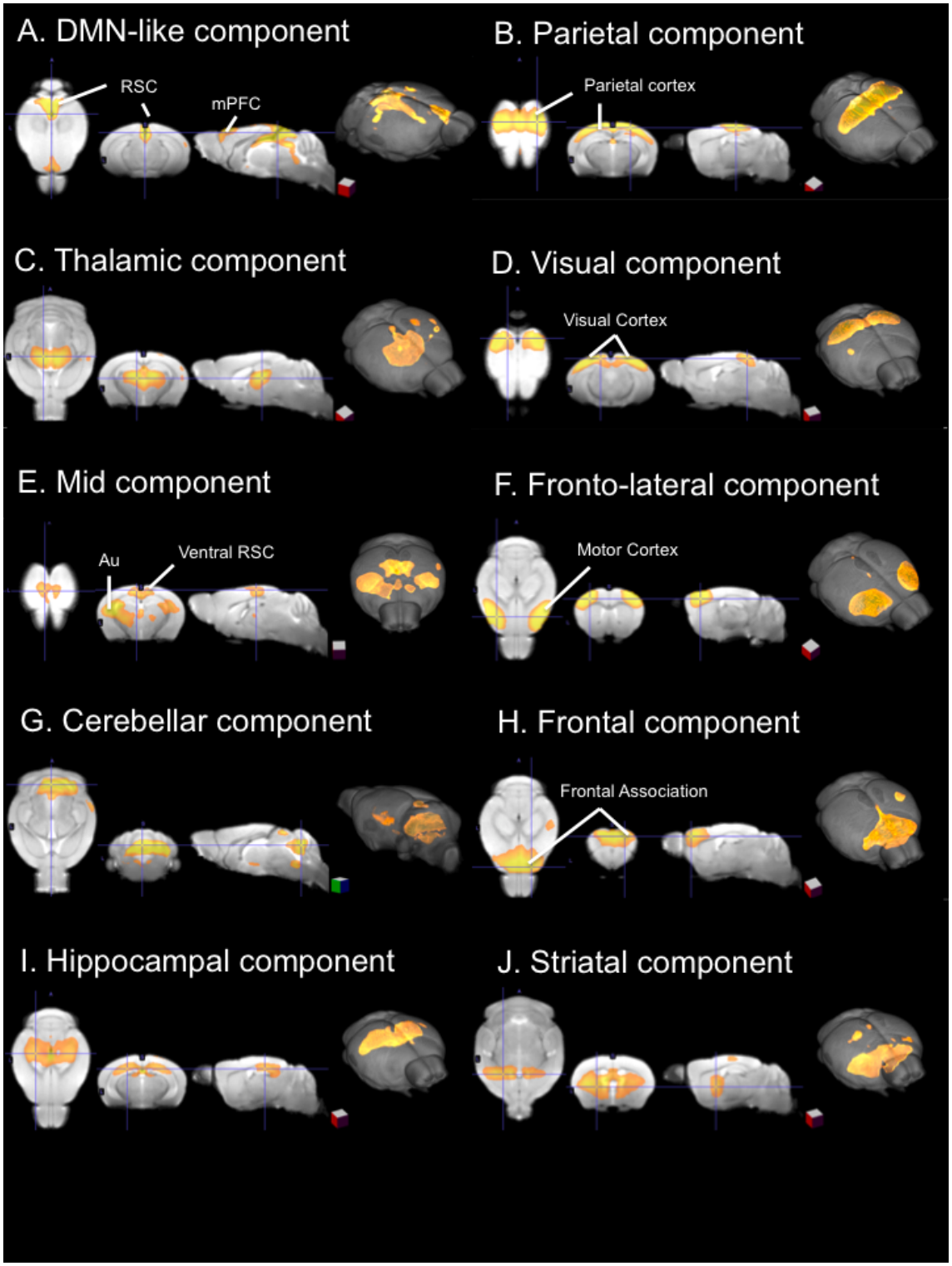

Figure 3.9: Extracted functional network components. A. DMN-like component, B. Mid-cortical component, C. Thalamic component, D. Visual component, E. Mid component, F. Fronto-lateral component, G. Cerebellar component, H. Frontal component, I. Hippocampal component, J. Striatal component

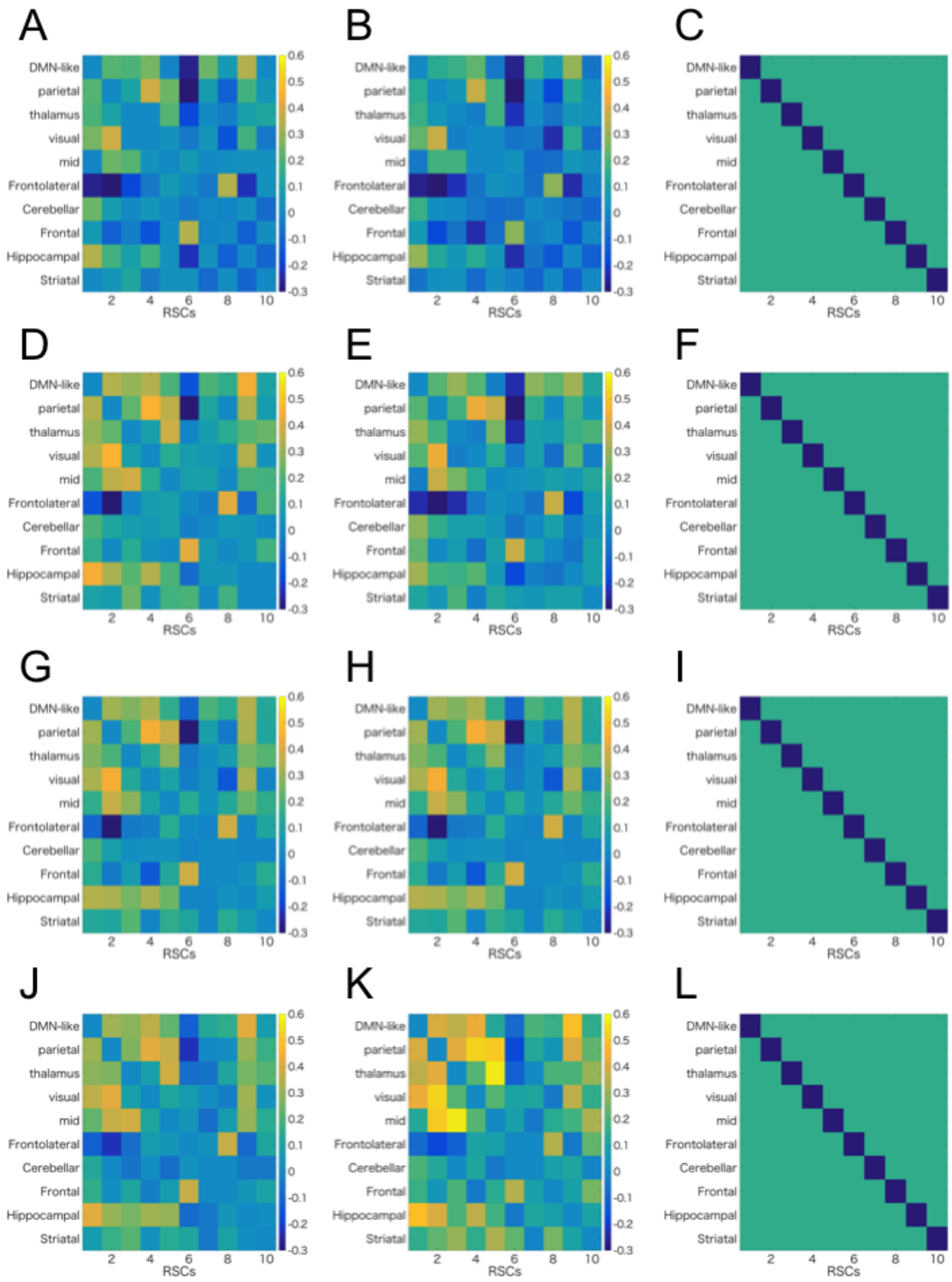

Figure 3.10: We extracted time-series from 10 resting-state networks, and calculated Pearsons' correlation among them. (A,D,G,J) We averaged correlation matrices in the SSRI-treated group from one week before, 1^{st} day, 1^{st} week, and 2^{nd} week sessions, respectively. (B,E,H,K) We also averaged correlation matrices in the control group from one week before, 1^{st} day, 1^{st} week, and 2^{nd} week sessions, respectively. (C,F,I,L) We tested whether there is a statistically significant difference (P_{FDR}<0.05). Blue and light green pixels indicate no value and no statistically significant difference, respectively. No FCs in any sessions exhibited significant differences.

3.6 Energy landscape analysis revealed the effect of SSRIs on transient brain dynamics

Conventional FC analysis could not reveal distinct changes in brain-wide functional networks. We then considered the possibility that averaging brain-wide dynamics with FCs over the ten-minute scans might neglect reconfiguration of brain dynamics on a shorter time scale. To check this possibility, we leveraged the energy landscape analysis (ELA), which approximates brain dynamics as transitions among attractors of different energy levels. ELA is a promising analytical method to detect changes in whole-brain dynamics by fitting time-series data to a simple stochastic model (see details in the Supplementary section.A.4).

3.6.1 Representative brain state patterns by energy landscape analysis

We first binarized time courses of the ten sICA components and obtained eight energy local minima by fitting all data from all sessions to a Boltzmann machine model (Figure.3.11 A-B). The eight states were symmetrical brain patterns, for which active and inactive states are complementary. We found two dominant states, 1^{st} and 2^{nd} states and 7^{th} and 8^{th} states (Figure. 3.11A.). All active and inactive components were composed of the dominant states. The 3^{rd} and 6^{th} states are the intermediate states between the dominant states. 3^{rd} state comprises the active posterior brain components including the DMN-like component, the parietal component, the visual component, the cerebellar component, and the hippocampal component, while the 6^{th} state contains active anterior components, the thalamic component, the mid cortical component, the frontal lateral component, the frontal component, and the striatal compoment. The 4^{th} and 5^{th} states are minor states.

Next, we defined the local minima as the representative states, and categorized neighboring states of each local minimum as the attractor basin. Brain activity patterns in each session were transformed to a series of attractor states. We then compared the percentage of time in each attractor state from one week before to 2^{nd} week sessions in SSRI and control groups (Figure.3.11C-F). The time spent in states 3 and 6 in the SSRI group was significantly smaller in the 2^{nd} week session ($P < 0.005$;Figure.3.11F.).

This result implies that the energy landscape is reshaped by chronic SSRI treatment. In order to confirm whether the intermediate states are prominently diminished in SSRI groups, we separately applied ELA to SSRI and control imaging data from one week before to 2^{nd} week sessions, and defined the attractor states in the same manner as with all imaging data (Figure.3.12 and 3.13). ELA with SSRI data yielded six representative states, excluding those corresponding to the intermediate states identified from all data (Fig 3.12 A). On the other hand, ELA with control data resulted in the corresponding eight states (Figure. 3.13 A).

Additionally, we examined whether intermediate states from the control group could detect energy landscape differences in the SSRI group. Our analysis showed that state duration in the intermediate states are statistically smaller in the SSRI group compared to the control group only in the 2^{nd} week session (Figure. 3.13.C-F).

These analyses indicate that long-term serotonergic medication, but not acute medication reshapes brain activity patterns.

We further investigated how durations in the 3rd and 6th states changed across imaging sessions in SSRI or control groups (Figure. 3.14A-C.). We refer to the 3^{rd} and 6^{th} states as intermediate states. The results revealed that change of state duration in intermediate states in the 2^{nd} week session increased significantly in the control group only in the 2^{nd} week session ($P < 0.005$, unpaired t-test; Figure. 3.14). Since there is no increase of state duration in the SSRI group, the results suggest that long-term serotonergic antidepressant treatment suppresses the increase in state duration.

3.6.2 Change of modular structure underlying brain activity patterns in the intermediate states

We further analyzed what brain dynamics corresponding to the attractor states 3^{rd} and 6^{th}, which we call "intermediate states," which were affected by chronic SSRI application (Figure.3.15). First, original BOLD signals during the intermediate states in the ELA were extracted and Pearsons' correlations among the ten sICA components were calculated(Figure. 3.16.A-D). We examined alteration of modular structure by calculating modular integration and segregation with averaged within-module FCs and modular segregation with averaged across-module FCs. There was a significant increasing trend in modular integration (MANOVA, session, $P = 0.104$, group: $P < 0.005$) and a decreasing trend in modular segregation in the control group (MANOVA, session, $P = 0.162$, group: $P < 0.001$). However, we could not identify such trends in the SSRI group.

In summary, our observations imply that SSRI administration suppresses reshaping of modular structures.

3.6.3 Modular integration and segregation alters along sessions

Next, we examined the possibility that long-term serotonergic antidepressants impact the association between brain state dynamics and modular structures. Association between brain state dynamics and modular structures is initially examined between sessions. However, we could not find any significant correlation between them (data not shown). We assumed that the association is not directly reflected. Therefore, linkage between alteration of brain state dynamics and modular structures across sessions was further studied. The observations resulted in statistically significant correlation

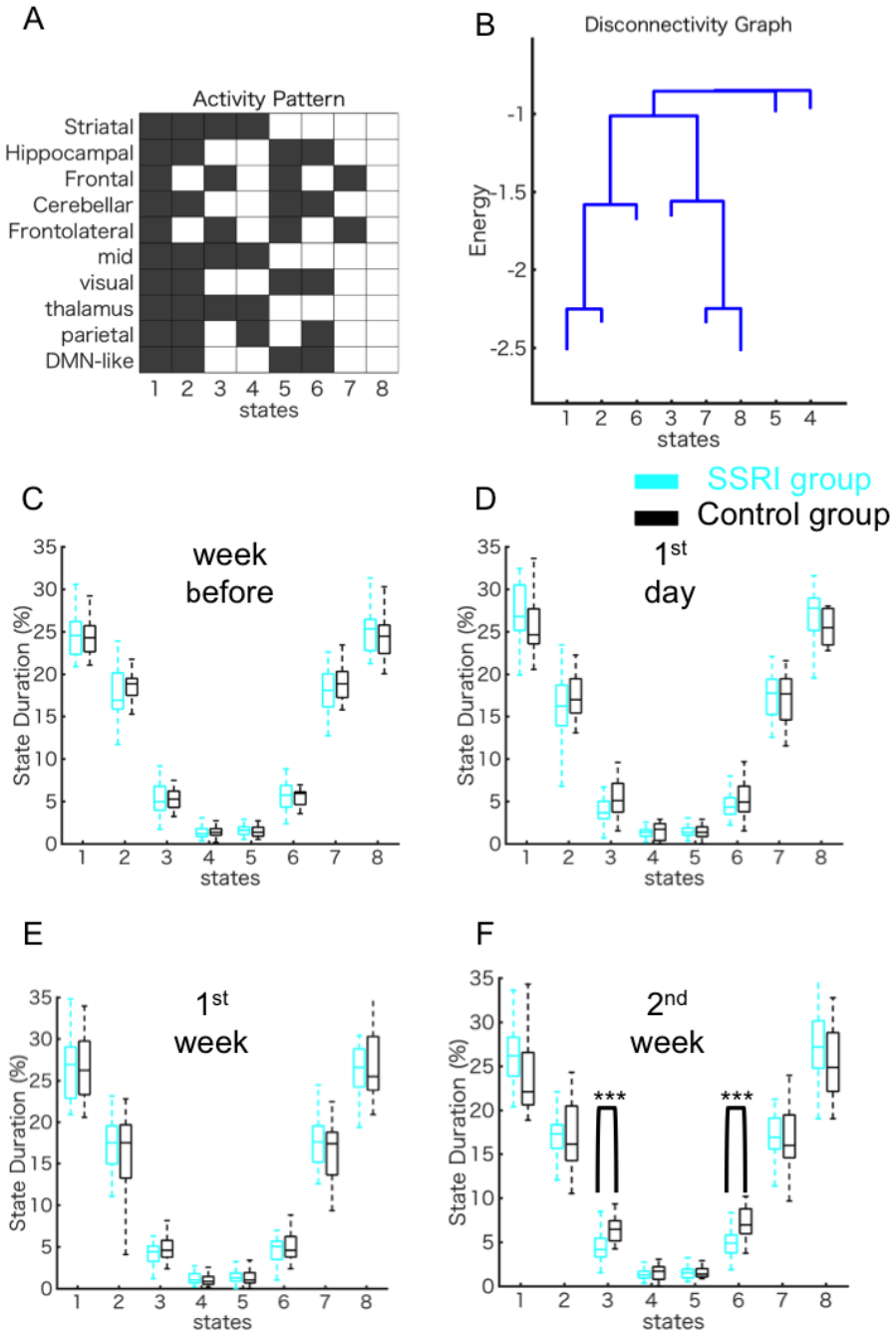

Figure 3.11: (A) Local minima and their activity patterns from all data. We applied ELA to all imaging data including one week before to 2^{nd} week sessions from both groups. We identified 8 activity patterns as local minima from the data. Given each local minimum, we also defined corresponding states in which activity are attracted to each local minimum. (B) Disconnectivity graph. We visualized disconnectivity for local minima. (C-F) Percent stay in each session. Using 8 states, we compared dominance of each state in the SSRI-treated group and control group from one week before to 2^{nd} week sessions, respectively. We found that states 3 and 6 were statistically smaller in the SSRI group (P_{FDR}<0.005).

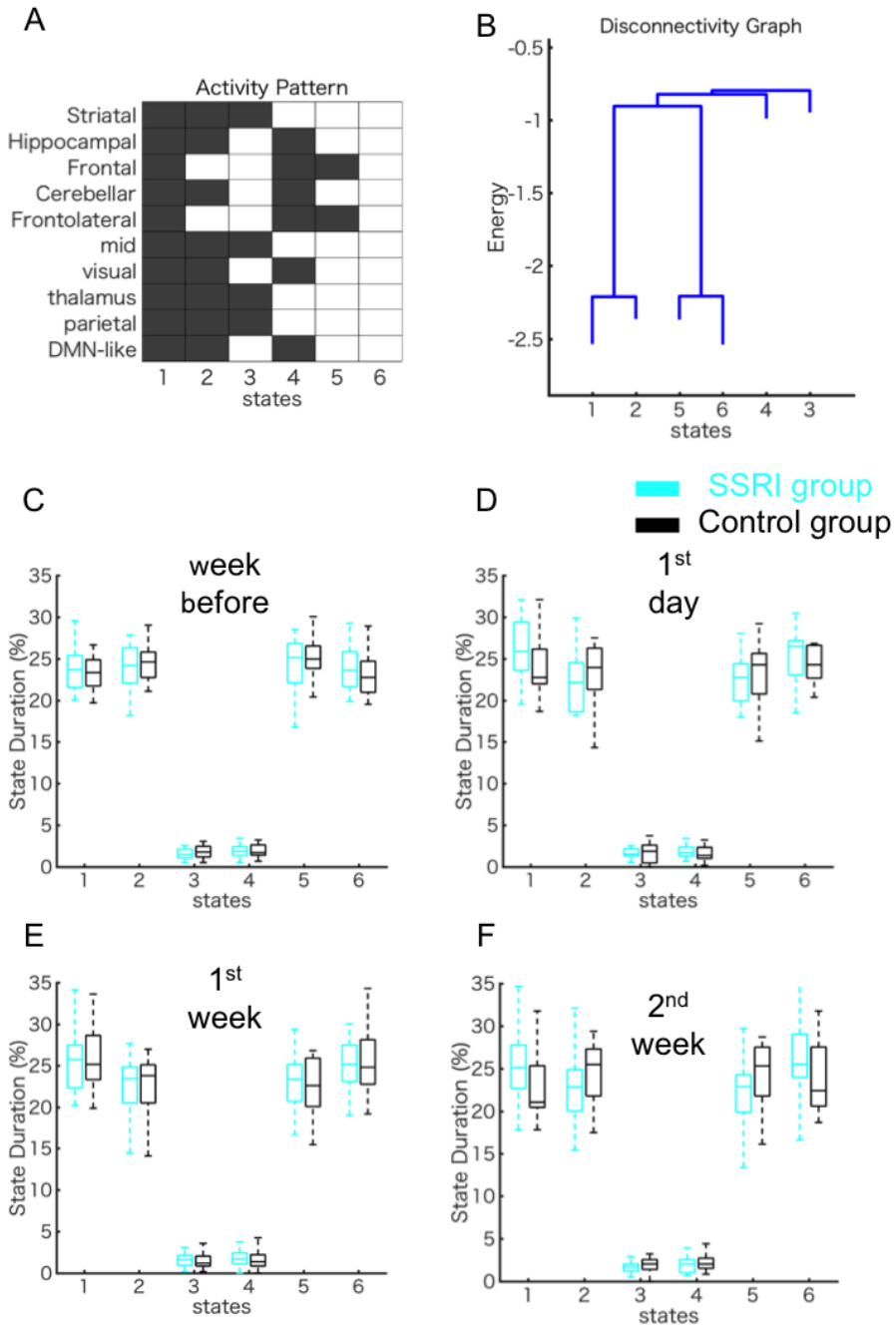

Figure 3.12: Local minima and their activity patterns only from SSRI data. We applied ELA to imaging data, including one week before to 2^{nd} week session from SSRI group. We identified 6 activity patterns that appear in all experimental and control data. Given each local minimum, we also defined corresponding states in which activity is attracted to each local minimum. Disconnectivity graph. We visualized disconnectivity graphically for local minima. C-F. Using given 6^{th} states, we compared dominance of each state in the SSRI and control groups from week before to 2^{nd} week sessions, respectively. No patterns exhibited significant differences.

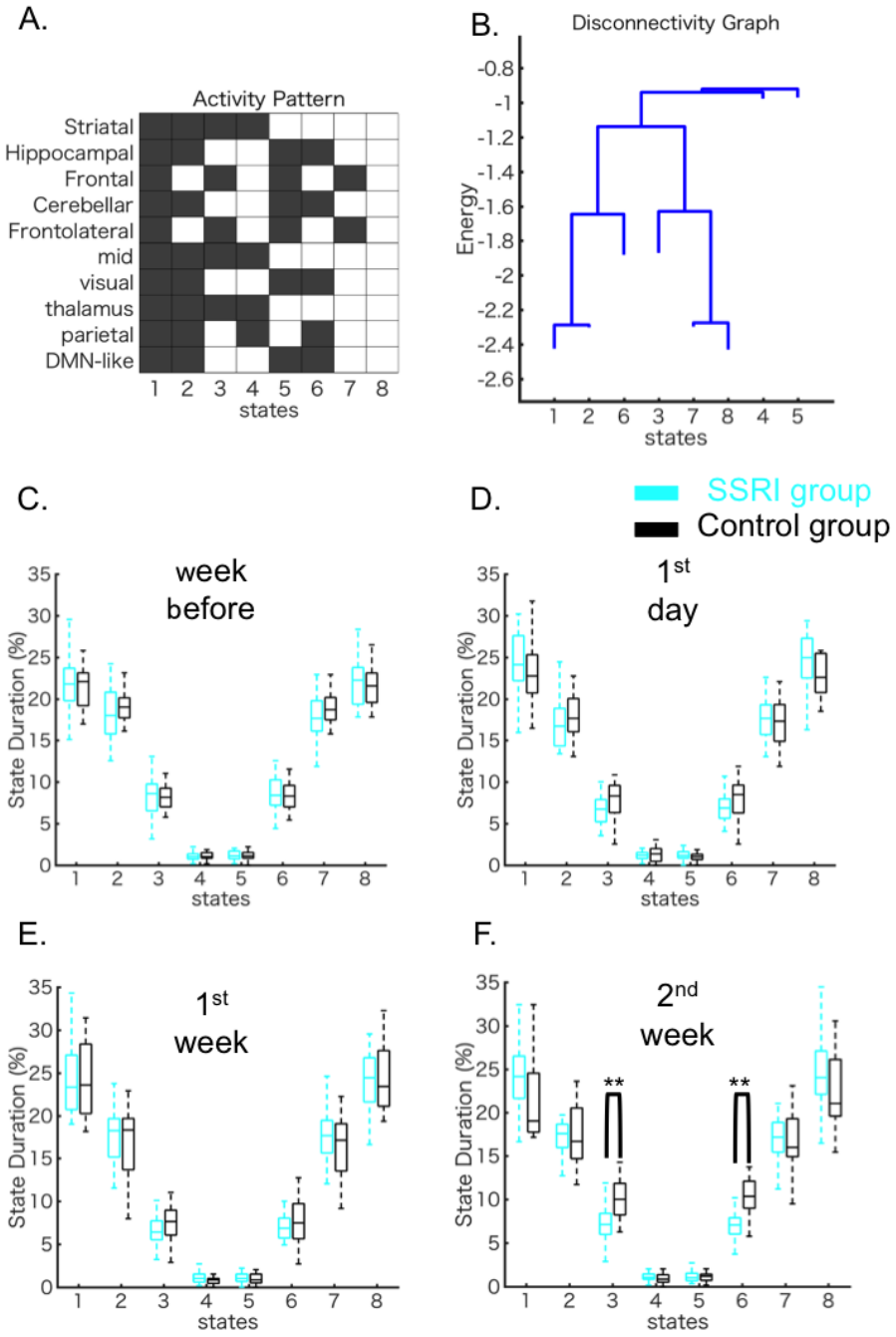

Figure 3.13: Local minima and their activity patterns only from control data. We applied ELA to imaging data including one week before to 2^{nd} week sessions from control. We found all 8 activity patterns as local minima correspond to the pattern from all imaging data. Given each local minimum, we defined corresponding states in the same manner of the all data case. Disconnectivity graph. We visualized disconnectivity graph for local minima. C-F. Using 8 states, we compared dominance of each state in the SSRI and control groups from one week before to 2^{nd} week sessions, respectively. As with all data, we found that states 3^{rd} and 6^{th} were statistically smaller in the SSRI group ($P_{FDR} < 0.005$).

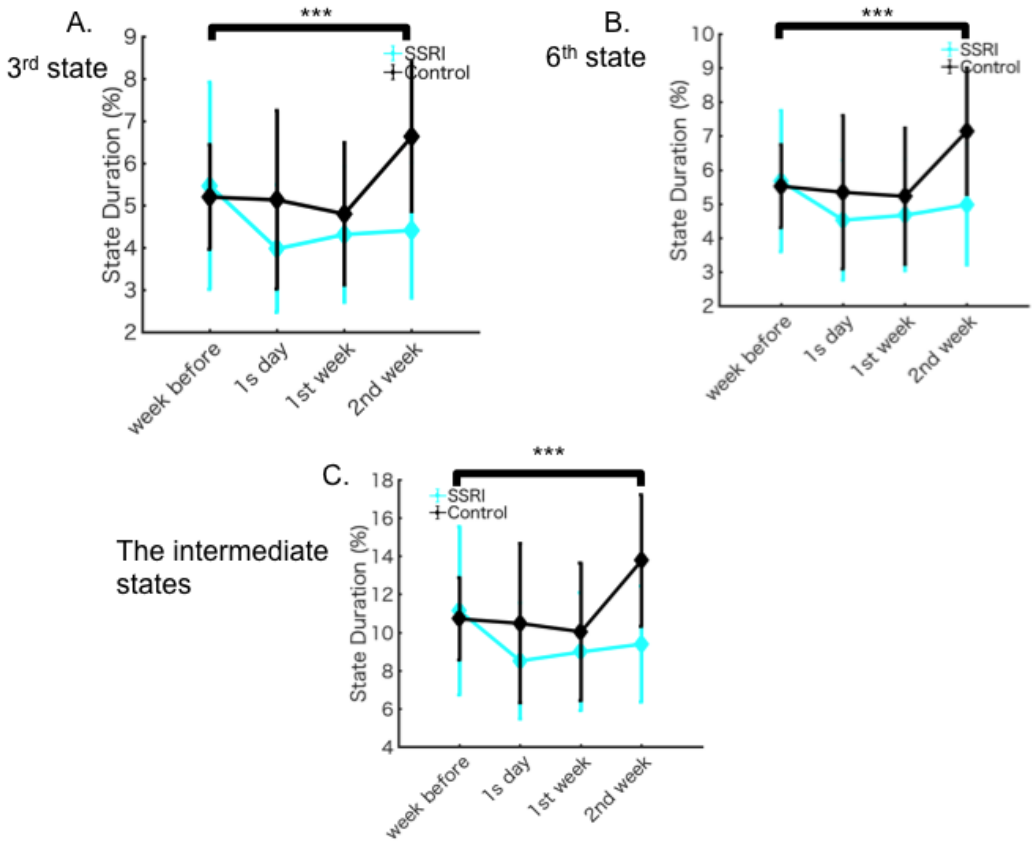

Figure 3.14: A-B. Changes of state duration of 3^{rd} and 6^{th} states across sessions, respectively. There were significant differences between one week before and 2^{nd} week sessions in the both 3^{rd} ($P < 0.005$, unpaired t-test) and 6^{th} states ($P < 0.005$, unpaired t-test), respectively. C. Changes of state duration of concatenated intermediate states across sessions. There were also significant differences between one week before and 2^{nd} week sessions in the intermediate state ($P < 0.005$, unpaired t-test).

between alteration of modular integration and state duration across sessions in the SSRI group (1^{st} day vs. week before: $r = 0.51$, $P < 0.01$; 1^{st} week vs. week before: $r = 0.61$, $P < 0.001$, $2^{nd} week vs. week before: r = 0.45, P_{uncorrected} < 0.05$) but not consistent in control group (1^{st} day vs. week before: $r = 0.41$, $P = 0.08$; 1^{st} week vs. week before: $r = 0.58$, $P < 0.005$, 2^{nd} week vs. week before:$r = 0.31, P = 0.21$;Figure.3.17.). However, we could not identify such an association in modular segregation (Figure.3.18.).

These results suggest that serotonergic antidepressant treatment indirectly shapes the relationship between modular integration of functional networks and brain state dynamics.

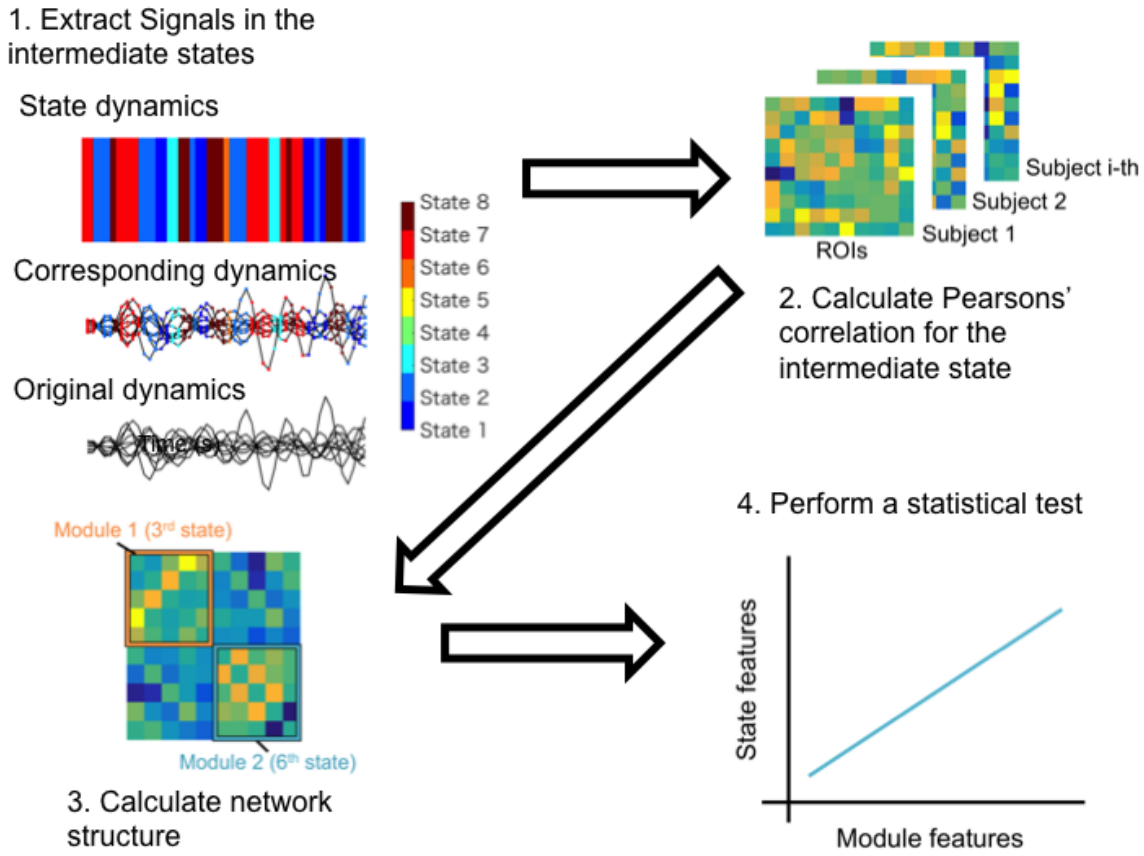

Figure 3.15: We further confirmed whether brain state dynamics are associated with underlying functional module structure in intermediate states. First, we segregated the original time series from state dynamics defined by corresponding states into time series in states. Next, we formed functional network matrices for states by calculating Pearsons' correlation among the components. Network analysis was further perfomed by calculating modular integration and segregation. We finally checked association with module features, including average within-module functional connectivity and across-module functional connectivity.

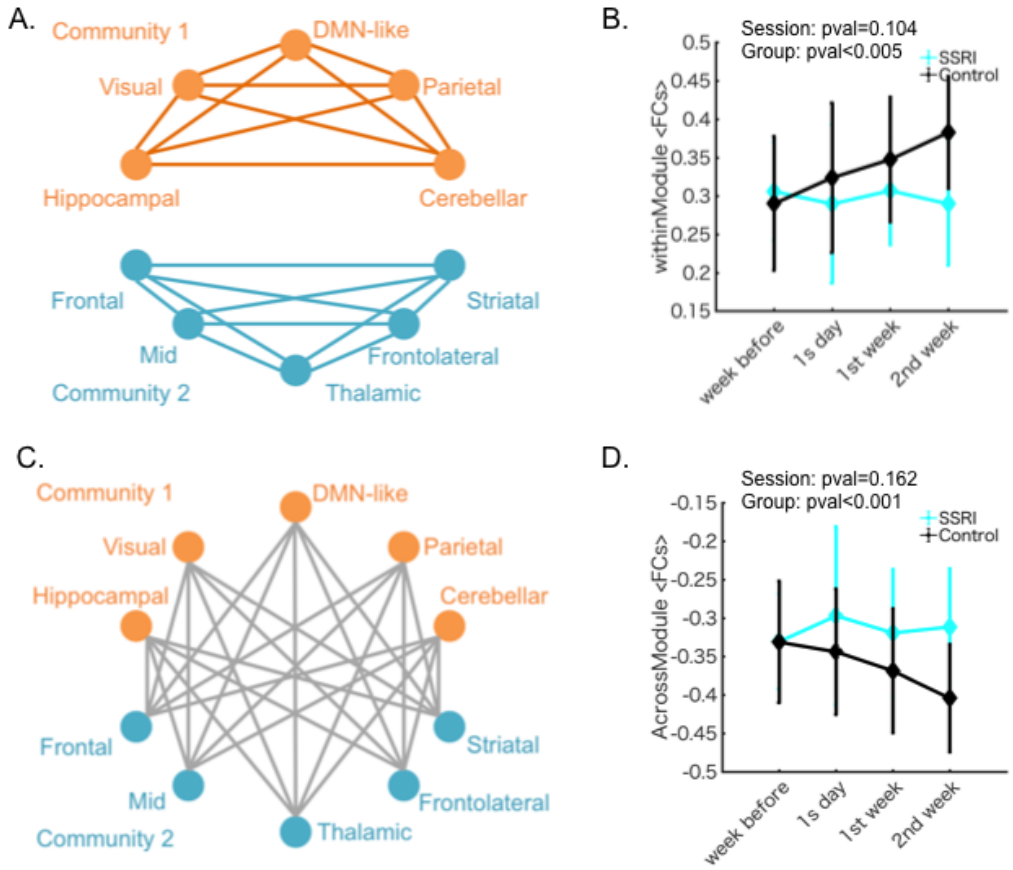

Figure 3.16: A. A representative figure of within-module FCs summing total FCs in two modules in the intermediate states. We calculated average within-module FCs based on module partitioning. B. Accordingly, we summarized change of within-module FCs between the SSRI and control groups along sessions MANOVA, session: $P = 0.104$, Group difference: $P < 0.005$). C. A representative figure of across-module FCs summing FCs across two modules, but not within modules in intermediate states. We measured average across-module FCs. D. we also compared changes of across-module FCs between SSRI and control groups.

3.7 Intermediate states in ELA are correlated with anxiety-like behaviors.

Finally we tested whether brain activity patterns identified by ELA and affected by chronic SSRI dosage were correlated with behavioral performances affected by chronic SSRI, namely, the average speed in the open-field test and percent immobility in the open-field and elevated plus maze tests.

We performed correlation analyses of individual subject data and found that the duration of intermediate states was significantly correlated with percent immobility in the EPM test in the SSRI group, but not in the control group (SSRI: $r = 0.478, P < 0.01$, Control: $r = 0.250, P = 0.302$; Figure. 3.19A.).

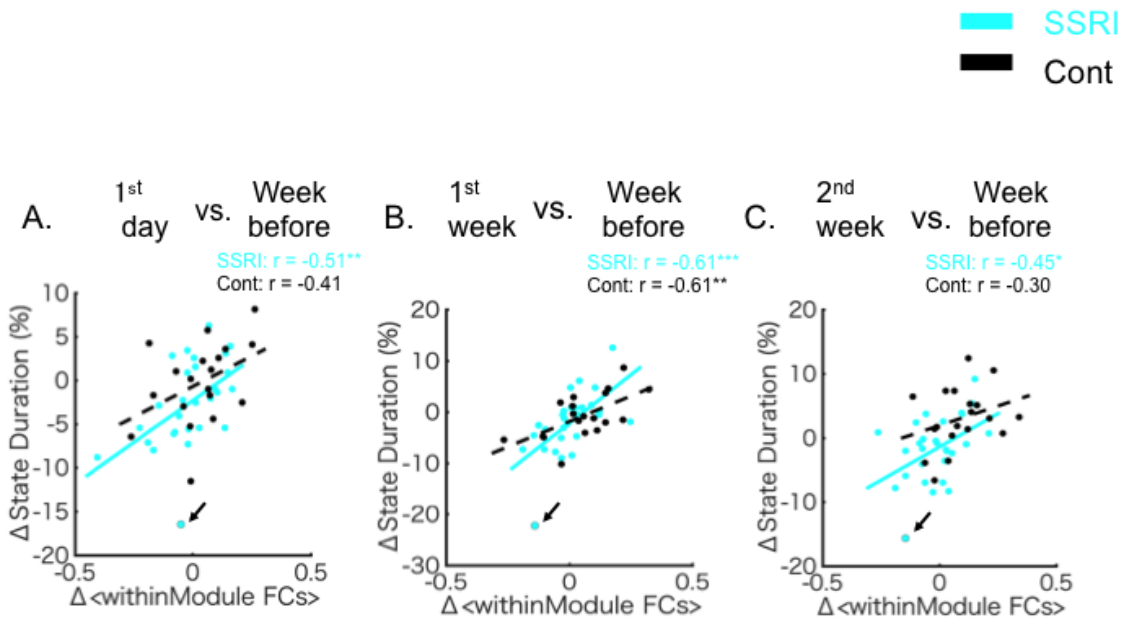

Figure 3.17: A. Correlation between change of average within-module FCs and change of appearance of the intermediate states in one week before versus 1^{st} day sessions (SSRI: r=-0.51, Control: r=-0.41). B. The correlation in one week before versus 1^{st} week sessions (SSRI: r=-0.61, Control: r=-0.61). C. Correlation between them in one week before versus 2^{nd} week sessions (SSRI: r=-0.45, Control: r=-0.30). Arrowed dots are outliers but we found no significant correlation with and without outliers.

Furthermore, we examined whether durations in states were correlated with immobility. In the SSRI group, the time in the 3^{rd} state was significantly correlated with immobility in the EPM test (SSRI: $r = 0.523, P < 0.005$, Control: $r = 0.183, P = 0.3454$; Figure. 3.19B.)

Taken together, since intermediate states in the SSRI group, but not the control group were correlated with behavioral performance, our results indicate that the degree of reduction of the intermediate brain state, especially state 3, in the chronic SSRI group was correlated with reduced immobility time in a novel anxious environment.

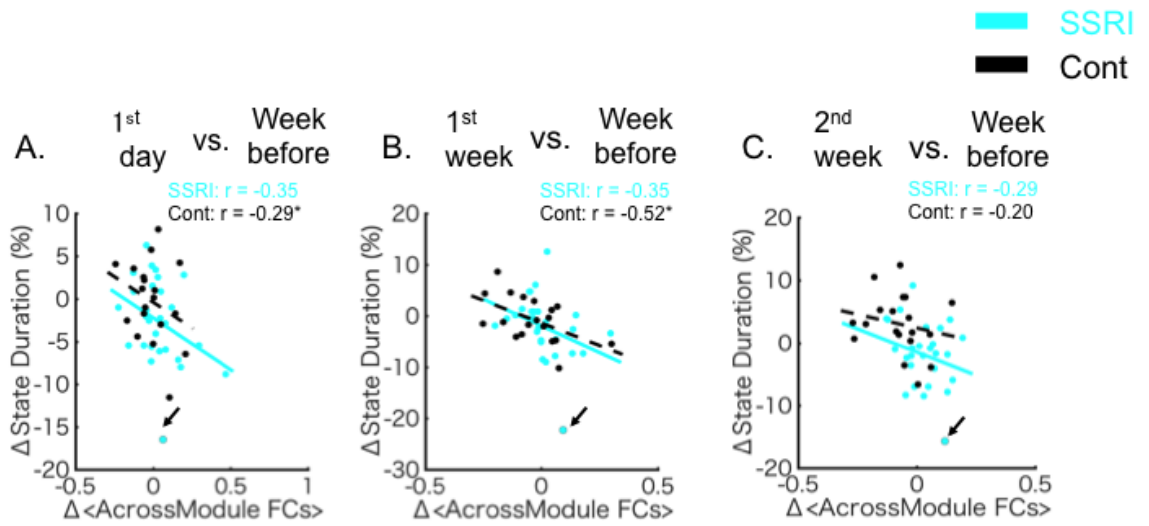

Figure 3.18: A. Correlation between change of average across-module FCs and change of appearance of intermediate states in one week before versus 1^{st} day sessions (SSRI: $r = -0.35$, Control: $r = -0.29$). B. The correlation between one week before and 1^{st} week sessions (SSRI: $r = -0.35$, Control: $r = -0.52$). C. Correlation between them in one week before versus 2^{nd} week sessions (SSRI: $r = -0.29$, Control: $r = -0.20$).

3.8 Discussion

In the present study, we studied the influence of chronic serotonergic antidepressants on behaviors, functional connectivity and brain-wide dynamics with energy landscape analysis. Our results showed that spontaneous locomotion, but not anxiety-like behaviors was altered by long-term serotonergic antidepressant administration (Figure.3.2.). Our seed-based FC analysis revealed reshaping of the cortico-limbic circuit across SSRI administrations. We also found that long-term serotonergic antidepressants suppressed changes of state duration in intermediate states(Figure.3.14.A-C.), also reflects active exploration in a novel anxious environment(Figure.3.19.A-B.). Furthermore, alteration of modular integration underlying brain activity patterns is associated with alternation of brain-wide dynamics in the SSRI group, but not the control group(Figure.3.17).

OF and EPM tests are common methods to observe anxiety-like behaviors and spontaneous locomotion[108]. Our observation showed average speed and activity time

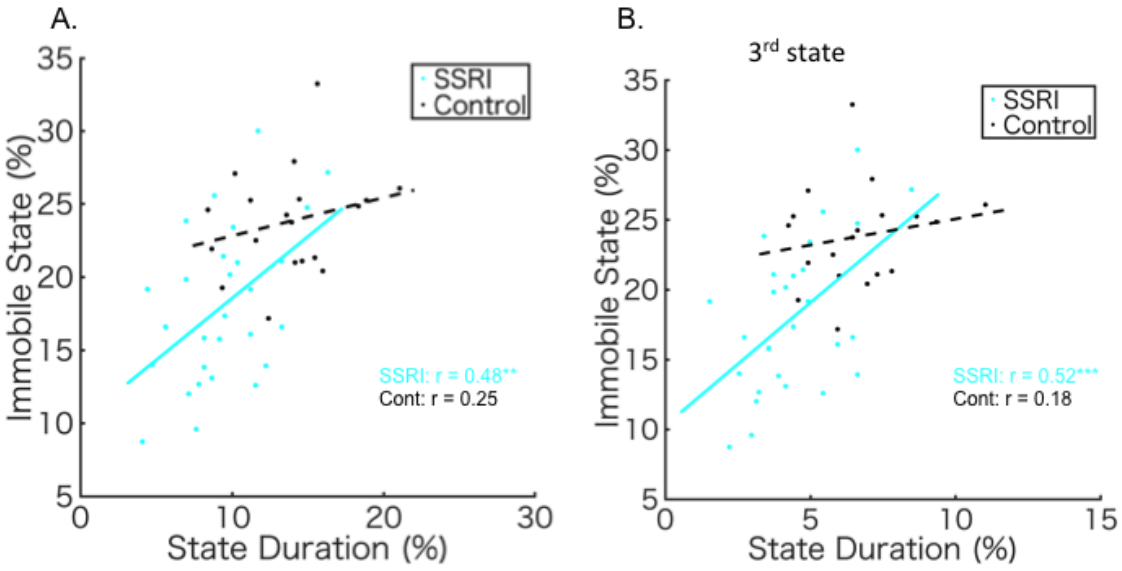

Figure 3.19: A. We quantified Pearsons' correlation between state duration in the intermediate state and immobile state in EPM in SSRI groups. We found significant correlation only in the SSRI group (SSRI: r=0.48, $P < 0.005$; control: r=0.25, $P = 0.302$). B. There was significant correlation between state duration in the 3^{rd} state and immobility (SSRI: $r = 0.523, P < 0.005$, Control: $r = 0.183, P = 0.3454$).

in the OF test were increased, but only active time in the EPM test was enhanced. Furthermore, individual behavioral performance between two tests were uncorrelated. This behavioral result implies that long-term serotonergic antidepressants did not influence general motor output, but possibly a motivational factor. The serotonin system has been suggested to work together with the reward system, including the striatum, nucleus accumbens (NAc), and VTA [114, 123]. Promoted spontaneous locomotion may be attributed to synaptic plasticity in the reward system[21] or neurogenesis[84] by chronic serotonergic antidepressants. Consistently, a previous study revealed that long-term DRN serotonergic stimulation enhances average moving time in the OP test, but did not affect speed and motor control in the motor rod test [38].

Meanwhile, we could not observe any mean difference over anxiety-like behaviors. However, we found higher individual differences of active exploration in the EPM test. SSRIs can require several weeks of intakes to work, and transient and intermediate time courses of intake sometimes negatively impact symptoms of MD patients. Hence, 19-day intakes may retain negative effects. Individual molecular profiles in those regions

may influence expression of anxiety-like behaviors.

Exploiting conventional seed-based FC analysis, we found that FCs between BST and vRSC varied across sessions. This finding concurs with the concept that BST is associated with acute effects of serotonergic antidepressant treatment[129]. Furthermore, the ventral RSC is a part of the DMN, which is one of the key regions for mood abnormalities in MD patients[77, 78]. A human functional imaging study[74] revealed that the BST is functionally linked to the posterior cingulate cortex (PCC), a homolog of the RSC in the mouse brain[122]. Modulation of depressive symptoms by serotonergic antidepressants can occur due to control of the neural circuit between the BST and DMN.

With energy landscape analysis, we studied the influence of serotonergic antidepressants on brain dynamics and behavioral performance combining conventional FC analysis and energy landscape analysis. Although conventional FC analysis did not exhibit any statistical difference, data-driven analysis with ELA revealed two intermediate brain states that did not appear in the SSRI group. This is because state duration of the intermediate states increased in the control group during imaging sessions, but the duration remains no different in the SSRI group. Furthermore, activity patterns of intermediate states were identical to two partitioned modules. Module integrity did not directly reflect brain state dynamics, such as state duration or state transitions. However, we found a change of module integrity was associated with a change of brain dynamics during sessions in the SSRI group, but not in the control group. Finally, brain state dynamics of intermediate states were linked to an active exploration state in a novel anxious EPM test. These findings suggest that serotonergic antidepressants suppress large-scale brain state dynamics, which underlie immobility in the EPM test by affecting functional network structure of the state.

Our study supports the notion that SSRIs influence large-scale brain state dynamics in the mouse brain. Previous studies demonstrated that SSRIs influence regional synchronized activity and brain-wide functional network[105, 106, 131, 132, 164]. However, none of them provided evidence about brain dynamics. Our study further provided linkage between temporal variation in brain-wide dynamics and behavioral performance during rest. Although previous studies did not observe behavioral or state measures, we found long-term SSRI administration is linked to brain state dynamics.

One of our results about functional module structures underlying brain activity patterns via the energy landscape is consistent with results from a previous human imaging study [4]. Furthermore, it is consistent with our study, the human imaging study reported within and between module FCs' scores poorly predicted the appearance of brain states. Although brain state dynamics remains linked to its network structure, the network structure does not maintain a simple association between them. However, in the present study, fluctuation of within-module FC scores during imaging sessions was correlated with fluctuation in appearance of the intermediate states only in the SSRI group. Serotonergic antidepressants are able to influence the relationship between module network integrity and state dynamics.

Additionally, appearance of an intermediate state (3rd state) was positively correlated with immobility in the EPM test in the SSRI group. This showed that immobility in the EPM test does not reflect a general motor output, but rather vigor for exploration. Hence, at least the 3rd state might be associated with active exploration in the EPM test. In human functional imaging, there are some studies analyzing temporal shifting brain dynamics about major depressive disorder (MDD)[54, 103]. MDD subjects showed increased time in varying functional synchronous activity between the medial prefrontal cortex and the insular cortex, which is also associated with their rumination score [103]. Rumination is a distressing spontaneous thought as a typical symptom of MDD subjects[35, 67]. Resting-state functional dynamics have been recently featured to study spontaneous thoughts since resting-state dynamics are deemed to reflect imagination or internal thoughts without external stimuli. Abnormal brain dynamics in mental disorders are thought to reflect internal mental processes of subjects [35]. The core of such spontaneous thought is suggested to be associated with the posterior parietal cortex (a homolog of retrosplenial cortex), hippocampus, parietal cortex, and visual cortices. Although we could not discern a clear association between modular partitioning and certain functioning, module partitioning in the $3^r d$ state retains similar components. Since SSRIs are a clinical drug intervention to alleviate such symptoms, this modular partitioning may reflect internal processes in the subjects and might be useful to observe abnormalities in animal models of depression.

It is also worth mentioning state appearance of intermediate states in the control group. Our observation showed enhanced state appearance along imaging sessions. In spite of acclimation, long-term repetition of awake imaging with mice might cause excessive stress, contributing to the enhancement in the control group, which showed lower active time in a novel environment. In contrast, the SSRI group displayed no alteration during sessions. One study previously found that intake of imipramine, a serotonin and norepinephrine antidepressant, reversed the signature of a depression-like phenotype, and evoked resilience-related gene expression [5]. One of the efficacious serotonergic antidepressants can provoke neural circuits of stress-resilience. This notion is consonant with another theory that serotonergic antidepressants normalize abnormal activity in MDD patients[131, 132]. Furthermore, one study advanced the theory that serototonergic antidepressants make brain responses robust against interferent stimuli[165]. In this regard, serotonergic antidepressants might normalize brain dynamics confounded by stress. However, from another perspective, serotonergic antidepressants stabilize brain dynamics against stress.

It is noteworthy to discuss key limitations of the experiments. First, rs-fMRI for rodents requires body fixation, and causes loud imaging noise. Although we acclimatized the mice to reduce imaging stress, it might have caused interaction between cumulative noise and chronic SSRI administration. Second, there are significant differences between the mouse brain and the human brain. It is well known that these brains exhibit prominent differences in cortical architecture. We found consistent responses in affective networks after SSRI administration, but other cortical regions may respond to SSRI and stress. It would be worth validating the functional differences in brains of MDD patients and animal models of depression, as a translational study. Third, SSRI

administration is a systematic way to control brain dynamics. Therefore, it is challenging to infer causal relationships between brain responses and serotonin sub-systems such as DRN and MRN. It is interesting to utilize chemogenetics or optogenetics to target serotonergic influences to specific areas of the brain. For example, a recent report employed chemogenetics with rsfMRI and positron emission tomography (PET). Correia et al. reported that short-term and long-term serotonin transmission exhibit opposite influences on spontaneous locomotion [38]. Transient serotonin transmission under different synaptic serotonin levels would be helpful to reconcile dichotomous serotonergic effects on spontaneous locomotion.

Further studies are required to understand serotonergic control of functional architecture and brain-wide dynamics under transient and repetitive administration of serotonergic medications. Nonetheless, this study offers new insights regarding effects of serotonergic antidepressants on brain-wide dynamics.

Chapter 4

Brain-wide modulation of serotonin neurons with optogenetics

4.1 Aims

In this study, we aim to investigate serotonin control of brain-wide dynamics by stimulating the major serotonin subsystem, the dorsal raphe nucleus (DRN), with optogenetic fMRI. Optogenetic fMRI (ofMRI) is a recent advancement employing a combination of optogenetics and fMRI, which allows us to evaluate brain-wide causal control by a specific neuronal system [11, 115]. As the stimulation target, we chose the DRN, which sends numerous serotonergic neurons into depression-related brain regions such as the mPFC, striatum, and VTA. The project was done as a part of a collaborative study with Dr. Abe, Dr. Takata, and Dr. Tanaka (for optogentic fMRI setups and analyses), and with Dr. Miyazaki for a delayed reward task setup. I performed all imaging and behavioral experiments and analyses.

4.2 Methods

4.2.1 Animal subjects

One adult C57BL/6 male transgenic mouse (id: TS258) was used for the experiment. The channelrhodopsin 2 variant (C128S) was expressed in central serotonin neurons by targeting the tryptophan hydroxylase 2 (Tph2) promoter [139]. The C128S was step-function opsin, which can produce sustained depolarisation [12]. This opsin enables us to cause sustained neural activities without excessive laser heat, which can cause artifacts [33]. After surgery, the subject underwent habituation training [210], an MRI session, and a reward delay task in turn.

4.2.2 Streotaxic surgery

The subject was initially sedated with 3% isoflurane, and we administered three types of mixed anesthetic agents (1 (mg/mL) of medetomidine, 5.0 (mg/mL) of midaloram, and 5.0 (mg/mL) of butorphanol) [104]. We removed the head skin and fixed a plastic bar (3x3x27mm) to the mouse skull with dental cement. We also implanted an optical fiber toward the DRN. After at least one week of recovery, mice were habituated to the MRI environment for another week. Mice subsequently underwent imaging sessions.

4.2.3 MRI experiments

A mouse was placed in the MRI animal bed. After we confirmed that its body temperature was stable at 36 ± 0.5 (C°), T2-weighted structural imaging and three T2* functional imaging sessions were performed. MRI images were acquired with a 11.7 tesla MRI scanner for small animals (Biospec 117/11 system, Bruker Biospin, EmbH, Ettlingen, Germany) with a cryogenic quadrature RF surface probe (Cryoprobe, Bruker BioSpin AG, Fällanden, Switzerland). We performed T2-weighted structural imaging with a fast-spin echo sequence with subsequent parameters: 140 x 140 matrix, 13.5 x 13.5 mm^2 field-of-view, repetition time(TR)/effective echo time(TE) 4000/18.75 (ms), 32 coronal slices, slice thickness: 300 μm.

After T2-weighted structural imaging was performed, a functional MRI session was further executed. A functional MRI session was composed of three imaging runs, a resting-state run (without any stimulation), a blue-light stimulation run, and a yellow-light stimulation run. All functional imaging was performed using GE-EPI sequence with following parameters: 67 x 67 matrix, 13.5 x 13.5 mm^2 field-of-view, TR/TE 1000/10.7 (ms), flip angle: 50°, bandwidth: 333k(Hz), 32 coronal slices and slice thickness: 300 μm, and 640 repetitions.

Resting-state fMRI was initially performed. In the opto-fMRI session, we initiated blue stimulation 40s after the onset of imaging. We repeated 5s blue-light stimulation (2.7-2.9 (mW), 465 (nm)) 10 times, once every 60s. Yellow-light stimulation (1.2-1.4mW, 595 nm) followed 20s after the onset of blue light stimulation. We also applied a yellow light opto-fMRI session instead of blue illumination. 5s yellow light was repeated every 60s x 10. Another yellow illumination was followed 20s after the onset of yellow light stimulation. We removed the first 10 images from subsequent analysis.

4.2.4 Pre-processing

Data were pre-processed and activation maps were calculated using SPM12 (Wellcome Trust Centre for Neuroimaging, London, UK). We performed realignment, motion correction, co-registration, normalization, and spatial filtering (4 mm, FWHM Gaussian kernel).

4.2.5 A reward delay task

We leveraged a reward-delay task in which subjects were required to maintain a nose-poke to obtain delayed rewards [139] (Fig. 4.3 A). Subjects were trained to initiate trials by nose-poking into a tone site 500 (ms). In short, the reward-delay task is composed of reward trials (75%) and omission trials (25%). We adopted two types of stimulation protocols (Fig. 4.3 B). In the onset of reward and omission trials, either blue or yellow illumination was delivered. In the reward trials, blue/yellow light stimulation was delivered for 800 (ms) at the onset of each trial, and yellow light was delivered when subjects waited for 6 (s). However, yellow illumination was also given when subjects failed to wait for 6 (s). On the other hand, in omission trials, yellow stimulation was given when mice gave up waiting for delayed rewards while light stimulation was delivered in the same manner as in reward trials. In the pilot experiment, we fixed a 6 (s) reward delay in reward trials, while no reward was given in omission trials.

4.3 Optogenetic phasic stimulation of DRN serotonin neurons

First, we sought to investigate whether optogenetic stimulation evoked BOLD signals with the general linear model to map observe whole-brain stimulation contrast. However, we could not observe any BOLD responses. Next, we sought to study whether optogenetic stimulation evoked BOLD signals in DRN. We extracted an averaged time series of BOLD signals from DRN using the Allen brain template (Supplementary Figure.A.4 A-E.). As selection criteria for putative BOLD signals, we thresholded BOLD signals by the total average, and selected the average positive response ($40(s)$ duration $5(sec)$ after the onset of each stimulation) considering slow rising of BOLD signals. The last three stimuli were selected as putative responses. Furthermore, in order to validate this assumption, we again leveraged the general linear model (GLM) to map spatial activation patterns correlated with the last three stimuli. Consistent with the hypothesis, prominent activation originating from the DRN, mPFC, left CPu, right Cpu, and VTA was found (Figure. 4.1 and Figure. 4.2 A,C,E,G, and I). Furthermore, activation from the insular cortex, the hypothalamic regions, and retrosplenial cortex (RSC) were also found. Meanwhile, BOLD signals could be led by visual stimuli due to illumination leaks from an optic fiber. Therefore, we checked whether signals were evoked by yellow illumination. However, we could not observe such activation in either a resting-state or during yellow stimulation runs. Finally, we found a significant correlation between motion artifacts and BOLD signals (Supplementary Table.A.2; Supplementary Figure.A.4.). Hence, our results suggest that stimulated DRN serotonin neurons potentially evoked BOLD responses in those target regions, but motion artifacts may also have induced the BOLD signals.

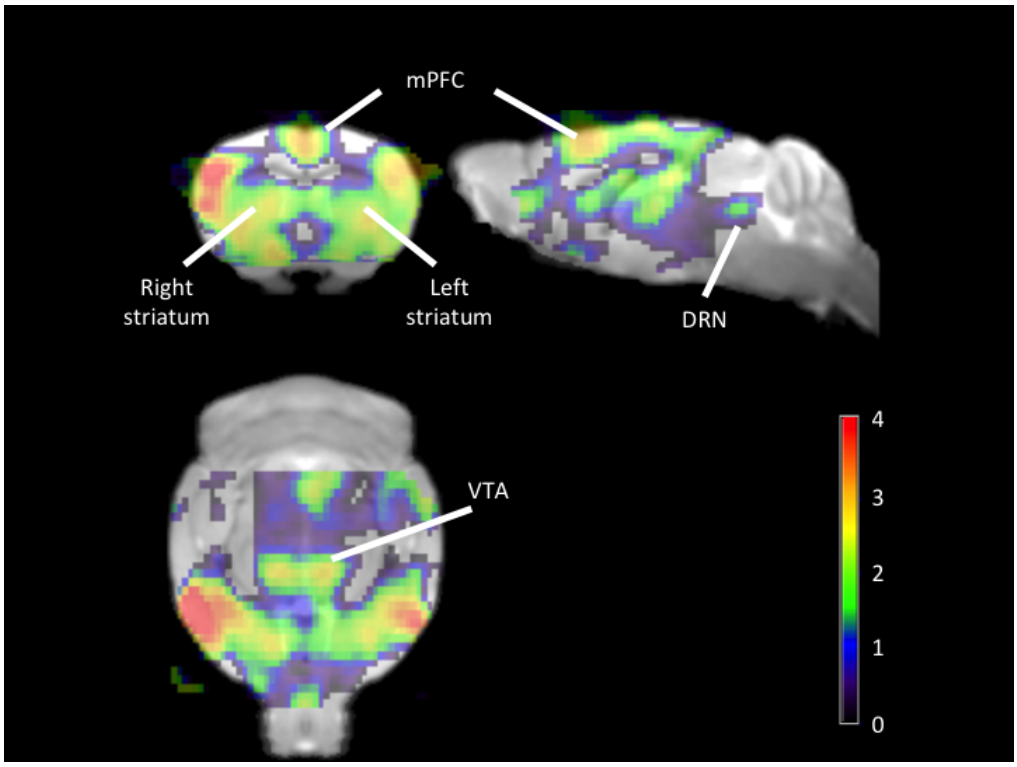

Figure 4.1: Activation map by the general linear model (GLM). The color bar indicates uncorrected Student's t-test values. The map implies prominent activation in DRN, mPFC, left striatum, right striatum, and VTA.

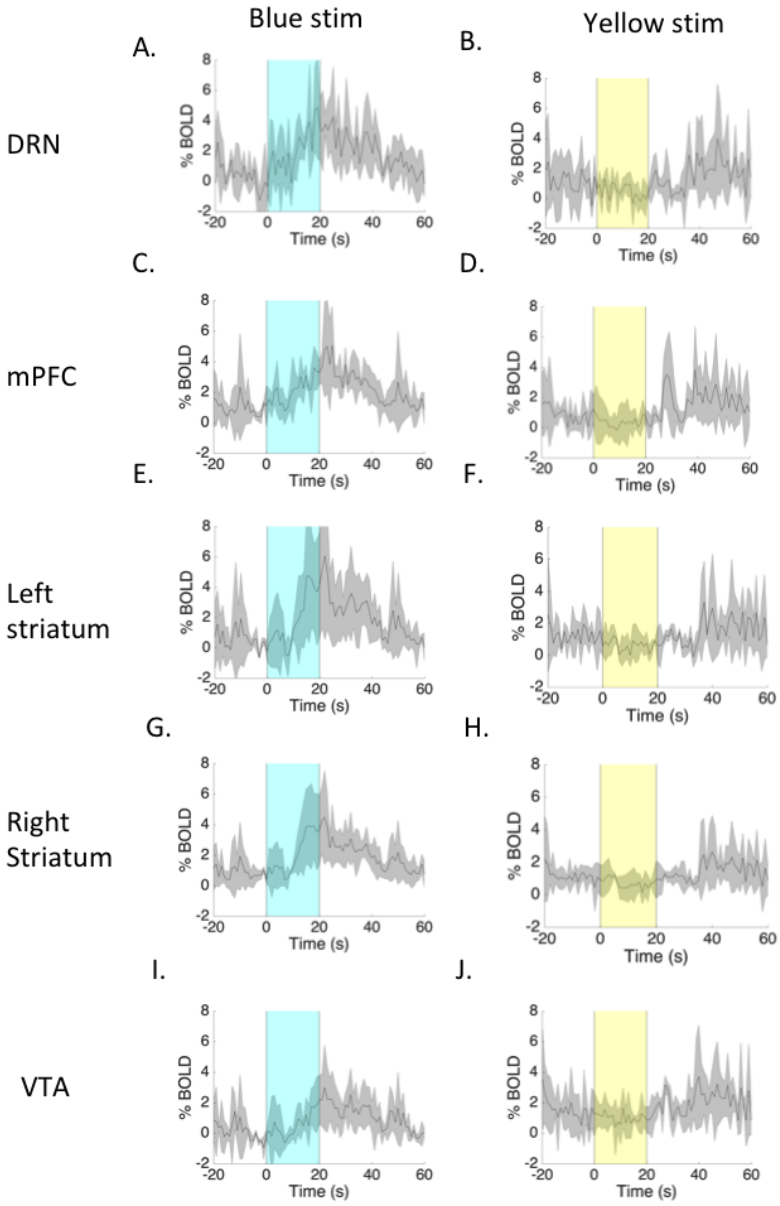

Figure 4.2: A,C,E,G,I: Averaged BOLD signals in the last three stimulations from DRN, mPFC, left striatum, right striatum, and VTA in the blue-illumination trial. B,D,F,H,J: Averaged BOLD signals in the last three stimulations from DRN, mPFC, left striatum, right striatum, and VTA in the yellow illumination run. Blue and yellow background colors indicate time courses of optogenetic blue and yellow illuminations for $20(s)$, respectively.

4.4 Transient activation promotes waiting for delayed rewards

We investigated whether the evoked BOLD responses with subject TS258 were produced by optogenetic stimulation. In order to validate it, we utilized a reward delay test that we previously used to observe the influence of optogenetic stimulation on waiting behaviors [139]. In the previous study, TPh2 transgenic mice showed longer waiting times in omission trials in blue light stimulation trials. Therefore, TS258 was subsequently trained to perform a reward delay task. We tested whether blue light stimulation to DRN serotonin neurons elongates waiting time in omission trials with this subject (Fig. 4.3 C and D). We found that TS258 showed significantly longer waiting time under blue light stimulation ($P = 1e^{-6}$, U-test; blue stim: mean time=11.96(s), $SD = 1.82$; yellow stim: mean time=10.91(s), $SD = 1.64$). Furthermore, mean waiting ratio was 1.096(s), which is consistent with previous experiments. Hence, we concluded that DRN serotonin stimulation induced longer waiting for delayed rewards with TS258.

4.5 Discussion

Here, we conducted a pilot experiment to assess to specific DRN serotonin regulation of brain dynamics with ofMRI in awake mice. Our pilot experiment with a single subject showed that optogenetic activation of DRN serotonin neurons evokes BOLD responses in the mPFC, the insular cortex, the striatum, and the VTA although BOLD responses may have been evoked by motion artifacts. Furthermore, in order to confirm optogenetic activation of serotonin neurons, we also conducted a waiting task for delayed rewards with the same subject[139]. Consistent with our previous research, optogenetic activation elongates waiting time for delayed rewards. Hence, we concluded that evoked BOLD signals originated from optogenetic activation of DRN serotonin neurons.

Our attempt entails two potential methodological advances. Our ofMRI was performed with mice in an awake state. In previous studies, anesthesia was introduced to prevent motion artifacts during imaging possibly due to leaks of illumination [62, 111, 118]. However, anesthesia can lessen BOLD responses, and the choice and level of anesthesia can ambiguate interpretations of evoked signals [56]. Three preparations, introduction of step function opsin expressed in transgenic mice, stereotaxic surgery with a mixture of dental cement and carbon, and acclimation training with visual stimuli, could be helpful to perform optogenetic fMRI in awake animals.

Recent opto-fMRI studies focus on phasic optogenetic manipulation of neuromodulatory systems, especially of the dopamine system [53, 62, 111, 118]. These studies leveraged the major advantage of ofMRI to access direct and indirect modulation of neuronal dynamics among distant brain regions, and successfully showed dopamine

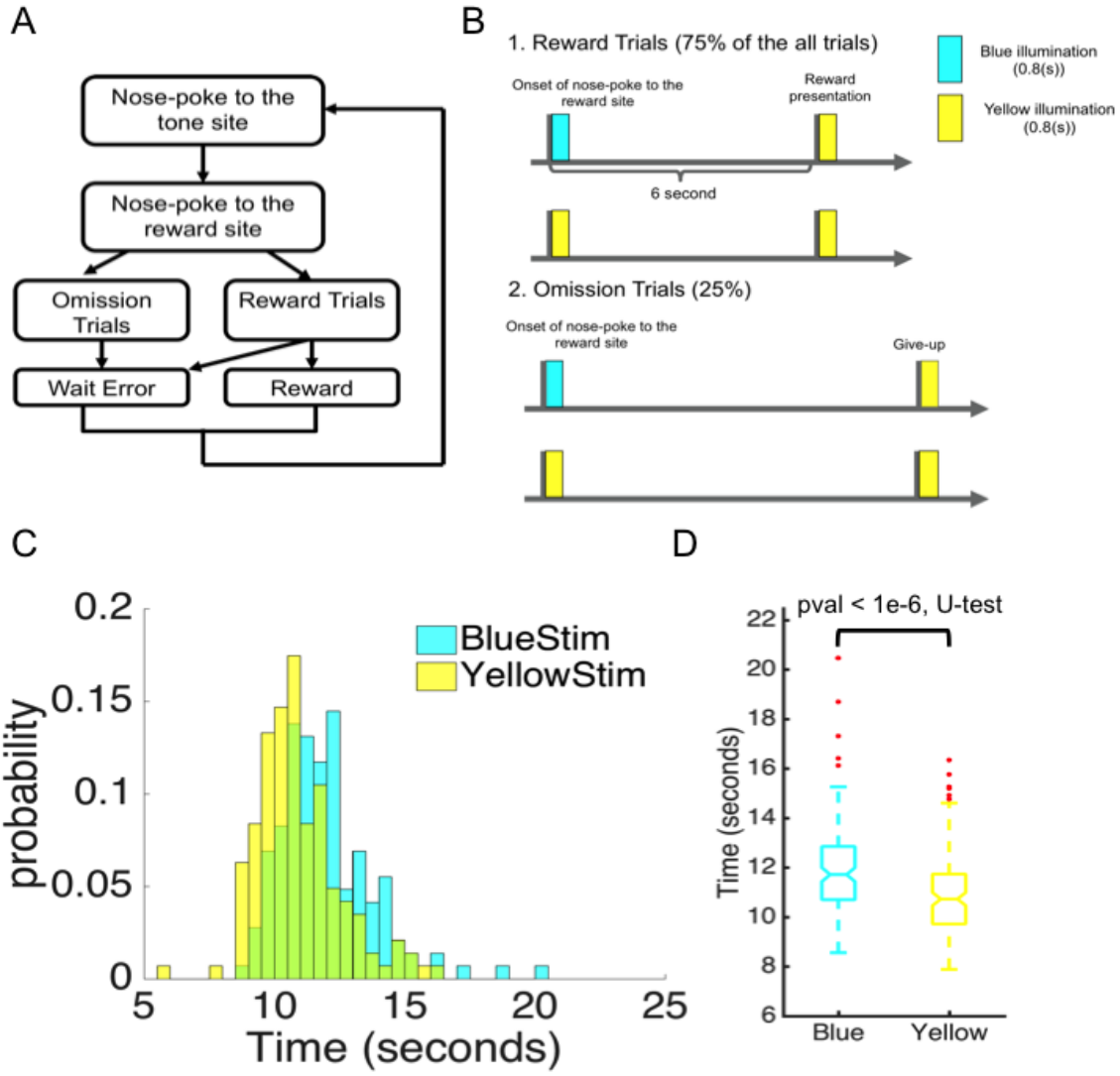

Figure 4.3: A. Schematic diagram of the reward delay task [139]. A mouse was required to nose-poke a tone site in an experimental chamber to initiate a trial. If the mouse successfully nose-poked the tone site for 500 ms, a tone was given. The mouse was required to maintain the nose-poke in a reward site in the chamber. If mice maintained the nose-poke at the site for 6 (s), a reward was given in 75 % trials. On the other hand, in the 25% omission trials, rewards were never given. Therefore, the mouse needed to determine when to give up waiting. The mouse repeated the procedure for multiple trials in order to obtain statistically significant number of data points. B. Stimulation time-course. Random blue- or yellow-light stimulation was given to serotonergic neurons at the onset of trials after each nose-poke to the tone site. Additional yellow illumination was applied at the offset of the trial by reward presentation or by ceasing to wait. C. We counted waiting time in both blue- and yellow-stimulation trials separately from omission trials. Mean time for blue-illumination trials was $11.96(s)$ and $10.9(s)$ for yellow-stimulation trials. D. We tested whether blue illumination successfully stimulates DRN serotonin neurons. There was significantly higher waiting time in blue illumination wait error trials than in yellow illumination wait error trials ($P < 10^{-6}$, U-test).

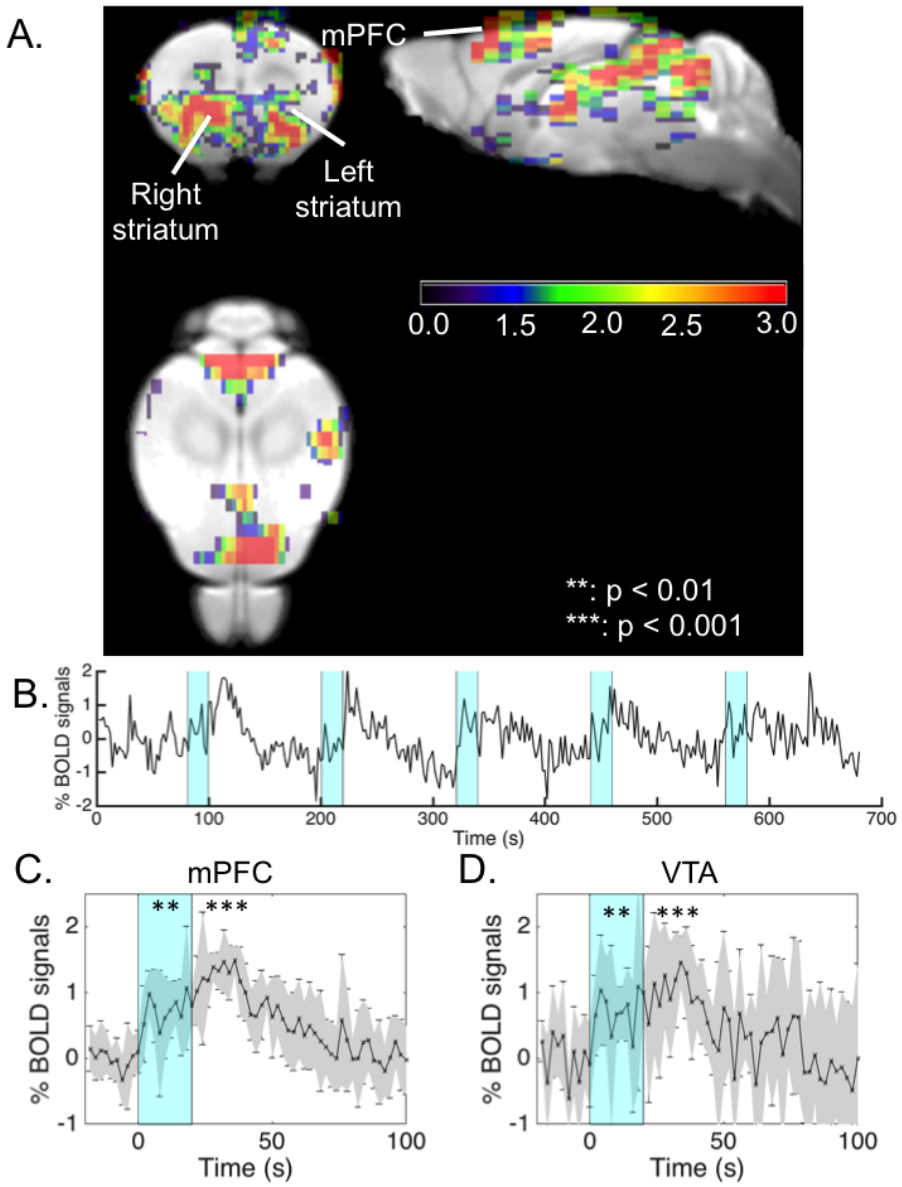

Figure 4.4: Replication of an activation map by DRN serotonin neurons with another subject (TS339). A. Activation map by DRN serotonin neurons (Blue light: 10.0mW, Yellow light: 7mW) Considering possible artifacts in a pilot study, we introduced a head fixation with dental cement with carbon, acclimation with visual illumination, and higher intensity of illumination. We applied GLM for all activation in an imaging session. We found an activation in the mPFC and striatum. A color bar indicates statistical t-score. B. Time-couse of BOLD signals in the mPFC. Blue highlight indicates 20s stimulation course. C,D. Average BOLD responses in the mPFC and VTA. We overlaid BOLD responses by blue light stimulationin the mPFC(Figure.4.4.C) and VTA(Figure.4.4.D). We found statistical significance in BOLD signals during blue-light stimulation and 20 second later compared to the baseline, which is defined by mean of 20 s BOLD signals(** indicates uncorrected $P < 0.01$, *** indicates uncorrected $P < 0.005$).

modulation in the mPFC and structually non-connected regions, such as the NAc. A recent study also attempted to apply chemogenetics to map brain-wide DRN serotonergic activation [71]. It would be useful to observe brain-wide tonic modulation by chemogenetic or optogenetic activation of serotonin system, since the system has a slow impact on brain dynamics by acting on metabolic receptors [30]. For example, depression and stress vulnerability are encoded in spatial-temporal dynamics [54, 94, 103]. Such spatial-temporal dynamics could be modulated non-linearly by tonic serotonin modulation. Additionally, a recent study also revealed that daily repetitive optogenetic stimulation of the DRN serotonin system promoted spontaneous locomotion opposite to transient optogenetic stimulation [38]. Long-term modulation may underlie slow therapeutic efficacy of serotonin antidepressants. Such slow modulation is possibly better clarified by dissecting spatio-temporal dynamics with optogenetic fMRI and network analysis.

It is necessary to mention critical limitations of the study. The pilot experiment revealed the possibility of accessing brain regulation with optogenetic DRN serotonin stimulation. However, we failed to replicate putative and similar activation maps. We speculate that illumination-induced motion artifacts and diminishing light intensity are the two major confounding factors. First, illumination leaks may cause motion artifacts by surprising subjects. As correlation between motion artifacts and BOLD responses, we identified light leaks from the skull. Furthermore, we confirmed that motion noise in opto-fMRI sessions showed higher variance compared to resting-state imaging. To reduce such noise, we fixed an optic fiber with a mixture of dental cement and carbon powder. Carbon prevents illumination leaks from the mouse skull. Additionally, we also introduced blue-light stimulation during acclimation training prior to the imaging session. Our follow-up experiment showed that training successfully decreases motion artifacts. However, we could not replicate putative evoked signals with the training. This might be due to a second factor, diminished light intensity. In the pilot and follow-up experiments, we used a cannula (diameter: 400 μm) to illuminate tissues. We found that maximum light intensity decreased from 2.7 mW to 1.2 mW (465 nm), presumably by repetitive use of the cannula. Introduction of higher light intensity may allow us to replicate the result. A recent attempt showed a replication by considering these factors4.4.

Application of ofMRI to the serotonin system has promise to uncover its complicated role of brain modulation. Our ofMRI approach with step-function opsion aimed at both phasic and tonic modulations in a serotonin subsystem. We attempted to develop the procedure, and performed preliminary experiments. However, we failed to establish a protocol for further validation. Nonetheless, our pilot experiment opens a new possibility to access serotonin modulation of brain-wide dynamics.

Chapter 5

Discussion

5.1 Summary of the experiments

In the SSRI project, we found that a serotonergic antidepressant influenced spontaneous locomotion and a DRN-related affective system. Furthermore, such spontaneous locomotion was associated with large-scale brain dynamics. Preliminary optogenetic functional mapping showed brain responses from anatomically known DRN terminal targets, and our replication of functional mapping by optogenetic stimulation will be used for further validation of the results.

5.2 General limitation of the studies

It is worth noting general limitations of studies of relying upon resting-state fMRI and a brain atlas.

Due to its convenience and task information, resting-state fMRI has been utilized to reveal abnormal brain dynamics from subjects with mental disorders. However, some personal characteristics such as aggressiveness and resilience, the capability for rapid recovery from mental stresses, might be challenging to capture. Task fMRI is predominant in human studies, but there are few rodent studies. The main hindrance to employing task fMRI with rodents is body fixation during imaging. Although some studies focused on sensory-evoked brain response in rodent studies, body fixation during imaging is the most difficult task, especially for studies that require body movement, such as goal-directed decision making and spontaneous locomotion. One possibility to enhance flexibility of subject movement is to introduce a treadmill type of animal bed. Brain imaging studies employ treadmills with head-fixation. An additional advantage of a treadmill is potential reduction of stress by body fixation. Although acclimation training with body fixation induced significant reduction of stress responses, long-term

training can be stressful. As we found state duration of the intermediate state may be caused by repetitive body fixation stresses. A treadmill type of an animal bed may be able to prevent such confounding factors. However, a treadmill could degrade signal-to-noise ratio of brain imaging due to movement. Establishing a training protocol for a treadmill would be critical for its introduction.

Another significant limitation of the present studies is creating translational functional brain maps across species. Pre-clinical trials are used to validate effectiveness of treatment with animals, but not with humans, for ethical reasons. Although there has not been any one-to-one quantitative mapping, quantitative translational brain mapping using the same methodology, including fMRI would be worthwhile to fill the anatomical and functional gap across species. In this study, we confirmed that homologs of putative brain regions were consistently influenced in the mouse brain. However, there is room for improvement in future studies. Our brain atlas is based on brain parcellation from the Allen brain atlas, which is designed for divisions of the mouse brain by cell-type. There have been some attempts to coordinate homologs across multiple species [9, 122, 127, 143, 197]. It should be beneficial to take advantage of brain differences to create a translational functional map. Furthermore, there are some human brain regions that do not exist in the rodent brain. For example, the rodent brain does not have regions homologous to the dorsolateral prefrontal cortex (dlPFC) and the posterior cingulate cortex (PCC), although there are some partial anatomical overlaps. These regions serve a social function, notably the theory of mind and subjectivity. Those functions are key to abnormalities in mental diseases. Therefore, the major difficulty in evaluating animal models of mental diseases is due to their anatomical distinctions. Nonetheless, it would be worth reconciling the anatomical gap in order to establish an interspecific pre-clinical translational map.

Finally, it is noteworthy that strong illumination intensity can be the key for optogenetic fMRI, but a dilemma can emerge. Induction of strong optogenetic activation might induce biologically implausible brain responses although fMRI might not detect weak activation by weaker optogenetic stimulation. The dilemma require balanced control of a system invasion. However, it is unclear whether identifying an appropriate balance is possible, unless a system is fully explored. Hence, determination of balanced stimulation is a challenge to be discussed in the field.

5.3 Future research direction

In the optogenetic preliminary study, we successfully replicated functional mapping of DRN serotonergic neurons. I would like further to statistically validate phasic and slow serotonergic regulation by daily repetitive optogenetic stimulation. Correia et al. revealed that antithetical effects of serotonin on spontaneous locomotion by phasic activation and long-term activation. Optogenetic fMRI may show distinctive functional mapping by repetitive stimulation of the DRN serotonin system due to synaptic plasticity. From the SSRI project, we also found SSRI influence on functional connectivity

and brain attractor dynamics. The previous human study showed abnormal functional connectivity in the affective network and the default mode network (DMN) in MD subjects. Serotonergic antidepressants has been hypothesized to normalize abnormal functional connections in the affective network and DMN in MD subjects[131, 132]. Consistent with the notion, our findings showed acute SSRI influence on functional connectivities in those functional networks between BST and dRSC, and DRN and thalamic RT. Rodent fMRI studies also showed SSRI involvement in the functional networks [71, 82]. For example, Hai et al. found signal reduction in BST by infusion of an acute serotonergic antidepressant into the Cpu [82]. Another study by Giorgi et al. revealed increased activity in the DRN and the thalamic area by chemogenetic activation of serotonin systems [71]. Especially, the BST circuit is modulated by serotonin for anxiety-like behaviours [129]. It will be interesting to observe influence on the BST circuit by acute and chronic serotonergic antidepressants in human imaging.

Furthermore, recent human studies with MD subjects showed abnormal dynamic functional connectivity, which is associated with depression scores[103, 213]. One of the representative symptoms in MD subjects is rumination, repeated distressing thoughts. Since rumination is a mental state of repetitive stress, such a mental state might be represented by a brain state [35]. Therefore, depressed subjects can be defined by the abnormal appearance of ruminative brain states. Our findings about a serotonergic antidepressant on brain attractor dynamics implicates normalization of the such ruminative brain state dynamics by a serotonergic antidepressant. Moreover, psychotherapies including cognitive behavioral therapy and mindfulness-based cognitive therapy for depression may exhibit a similar normalizing influence on ruminative brain state dynamics[58, 128]. It is also interesting to address the question of whether long-term serotonin activation reshapes brain state dynamics against stresses[72]. The serotonergic system might be linked to temporal internal processes [34, 35]. Another potential project would be to investigate how human brain state dynamics respond to serotonergic antidepressants with ELA. Functional imaging with experience sampling using human subjects would enable us to clarify the influence of antidepressants on the internal process.

As a general research direction, the aforementioned limitation will be a potential research target. First, introduction of a foot-free rodent MRI apparatus, such as a treadmill, might be the next target. Serotonin serves multiple functions in spontaneous and goal-directed behaviors. Task fMRI enables us to capture serotonergic regulation of task-relevant brain activation during these tasks.

Next, a translational functional map between human and rodent brains should be beneficial. Rodent fMRI allows us to observe brain-wide dynamics of the rodent brain with the same methodology as in human fMRI. This is advantageous to validate underlying neural mechanisms in pharmaceutical pre-clinical tests with animal models of depression and other mental disorders. There are three conventional criteria in animal models of mental disorders, which are based on three non-neuronal validities: construct, face, and predictive validities. Construct validity is about the cause of a behavioral abnormality, such as social defeat in animal models of depression. Face

validity is similar to symptoms, such as learned helplessness and reduction of social interaction in the models [32, 72]. Last, predictive validity is whether drug treatment has the same recovery effect on the models. Ethological observation suffices for those criteria, but underlying neuronal mechanisms may differ. It has been suggested to introduce other validities such as homological and mechanistic validities in order to further legitimize animal models of mental disorders [10]. Concomitantly, multiple groups have identified depression-related neuro-markers using fMRI studies [96, 172]. It has also been found that depression-related target regions showed abnormal brain activity patterns in rodent studies. RsfMRI for the rodent brain is a promising tool to validate mechanistic and remission validity collaboratively with human fMRI studies.

Furthermore, multi-modal and integrative approaches would reveal complicated serotonin modulation of brain dynamics and mental processes. Methodological and computational advances have enabled us to collect and analyze large datasets [26, 110, 169]. A recent trend in neuroscience is to facilitate multi-modal databases, including genetic expression, structural projections, electrophysiological data, BOLD signal data, behavioral data, diagnostics, and etc. For example, the Allen Brain Institute (ABA) [179] has started opening genetic, anatomical, and functional datasets of the human and mouse brains. The Human Connectome Project (HCP) [188] collects task-free fMRI, task-fMRI, EEG, MEG, and behavioral results, and questionnares from each of over 1000 subjects, enhancing neuro-imaging genetics through meta analysis (ENIGMA) [100, 147]. Those databases make it possible study relationships among different modalities. The serotonin system has multiple components, such as 9 nuclei, over 14 receptors, sub-types of transporters, wide-spread projections, and stimulus-sensitive regulation. Hence, a multi-modal approach allows us to examine nonlinear relationships of each component.

Integrative approaches are also a promising tool to unite multi-modal datasets of the serotonin system. The conventional integrative approach is model-based analysis. Model-based approaches became well-known due to the dopamine temporal difference error hypothesis in reinforcement learning [45, 57, 166]. In a framework of a model-based approach, cognitive models are hypothesized to underlie task behaviors, usually goal-directed behaviors, and to fit models to neuronal and behavioral data to analyze contributing factors. Several groups leverage this approach to decode serotonin modulation in goal-directed behaviors [120, 123, 136, 138–140]. This approach is helpful to understand relationships between cognitive process and neuronal dynamics. On the other hand, another recent integrative approach focuses on understanding emergent properties of functional dynamics based on anatomical projections [48, 49, 51]. Resting-state brain dynamics is spatio-temporarily organized and retains task-relevant information. Resting-state functional dynamics can underlie task-relevant brain responses and behavioral performances.

Along with this trend, researchers have started to apply this integrative approach not only to the human brain, but also to the mouse brain. For example, the Virtual Mouse Brain (TVMB) is the connectome-based simulation platform to emulate brain-wide dynamics by leveraging anatomical projections from ABA and neuronal models

[134]. Although the TVMB does not explicitly consider neuro-modulatory regulation, it can be extended to exploit data from neuromodulatory regulation by regulating the global coupling parameter, which controls the amplitude of neural firing. The serotonin system regulates multiple regions, predominantly by metabolic receptors, and its slow and widespread regulation may cause nonlinear dynamics, which have been challenging to delineate by conventional methods. Additionally, while this is computationally very expensive, it is easy to take into account receptor regulation in neuronal models. Therefore, this connectome-based integrative approach has potential to explain slow and nonlinear modulation of the serotonin system. This connectome-based integrative approach can be categorized as data-driven modeling, which explicitly exploits empirical data to construct hidden dynamics with approximate equations. Such data-driven modeling may foster understanding of the serotonin system and clinical effects of serotonergic antidepressants.

Taken together, by exploiting new data platforms and large datasets, it is promising to integrate multi-modal data and to disentangle the complexity of the serotonergic system from an integrated perspective, considering molecular, anatomical, physiological, and network variables. Exploiting brain-wide functional data from my concurrent studies will contribute to future studies.

Conclusion

In this thesis, I studied long-term modulation and phasic activation of the serotonin system using pharmacology and optogenetics. In the first experiment, I explored the influence of serotonergic antidepressant treatment on spontaneous locomotion and anxiety-like behaviors, brain dynamics, and the linkage between behaviors and brain dynamics. My results delineated resultant changes in spontaneous locomotion and functional connections in the affective system. Furthermore, network dynamics analysis revealed maintenance of dynamic brain states, which is linked to active exploration by serotonergic antidepressant treatment. My results suggest an influence of serotonergic antidepressant treatment on abnormal brain activity by balancing brain state dynamics. In the second experiment, I preliminarily showed that phasic optogenetic activation of DRN serotonergic neurons revealed BOLD responses in affective brain regions among the projection regions of the DRN.

Further investigation is required to understand the relationship between serotonergic regulation of brain dynamics and behaviors. Nonetheless, my findings have enabled new understanding of short- and long-term serotonergic modulation of brain-wide dynamics.

Appendix A

Supplementary information

A.1 Software

A.2 Atlas Creation

We utilized an anatomical template from the Allen brain atlas (ABA) for the C57BL6J mouse. First, we transformed a nissel image template from ABA to fit a C57BL6J T2 template [87] with advanced normalization tools (ANTs; see Supplementary Table A.1). Next, we used the transformation coordinates in the previous step to fit corresponding labels to the T2 template by interpolating with the nearest neighbor method. Finally, we concatenated multiple labels for FC calculations, and bilateral 10 brain regions were defined including DRN and VTA.

A.3 Large-scale components creation with ICA

A.3.1 Preproecssing

We first performed realignment, co-registration, normalization and spatial smoothing with SPM12 (Supplementary Table. A.1). We applied linear trend filter and temporal filter ([0.01, 0.08] Hz) to all preprocessed data from the first sessions with REsting State fMRI data analysis Toolkit (REST). Next, we performed sICA analysis with Group ICA Of fMRI Toolbox (GIFT) with following parameters: the number of independent components n=30, ICA algorithm (Infomax), and ICASSO (10 runs and min/max cluster size=8/10; [88]). In order to obtain stable independent component, we performed ICASSO, which is a software for checking estimate reliability of ICA results. We selected 10 interpretable independent components out of 30 components

Software and Data	Source	Indentifier
MATLAB 2015b	Mathworks	https://jp.mathworks.com/products/matlab.html
Statistical Parametric Mapping 12 (SPM12)	University College London	http://www.fil.ion.ucl.ac.uk/spm/software/spm12/
functional connectivity toolbox (CONN)	The Gabrieli Lab, McGovern Institute for Brain Science	https://www.nitrc.org/projects/conn
Group ICA Of fMRI Toolbox (GIFT)	Mia lab. University of New Mexico.	http://mialab.mrn.org/software/
Advanced normalization tools (ANTs)	Penn Image Computing and Science Lab. University of Pennsylvania.	http://stnava.github.io/ANTs/
Resting-State fMRI Data Analysis Toolkit (REST)	State Key Laboratory of Cognitive Neuroscience and Learning, Beijing Normal University.	http://restfmri.net/forum/ index.php
C57BL6/J anatomical template	Department of Physiology, Keio University School of Medicine.	https://www.nitrc.org/projects/tpm_mouse/
C57BL6J/J brain parcellation	Allen Brain Institute	http://help.brain-map.org/display/mousebrain/API
C57BL6/J large-scale components	Doya Unit	available soon
R code for for advance normalization	Doya Unit	available soon
MATLAB codes for CONN Batch processing	Doya Unit	available soon

Table A.1: Software and Data

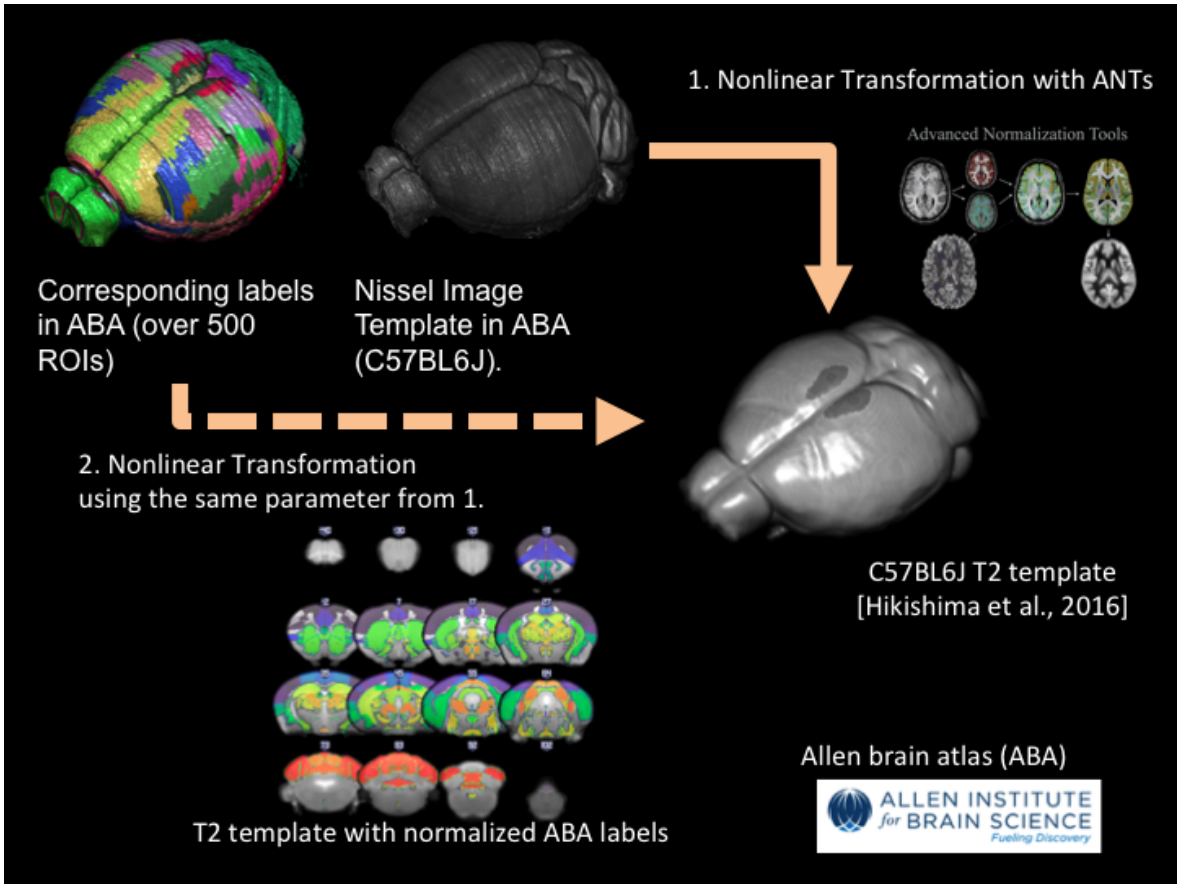

Figure A.1: We leverage Allen mouse brain atlas labels to extract functional connectivity among brain regions. First, we transformed a nissel image template to fit a C57BL6J T2 template with advanced normalization tools [87]. Next, we used the transformation corrdinates in the previous step to fit corresponding labels to the T2 template. Finally, we concatenated multiple labels for FC calculations, and 157 brain regions were defined including DRN, MRN, and VTA.

for the subsequent analyses such as large-scale FC analysis and ELA analysis.

A.4 Energy Landscape Analysis

The brain is a nonlinear dynamical system, and its neuronal dynamics represents cognitive information or mental states. In conventional literature in rs-fMRI studies, they are focused on functional dynamics in the over all time-series with FC analysis, and showed relevance in multiple cognitive functions. However, such methodology neglects time-varying shifts of signals, and it was urged to analyze a complex dynamics which is inherited in the brain in nature. To gain this goal, multiple groups started proposing methods to analyze neuronal dynamics taken by neural recording, EEG, MEG, and fMRI. Energy landscape analysis (ELA) is deemed as a promising analytical method for analyzing multivariate neural dynamics as a roaming ball in a landscape of information theoretic 'energy' but neither metabolic nor thermal energy [4, 60, 200–203]. ELAs originated from the Ising model in statistical mechanics to consider brain network dynamics as probabilistic models, and ELA revealed individual difference in conscious processing and abnormal dynamics in a mental disorder, autism [202, 203]. Here, we hypothesize that the mouse brain retains functional brain transitions between brain states, and SSRI can modulate configuration of an energy landscape. To test this, we utilized a pairwise maximum entropy model (MEM).

A.4.1 Pairwise maximum entropy model (MEM)

Pairwise maximum entropy model (MEM) is one way to describe energy landscape of neuro-imaging data [200, 201, 203]. The method analysis enables us to regard multivariate brain signals as a ball in an energy landscape. We only assume no information is available in advance for unbiased distribution estimation. Given such setting, the uncertainty miximization is the only reasonably possible method. It is known that the maximum entropy probability distribution by maximizing the entropy leads to the Bolztmann distribution [101]. The pairwise maximum entropy model adopts the Boltzmann distribution to infer the energy function.

The algorithm is calculated as shown below[200, 201, 203].

Step 1. set the N regions of interests (ROIs), and extract time-series $X_i(t)$ where represents time point $t = [1, \ldots, t_{max}]$ and a region of interest (ROI) $i = [1, \ldots, N]$.

Step 2. binarize neuroimaging signals $X_i(t)$ by thresholding the signals. We denote the binalized signals, $\{\ \sigma_i(1), \ldots, \sigma_i(t_{max})\ \}$.

$$\sigma_i(t) \quad = \quad \begin{cases} 1, & \text{if } X_i(t) \geq \ \langle X_i \rangle \\ -1, & \text{else} \end{cases} \tag{A.1}$$

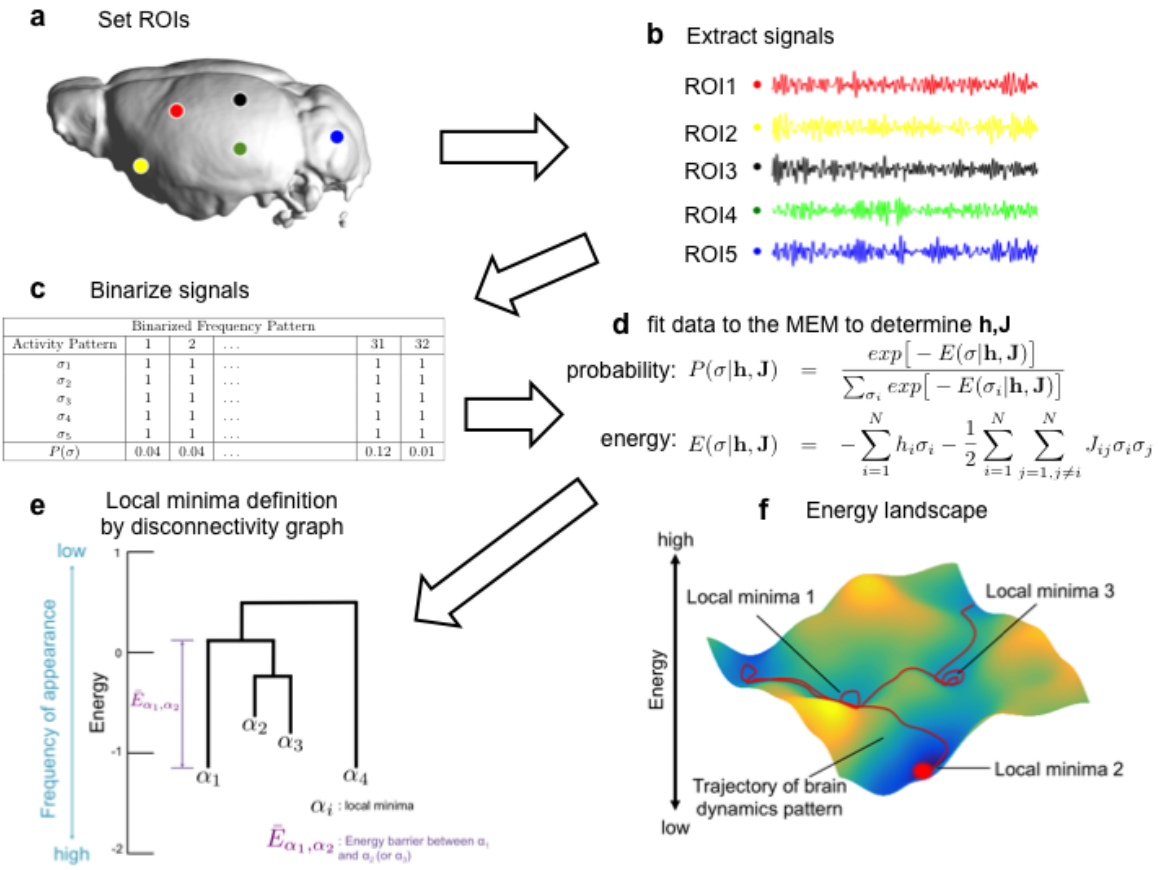

Activity Pattern	1	2	...	31	32
σ_1	1	1	...	1	1
σ_2	1	1	...	1	1
σ_3	1	1	...	1	1
σ_4	1	1	...	1	1
σ_5	1	1	...	1	1
$P(\sigma)$	0.04	0.04	...	0.12	0.01

Figure A.2: (a) Regions of interest. First, we choose regions of interest (ROIs) from the brain. (b) Signal Extraction. Extract signals from ROIs after preprocessing and denoising steps. (c) Binarization. Binarize the extracted signals. (d) Maximum entropy method. Apply the binarized signals to MEM algorithm AA.4.1 in order to optimize parameters h, J. We can define local minima based on the optimized parameters. The optimized parameters allows us to obtain local minima and related brain states. and (e) Disconnectivity graph. Calculate disconnectivity graph in order to visualize energy landscape of local minima. (f) Energy of local minima represents depth of energy landscape. Furthermore, empirical percent stay in each local minimum is associated with basin size, which is defined by corresponding activity patterns.

caution: thresholding is arbitrary but we used the time average $\langle X_i \rangle$ of original time-series for each region i.

Step 3. calculate the empirical frequency $P_{empirical}(\boldsymbol{\sigma})$ that represents appearance probability of each activity pattern.

Step 4. fit the Boltzmann distribution to the empirical data. The Boltzmann distribution is defined as

$$P(\boldsymbol{\sigma}|\mathbf{h},\mathbf{J}) = \frac{\exp\left[-E(\boldsymbol{\sigma}|\mathbf{h},\mathbf{J})\right]}{\sum_{l=1}^{2^N}\exp\left[-E(\boldsymbol{\sigma}^l|\mathbf{h},\mathbf{J})\right]} \tag{A.2}$$

where

$$E(\boldsymbol{\sigma}|\boldsymbol{h},\boldsymbol{J}) = -\sum_{i=1}^{N} h_i\sigma_i - \frac{1}{2}\sum_{i=1}^{N}\sum_{j=1,i\neq j}^{N} J_{ij}\sigma_i\sigma_j \tag{A.3}$$

$E(\boldsymbol{\sigma}|\mathbf{h},\mathbf{J})$ is the energy, and $\mathbf{h} = \{h_i\}, \mathbf{J} = \{J_{ij}\}(i,j = 1,\ldots,N)$.

A.4.2 Likelihood maximization for the pairwise MEM

We aim to gain a set of parameters, $\mathbf{h},\mathbf{J}$.

$$(\mathbf{h},\mathbf{J}) = \arg\max_{\mathbf{h},\mathbf{J}} \mathbf{L}(\mathbf{h},\mathbf{J}) \tag{A.4}$$

$$\mathcal{L}(\mathbf{h},\mathbf{J}) = \prod_{t=1}^{t_{max}} P(\boldsymbol{\sigma}(t)|\mathbf{h},\mathbf{J}) \tag{A.5}$$

We applied a gradient descent method [202] for likelihood maximization.

$$\begin{aligned} h_i^{new} - h_i^{old} &= \frac{\epsilon}{t_{max}}\frac{\partial}{\partial h_i}\log\mathcal{L}(\mathbf{h},\mathbf{J}) \\ &= \epsilon(\langle\sigma_i\rangle_{empirical} - \langle\sigma_i\rangle_{model}) \end{aligned} \tag{A.6}$$

where

$$\langle \sigma_i \rangle_{empirical} = \frac{1}{t_{max}} \sum_{t=1}^{t_{max}} \sigma_i(t) \tag{A.7}$$

$$\langle \sigma_i \rangle_{model} = \sum_{l=1}^{2^N} \sigma_i^l P(\boldsymbol{\sigma}^l | \mathbf{h}, \mathbf{J}) \tag{A.8}$$

$$\langle \sigma_i \sigma_j \rangle_{empirical} = \frac{1}{t_{max}} \sum_{t=1}^{t_{max}} \sigma_i(t) \sigma_j(t) \tag{A.9}$$

$$\langle \sigma_i \sigma_j \rangle_{model} = \sum_{l=1}^{2^N} \sigma_i^l \sigma_j^l P(\boldsymbol{\sigma}^l | \mathbf{h}, \mathbf{J}) \tag{A.10}$$

A.4.3 Derivation of the likelihood maximization

First, we derivate the equation (A.6). Here,

$$\begin{aligned}
\frac{\partial}{\partial h_i} \log \mathcal{L} &= \frac{\partial}{\partial h_i} \log \prod_{t=1}^{t_{max}} P(\sigma(t) | \mathbf{h}, \mathbf{J}) \\
&= \frac{\partial}{\partial h_i} \sum_{t=1}^{t_{max}} \log P(\sigma(t) | \mathbf{h}, \mathbf{J}) \\
&= \frac{\partial}{\partial h_i} \sum_{t=1}^{t_{max}} \log \frac{exp(-E(\sigma(t)|\mathbf{h}, \mathbf{J}))}{\sum_{l=1}^{2^N} exp(-E(\boldsymbol{\sigma}(t)|\mathbf{h}, \mathbf{J}))} \\
&= \sum_{t=1}^{t_{max}} \frac{\partial}{\partial h_i} \Big[-E(\boldsymbol{\sigma}(t)|\mathbf{h}, \mathbf{J}) - \log \sum_{l=1}^{2^N} exp(-E(\boldsymbol{\sigma}^l(t)|\mathbf{h}, \mathbf{J})) \Big]
\end{aligned} \tag{A.11}$$

We calculate the terms $\frac{\partial}{\partial h_i}\big[-E\big]$ and $\frac{\partial}{\partial h_i}\big[\log \sum_{l=1}^{2^N} exp(-E)\big]$, respectively.

$$\begin{aligned}
\frac{\partial}{\partial h_i}\big[-E(\sigma(t)|\mathbf{h}, \mathbf{J})\big] &= \frac{\partial}{\partial h_i}\Big[\sum_{i=1}^{N} h_i \sigma_i(t) + \frac{1}{2} \sum_{i=1}^{N} \sum_{j=1, j\neq i}^{N} J_{ij} \sigma_i(t) \sigma_j(t)\Big] \\
&= \sigma_i(t)
\end{aligned} \tag{A.12}$$

$$\begin{aligned}
\frac{\partial}{\partial h_i}\big[-\log\sum_{l=1}^{2^N} exp(-E(\sigma^l(t)|\mathbf{h},\mathbf{J}))\big] &= \frac{-1}{\sum_{l=1}^{2^N} exp(-E(\sigma^l(t)|\mathbf{h},\mathbf{J}))}\frac{\partial}{\partial h_i} exp(-E(\sigma^l(t)|\mathbf{h},\mathbf{J})) \\
&= -\frac{\sum_{l=1}^{2^N}\sigma_i^l(t) exp(-E(\boldsymbol{\sigma}^l(t)|\mathbf{h},\mathbf{J}))}{\sum_{l=1}^{2^N} exp(-E(\boldsymbol{\sigma}^l(t)|\mathbf{h},\mathbf{J}))} \\
&= -\sum_{l=1}^{2^N}\sigma_i^l P(\boldsymbol{\sigma}^l|\mathbf{h},\mathbf{J}) \\
&= -\langle\sigma_i\rangle_{model} \qquad \text{(A.13)}
\end{aligned}$$

Finally, we substitute the terms (A.12) and (A.13) into the equation (A.11).

$$\begin{aligned}
h_i^{new} - h_i^{old} &= \frac{\epsilon}{t_{max}}\frac{\partial}{\partial h_i}\log\mathcal{L}(\mathbf{h},\mathbf{J}) \\
&= \frac{\epsilon}{t_{max}}\sum_{t=1}^{t_{max}}\big[\sigma_i(t) - \langle\sigma_i\rangle_{model}\big] \\
&= \epsilon(\langle\sigma_i\rangle_{empirical} - \langle\sigma_i\rangle_{model}) \quad \textbf{(Q.E.D)} \qquad \text{(A.14)}
\end{aligned}$$

Next, we also derive $\epsilon(\langle\sigma_i\sigma_j\rangle_{empirical} - \langle\sigma_i\sigma_j\rangle_{model})$ from the equation (**??**). Here,

$$\begin{aligned}
\frac{\partial}{\partial J_{ij}}\log\mathcal{L}(\mathbf{h},\mathbf{J}) &= \frac{\partial}{\partial J_{ij}}\log\prod_{t=1}^{t_{max}} P(\boldsymbol{\sigma}(t)|\mathbf{h},\mathbf{J}) \\
&= \frac{\partial}{\partial J_{ij}}\sum_{t=1}^{t_{max}}\log P(\boldsymbol{\sigma}(t)|\mathbf{h},\mathbf{J}) \\
&= \sum_{t=1}^{t_{max}}\frac{\partial}{\partial J_{ij}}\Big[-E(\boldsymbol{\sigma}(t)|\mathbf{h},\mathbf{J}) - \log\sum_{l=1}^{2^N} exp(-E(\boldsymbol{\sigma}^l(t)|\mathbf{h},\mathbf{J}))\Big]
\end{aligned} \qquad \text{(A.15)}$$

In order to calculate the equation (A.15), we calculate $\frac{\partial}{\partial J_{ij}}\Big[-E\Big]$ and $\frac{\partial}{\partial J_{ij}}\Big[\log\sum_{l=1}^{2^N} exp(-E)\Big]$, respectively.

$$\begin{aligned}
\frac{\partial}{\partial J_{ij}}\big[-E(\boldsymbol{\sigma}(t)|\mathbf{h},\mathbf{J})\big] &= \frac{\partial}{\partial J_{ij}}\Big[\sum_{i=1}^{N} h_i\sigma_i(t) + \frac{1}{2}\sum_{i=1}^{N}\sum_{j=1,j\neq i}^{N} J_{ij}\sigma_i(t)\sigma_j(t)\Big] \\
&= \sigma_i(t)\sigma_j(t) \qquad \text{(A.16)}
\end{aligned}$$

$$\begin{aligned}
\frac{\partial}{\partial J_{ij}} \log \sum_{l=1}^{2^N} exp(-E(\boldsymbol{\sigma}^l(t)|\mathbf{h},\mathbf{J})) &= \frac{1}{\sum_{l=1}^{2^N} exp(-E(\boldsymbol{\sigma}^l(t)|\mathbf{h},\mathbf{J}))} \sum_{l=1}^{2^N} \frac{\partial}{\partial J_{ij}} exp(-E(\boldsymbol{\sigma}^l(t)|\mathbf{h},\mathbf{J})) \\
&= \sum_{l=1}^{2^N} \sigma_i^l \sigma_j^l \frac{exp(-E(\boldsymbol{\sigma}^l(t)|\mathbf{h},\mathbf{J}))}{\sum_{l=1}^{2^N} exp(-E(\boldsymbol{\sigma}^l(t)|\mathbf{h},\mathbf{J}))} \\
&= \sum_{l=1}^{2^N} \sigma_i^l \sigma_j^l P(\boldsymbol{\sigma}^l|\mathbf{h},\mathbf{J}) \\
&= \langle \sigma_i \sigma_j \rangle_{model} \qquad (A.17)
\end{aligned}$$

By substituting terms (A.16) and (A.17) into the equation (A.15),

$$\begin{aligned}
J_{ij}^{new} - J_{ij}^{old} &= \frac{\epsilon}{t_{max}} \sum_{t=1}^{t_{max}} \frac{\partial}{\partial J_{ij}} \Big[-E - \log \sum_{\sigma'} exp(-E) \Big] \\
&= \frac{\epsilon}{t_{max}} \sum_{t=1}^{t_{max}} \big[\sigma_i(t)\sigma_j(t) - \langle \sigma_i \sigma_j \rangle_{model} \big] \\
&= \epsilon(\langle \sigma_i \sigma_j \rangle_{empirical} - \langle \sigma_i \sigma_j \rangle_{model}) \quad (\textbf{Q.E.D}) \qquad (A.18)
\end{aligned}$$

A.4.4 Energy barriers

Furthermore, the energy barrier for the transition from $\sigma^{(\alpha)}$ to $\sigma^{(\beta)}$ is calculated by $\bar{E}_{\alpha\beta} - E(\sigma^{(\alpha)})$.

The algorithm is to calculate $\bar{E}_{\alpha\beta}$ shown as below.

Step 1. ascendingly enumerate local minimums.

Step 2. pick up the un-used smallest local minimum, and finalize $\bar{E}_{\alpha\alpha} = E(\sigma^{(\alpha)})$, $\bar{E}_{\alpha\beta} = E(\sigma^{(\beta)})$ for all neighboring local minimums of $\sigma^{(\alpha)}$.

Step 3. Initialize $\bar{E}_{\alpha\beta'}$ for non-neighboring $2^N - N - 1$ local minimums $\sigma^{(\beta')}$ with ∞.

Step 4. Using each finalized $\sigma^{(\beta)}$, update $E_{\alpha\beta'}$ for its all unfinalized neighbors with

$$\bar{E}_{\alpha\beta'}^{new} = \begin{cases} min(\bar{E}_{\alpha\beta'}^{old}, \bar{E}_{\alpha\beta}), & (\bar{E}_{\alpha\beta} \geq E(\sigma^{(\beta')})) \\ E(\sigma^{(\beta')}), & (\bar{E}_{\alpha\beta} < E(\sigma^{(\beta')})) \end{cases} \qquad (A.19)$$

In this way, we finalize β', which are neighbors of β.

Step 5. set $\beta = \beta'$, $\beta' =$ neighbors of finalized β'.

Step 6. Repeat Step. 4 and 5 until all the pairs local minimums $\bar{E}_{\alpha\beta}$ for a given $\sigma^{(\alpha)}$ are finalized.

Step 7. Repeat Step. 2-6 with un-used smallest local minimum until all the given paris $\bar{E}_{\alpha\beta}$ are finalized.

A.4.5 Basin Size

We defined local minima based on the algorithm in section A.4.4. We further can define basin size in which each brain activity pattern belongs to as shown below.

Step 1. set unused state σ^l, and move to smallest neighboring states.

Step 2. repeat Step1. until we reach the local minimum E(σ^α) which there is no smaller neighboring states. Then, we regard that the σ^l belongs to the local minimum σ^α.

Step 3. repeat Step 1. and 2. until we define where all states belong to.

Step 4. calculate a basin size based on the number of brain states, which belongs to a local minimum. We used the fraction of brain states given a local minimum to the number of possible brain states as a basin size in this study.

A.5 Louvain Algorithm

For network clustering, we exploited a modularity-maximization method, the Louvain algorithm. We describe mathematical definitions of modularity for signed graphs and the louvain algorithm as implemented in the Brain Connectivity Toolbox (see Supplementary Table.A.1).

A.5.1 Modularity-based partitioning approach

In our analysis, brain complex network are un-directed and fully connected. For n nodes, a network is composed of $\frac{n(n-1)}{2}$ positive or negative connections. We also denote positive and negative connections as following.

Regarding a positive or negative connection between node i and node j,

$$w_{ij}^{\pm} \subset (0, 1] \tag{A.20}$$

Algorithm 1 Louvain algorithm

```
1: procedure LOUVAIN(W)
2:     n: the number of nodes
3:     M: community assignments
4:     Q_old = −1, Q_new = 0: set initial modularity value
5:     while Q_new − Q_old > 1e^−10 do                ▷ fine tuning of modularity
6:         Q_old ← Q_new
7:         Q_0 ← −∞
8:         Calculate temporal modularity Q_cur based on M
9:         while Q_cur − Q_0 > 1e^−10 do                          ▷ main iteration
10:            for node_i  from <randomly sorted nodes> do
11:                c_x = ΔQ                                  ▷ c_x is a community id
12:                M_node_i ← c_x
               end
13:            Q_0 ← Q_cur
14:            Calculate modularity Q_curbased on revised M
           end
15:        Q_new ← Q_cur
       end
16:    return M, Q_new
```

The positive or negative strength $s^{\pm}$ of node i means the total values of positive or negative connection weights of the node i, respectively.

$$s_i^{\pm} = \sum_j w_{ij}^{\pm} \tag{A.21}$$

The positive or negative total weights v of a brain network is defined by the total values of all positive or negative links, respectively.

$$v^{\pm} = \sum_i \sum_j w_{ij}^{\pm} \tag{A.22}$$

Given the definitions, we first initialize assignments to community id. Modularity is then iteratively calculated by assigning each remaining community to each node, and a community id giving maximal modularity was reassigned to each node. Until modularity is stable, we continue iterating this process.

A.5.2 Louvain algorithm for weighted undirected graphs

Multiple network clustering methods have been suggest to partition network graphs into subdivisions for analyzing internal subgraphs. In this concurrent study, we employed a version of the Louvain algorithm for undirected and signed graphs [158]. Some studies removed negative connections due to uncertainty of interpretations. However, some information removals have been also pointed out. Hence, we consider negative

weights in functional brain networks as well. It is assumed that positive connections are the explicit core of module association of nodes, and negative connections are the implicit support of module associations among nodes.

For a undirected and signed graph, modularity Q has been proposed as following.

$$Q^{\pm} = \frac{1}{v^{\pm}} \sum_i \sum_j (w_{ij}^{\pm} - e_{ij}^{\pm}) \delta_{M_i M_j} \tag{A.23}$$

$$\delta_{M_i M_j} = \begin{cases} 1, & \text{if } M_i = M_j \\ 0, & \text{otherwise} \end{cases} \tag{A.24}$$

where $e_{ij}^{\pm} = \frac{s_i^{\pm} s_j^{\pm}}{v^{\pm}}$, and M_i indicates which module the node i belongs to.

We followed assumptions of the asymmetrical importance of positive and negative connections over functional brain networks. Finally, the modularity Q was used for the algorithm.

$$Q = Q^{+} + \frac{v^{-}}{v^{+} + v^{-}} Q^{-} \tag{A.25}$$

$$= \frac{1}{v^{+}} \sum_i \sum_j (w_{ij}^{+} - e_{ij}^{+}) - \frac{1}{v^{+} + v^{-}} \sum_i \sum_j (w_{ij}^{-} - e_{ij}^{-}) \tag{A.26}$$

A.5.3 Community Detection

We performed network clustering with a community detection algorithm, the Louvain algorithm [18, 144]. The Louvain algorithm is a clustering approach by maximizing the modularity. We adopted a version of the algorithm considering signed and undirected graphs [158], implemented in Brain Connectivity Toolbox (BCT) [157].

Because the Louvain algorithm is none-deterministic, in order to assess the robustness of the partition results, we applied this algorithm to the averaged functional network in the ELA-defined intermediate states from each session. 10000 independent runs were performed with randomly ordered initial clustering. Our results resulted in 100% consistent partitions for all sessions.

A.5.4 Module partitioning and the intermediate states

Previous human imaging study found association between brain states from ELA and underling functional modular structures. We also sought to investigate the functional mouse brain in our study. We then applied the community detection algorithm, Louvain algorithm for extracting modular networks to the functional connectivity matrix for each session. The result was that modular partitioning was identical to the binarized states in the intermediate states (Supplementary Figure. A.3).

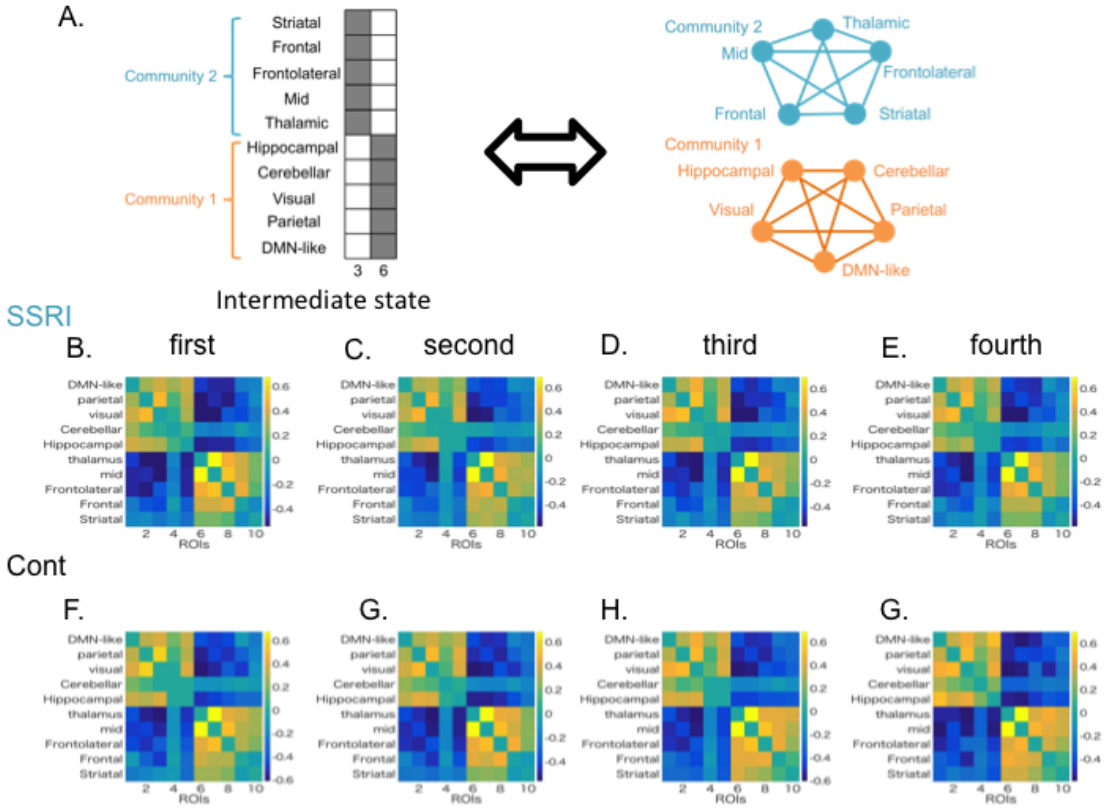

Figure A.3: A. We defined 3rd and 6th states as the intermediate states. Partition of the intermediate states is complementary each other. Network structure from brain signals may underly such cluster partition. Therefore, we compared between brain activity patterns and module partition in each session. We observed brain activity patterns matched to module partition in any sessions. B-E. Functional connectivity matrix aligned with the module partitioning result from first to fourth sessions in SSRI group, respectively. F-G. Functional connectivity matrix aligned with the module partitioning result from first to fourth sessions in control group, respectively.

A.6 Motion artifacts and BOLD signals

We sought to study whether there are motion artifacts in the sessions of resting-state, blue stimulation, and yellow light stimulation (Supplementary Figure.A.4). Motion artifacts of x, y, and z axes were detected by thersholding voxel size of the imaging sessions (200 μm). We found no artifacts in the resting state session and multiple artifacts in the blue and yellow sessions (Supplementary Table. A.2). As we found light leak from the skull during illumination, the finding suggest that light illumination induced motion artifacts. Furthermore, association between motion artifacts and BOLD signals in the DRN were studied in the sessions of resting-state, blue stimulation, and yellow light stimulation (Supplementary Table. A.2). We found significant correlation between motion artifacts and the BOLD signals. The finding suggest potential contamination of the motion artifacts in the BOLD signals.

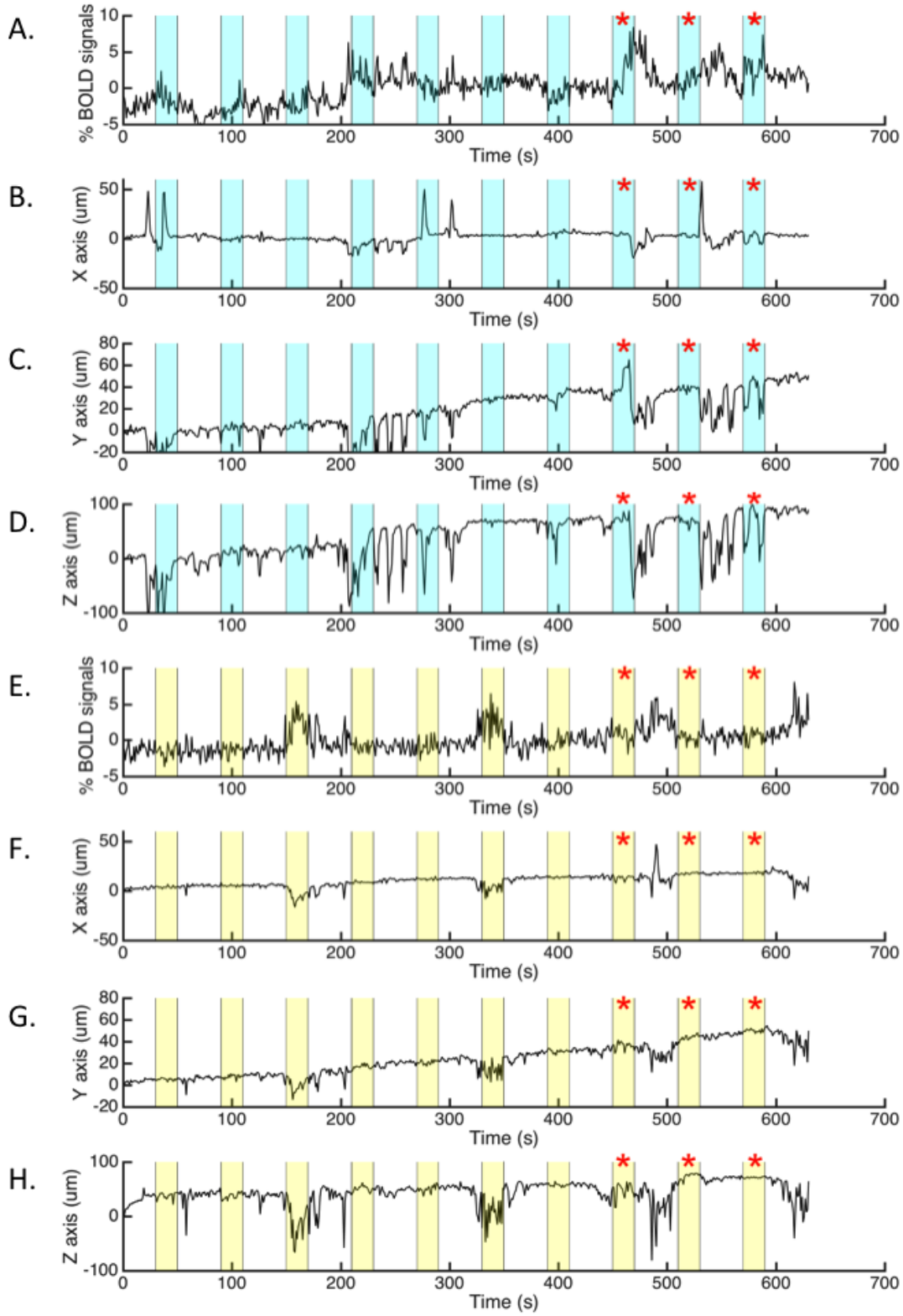

Figure A.4: A. time-series of BOLD signals from DRN in blue light session. B-D. X,Y,Z axis movements in the blue light stimulation, respectively. E. time-series of BOLD signals from DRN in the yellow light session. F-H. X,Y,Z axis movements in the yellow light stimulation, respectively. Blue and yellow color backgrounds indicate blue light and yellow light stimulation, respectively. * marks indicate selected stimulations for further analysis (Figure. 4.2).

Measure	REST session	Blue light session	Yellow light session
X axis artifact	0	6	1
Y axis artifact	0	13	4
Z axis artifact	0	50	39
diff X	a.v.=0.0357 (SD=5.7806)	a.v.= 0.0597 (μm) (SD=49)	a.v.=0.2331 (SD=33.3222)
diff Y	a.v.=0.1593 (SD=7.6838)	a.v.= 0.8045 (SD=79)	a.v.= 0.7929 (SD=45.3046)
diff Z	a.v.=0.2946 (SD=21.9261)	a.v.= 1.4171 (SD=79)	a.v.=1.0242 (SD=178.2535)
Corr with X axis	$r = -0.49$ ($P < 1e^{-12}$)	$r = -0.41$ ($P < 1e^{-8}$)	$r = -0.33$ ($P < 1e^{-5}$)
Corr with Y axis	$r = -0.49$ ($P < 1e^{-12}$)	$r = -0.42$ ($P < 1e^{-8}$)	$r = -0.61$ ($P < 1e^{-19}$)
Corr with Z axis	$r = -0.77$ ($P < 1e^{-35}$)	$r = -0.58$ ($P < 1e^{-17}$)	$r = -0.69$ ($P < 1e^{-26}$)

Table A.2: a.v.= avarage, SD = standard deviation

Bibliography

[1] Abrams, J. K., Johnson, P. L., Hollis, J. H., and Lowry, C. A. (2004). Anatomic and functional topography of the dorsal raphe nucleus. *Ann N Y Acad Sci*, 1018:46–57.

[2] Amat, J., Baratta, M. V., Paul, E., Bland, S. T., Watkins, L. R., and Maier, S. F. (2005). Medial prefrontal cortex determines how stressor controllability affects behavior and dorsal raphe nucleus. *Nat Neurosci*, 8(3):365–71.

[3] Arborelius, L., Nomikos, G. G., Grillner, P., Hertel, P., Hook, B. B., Hacksell, U., and Svensson, T. H. (1995). 5-ht1a receptor antagonists increase the activity of serotonergic cells in the dorsal raphe nucleus in rats treated acutely or chronically with citalopram. *Naunyn Schmiedebergs Arch Pharmacol*, 352(2):157–65.

[4] Ashourvan, A., Gu, S., Mattar, M. G., Vettel, J. M., and Bassett, D. S. (2017). The energy landscape underpinning module dynamics in the human brain connectome. *Neuroimage*, 157:364–380.

[5] Bagot, R. C., Cates, H. M., Purushothaman, I., Vialou, V., Heller, E. A., Yieh, L., LaBonte, B., Pena, C. J., Shen, L., Wittenberg, G. M., and Nestler, E. J. (2017). Ketamine and imipramine reverse transcriptional signatures of susceptibility and induce resilience-specific gene expression profiles. *Biol Psychiatry*, 81(4):285–295.

[6] Barrett, F. S., Workman, C. I., Sair, H. I., Savonenko, A. V., Kraut, M. A., Sodums, D. J., Joo, J. J., Nassery, N., Marano, C. M., Munro, C. A., Brandt, J., Zhou, Y., Wong, D. F., and Smith, G. S. (2017). Association between serotonin denervation and resting-state functional connectivity in mild cognitive impairment. *Hum Brain Mapp*.

[7] Bartelle, B. B., Barandov, A., and Jasanoff, A. (2016). Molecular fmri. *J Neurosci*, 36(15):4139–48.

[8] Bassett, D. S., Porter, M. A., Wymbs, N. F., Grafton, S. T., Carlson, J. M., and Mucha, P. J. (2013). Robust detection of dynamic community structure in networks. *Chaos*, 23(1):013142.

[9] Belcher, A. M., Yen, C. C., Stepp, H., Gu, H., Lu, H., Yang, Y., Silva, A. C., and Stein, E. A. (2013). Large-scale brain networks in the awake, truly resting marmoset monkey. *J Neurosci*, 33(42):16796–804.

[10] Belzung, C. and Lemoine, M. (2011). Criteria of validity for animal models of psychiatric disorders: focus on anxiety disorders and depression. *Biol Mood Anxiety Disord*, 1(1):9.

[11] Bernal-Casas, D., Lee, H. J., Weitz, A. J., and Lee, J. H. (2017). Studying brain circuit function with dynamic causal modeling for optogenetic fmri. *Neuron*, 93(3):522–532 e5.

[12] Berndt, A., Yizhar, O., Gunaydin, L. A., Hegemann, P., and Deisseroth, K. (2009). Bi-stable neural state switches. *Nat Neurosci*, 12(2):229–34.

[13] Berton, O., Covington, H. E., r., Ebner, K., Tsankova, N. M., Carle, T. L., Ulery, P., Bhonsle, A., Barrot, M., Krishnan, V., Singewald, G. M., Singewald, N., Birnbaum, S., Neve, R. L., and Nestler, E. J. (2007). Induction of deltafosb in the periaqueductal gray by stress promotes active coping responses. *Neuron*, 55(2):289–300.

[14] Bicks, L. K., Koike, H., Akbarian, S., and Morishita, H. (2015). Prefrontal cortex and social cognition in mouse and man. *Front Psychol*, 6:1805.

[15] Biswal, B., Yetkin, F. Z., Haughton, V. M., and Hyde, J. S. (1995). Functional connectivity in the motor cortex of resting human brain using echo-planar mri. *Magn Reson Med*, 34(4):537–41.

[16] Bland, S. T., Twining, C., Watkins, L. R., and Maier, S. F. (2003). Stressor controllability modulates stress-induced serotonin but not dopamine efflux in the nucleus accumbens shell. *Synapse*, 49(3):206–8.

[17] Blier, P. and Ward, N. M. (2003). Is there a role for 5-ht1a agonists in the treatment of depression? *Biol Psychiatry*, 53(3):193–203.

[18] Blondel, V. D., Guillaume, J. L., Lambiotte, R., and Lefebvre, E. (2008). Fast unfolding of communities in large networks. *Journal of Statistical Mechanics-Theory and Experiment*.

[19] Bouet, V., Klomp, A., Freret, T., Wylezinska-Arridge, M., Lopez-Tremoleda, J., Dauphin, F., Boulouard, M., Booij, J., Gsell, W., and Reneman, L. (2012). Age-dependent effects of chronic fluoxetine treatment on the serotonergic system one week following treatment. *Psychopharmacology (Berl)*, 221(2):329–39.

[20] Boureau, Y. L. and Dayan, P. (2011). Opponency revisited: competition and cooperation between dopamine and serotonin. *Neuropsychopharmacology*, 36(1):74–97.

[21] Branchi, I. (2011). The double edged sword of neural plasticity: increasing serotonin levels leads to both greater vulnerability to depression and improved capacity to recover. *Psychoneuroendocrinology*, 36(3):339–51.

[22] Brocka, M., Helbing, C., Vincenz, D., Scherf, T., Montag, D., Goldschmidt, J., Angenstein, F., and Lippert, M. (2018). Contributions of dopaminergic and non-dopaminergic neurons to vta-stimulation induced neurovascular responses in brain reward circuits. *Neuroimage*, 177:88–97.

[23] Bromberg-Martin, E. S., Hikosaka, O., and Nakamura, K. (2010). Coding of task reward value in the dorsal raphe nucleus. *J Neurosci*, 30(18):6262–72.

[24] Burghardt, N. S. and Bauer, E. P. (2013). Acute and chronic effects of selective serotonin reuptake inhibitor treatment on fear conditioning: implications for underlying fear circuits. *Neuroscience*, 247:253–72.

[25] Buzsaki, G. and Draguhn, A. (2004). Neuronal oscillations in cortical networks. *Science*, 304(5679):1926–9.

[26] Bzdok, D. and Yeo, B. T. T. (2017). Inference in the age of big data: Future perspectives on neuroscience. *Neuroimage*, 155:549–564.

[27] Calhoun, V. D., Miller, R., Pearlson, G., and Adali, T. (2014). The chronnectome: time-varying connectivity networks as the next frontier in fmri data discovery. *Neuron*, 84(2):262–74.

[28] Calizo, L. H., Akanwa, A., Ma, X., Pan, Y. Z., Lemos, J. C., Craige, C., Heemstra, L. A., and Beck, S. G. (2011). Raphe serotonin neurons are not homogenous: electrophysiological, morphological and neurochemical evidence. *Neuropharmacology*, 61(3):524–43.

[29] Celada, P., Puig, M., Amargos-Bosch, M., Adell, A., and Artigas, F. (2004). The therapeutic role of 5-ht1a and 5-ht2a receptors in depression. *J Psychiatry Neurosci*, 29(4):252–65.

[30] Celada, P., Puig, M. V., and Artigas, F. (2013). Serotonin modulation of cortical neurons and networks. *Front Integr Neurosci*, 7:25.

[31] Challis, C., Beck, S. G., and Berton, O. (2014). Optogenetic modulation of descending prefrontocortical inputs to the dorsal raphe bidirectionally bias socioaffective choices after social defeat. *Front Behav Neurosci*, 8:43.

[32] Chourbaji, S., Zacher, C., Sanchis-Segura, C., Dormann, C., Vollmayr, B., and Gass, P. (2005). Learned helplessness: validity and reliability of depressive-like states in mice. *Brain Res Brain Res Protoc*, 16(1-3):70–8.

[33] Christie, I. N., Wells, J. A., Southern, P., Marina, N., Kasparov, S., Gourine, A. V., and Lythgoe, M. F. (2013). fmri response to blue light delivery in the naive brain: implications for combined optogenetic fmri studies. *Neuroimage*, 66:634–41.

[34] Christoff, K., Gordon, A. M., Smallwood, J., Smith, R., and Schooler, J. W. (2009). Experience sampling during fmri reveals default network and executive system contributions to mind wandering. *Proc Natl Acad Sci U S A*, 106(21):8719–24.

[35] Christoff, K., Irving, Z. C., Fox, K. C., Spreng, R. N., and Andrews-Hanna, J. R. (2016). Mind-wandering as spontaneous thought: a dynamic framework. *Nat Rev Neurosci*, 17(11):718–731.

[36] Cohen, J. Y. (2015). Dopamine and serotonin signals for reward across time scales. *Science*, 350(6256):47.

[37] Cooney, R. E., Joormann, J., Eugene, F., Dennis, E. L., and Gotlib, I. H. (2010). Neural correlates of rumination in depression. *Cogn Affect Behav Neurosci*, 10(4):470–8.

[38] Correia, P. A., Lottem, E., Banerjee, D., Machado, A. S., Carey, M. R., and Mainen, Z. F. (2017). Transient inhibition and long-term facilitation of locomotion by phasic optogenetic activation of serotonin neurons. *Elife*, 6.

[39] Courtney, N. A. and Ford, C. P. (2016). Mechanisms of 5-ht1a receptor-mediated transmission in dorsal raphe serotonin neurons. *J Physiol*, 594(4):953–65.

[40] Cowen, P. (1991). Serotonin receptor subtypes: implications for psychopharmacology. *Br J Psychiatry Suppl*, (12):7–14.

[41] Crawford, L. K., Craige, C. P., and Beck, S. G. (2010). Increased intrinsic excitability of lateral wing serotonin neurons of the dorsal raphe: a mechanism for selective activation in stress circuits. *J Neurophysiol*, 103(5):2652–63.

[42] Crawford, L. K., Rahman, S. F., and Beck, S. G. (2013). Social stress alters inhibitory synaptic input to distinct subpopulations of raphe serotonin neurons. *ACS Chem Neurosci*, 4(1):200–9.

[43] Crockett, M. J., Clark, L., Apergis-Schoute, A. M., Morein-Zamir, S., and Robbins, T. W. (2012). Serotonin modulates the effects of pavlovian aversive predictions on response vigor. *Neuropsychopharmacology*, 37(10):2244–52.

[44] Crockett, M. J., Clark, L., and Robbins, T. W. (2009). Reconciling the role of serotonin in behavioral inhibition and aversion: acute tryptophan depletion abolishes punishment-induced inhibition in humans. *J Neurosci*, 29(38):11993–9.

[45] Daw, N. D., Kakade, S., and Dayan, P. (2002). Opponent interactions between serotonin and dopamine. *Neural Netw*, 15(4-6):603–16.

[46] Dayan, P. and Huys, Q. (2015). Serotonin's many meanings elude simple theories. *Elife*, 4.

[47] Dayan, P. and Huys, Q. J. (2008). Serotonin, inhibition, and negative mood. *PLoS Comput Biol*, 4(2):e4.

[48] Deco, G. and Kringelbach, M. L. (2016a). Metastability and coherence: Extending the communication through coherence hypothesis using a whole-brain computational perspective. *Trends Neurosci*, 39(3):125–135.

[49] Deco, G. and Kringelbach, M. L. (2016b). Metastability and coherence: Extending the communication through coherence hypothesis using a whole-brain computational perspective. *Trends Neurosci*, 39(3):125–135.

[50] Deco, G., Kringelbach, M. L., Jirsa, V. K., and Ritter, P. (2017). The dynamics of resting fluctuations in the brain: metastability and its dynamical cortical core. *Sci Rep*, 7(1):3095.

[51] Deco, G., Ponce-Alvarez, A., Mantini, D., Romani, G. L., Hagmann, P., and Corbetta, M. (2013). Resting-state functional connectivity emerges from structurally and dynamically shaped slow linear fluctuations. *J Neurosci*, 33(27):11239–52.

[52] Deco, G., Senden, M., and Jirsa, V. (2012). How anatomy shapes dynamics: a semi-analytical study of the brain at rest by a simple spin model. *Front Comput Neurosci*, 6:68.

[53] Decot, H. K., Namboodiri, V. M., Gao, W., McHenry, J. A., Jennings, J. H., Lee, S. H., Kantak, P. A., Jill Kao, Y. C., Das, M., Witten, I. B., Deisseroth, K., Shih, Y. I., and Stuber, G. D. (2017). Coordination of brain-wide activity dynamics by dopaminergic neurons. *Neuropsychopharmacology*, 42(3):615–627.

[54] Demirtas, M., Tornador, C., Falcon, C., Lopez-Sola, M., Hernandez-Ribas, R., Pujol, J., Menchon, J. M., Ritter, P., Cardoner, N., Soriano-Mas, C., and Deco, G. (2016). Dynamic functional connectivity reveals altered variability in functional connectivity among patients with major depressive disorder. *Hum Brain Mapp*, 37(8):2918–30.

[55] Denk, F., Walton, M. E., Jennings, K. A., Sharp, T., Rushworth, M. F., and Bannerman, D. M. (2005). Differential involvement of serotonin and dopamine systems in cost-benefit decisions about delay or effort. *Psychopharmacology (Berl)*, 179(3):587–96.

[56] Desai, M., Kahn, I., Knoblich, U., Bernstein, J., Atallah, H., Yang, A., Kopell, N., Buckner, R. L., Graybiel, A. M., Moore, C. I., and Boyden, E. S. (2011). Mapping brain networks in awake mice using combined optical neural control and fmri. *J Neurophysiol*, 105(3):1393–405.

[57] Doya, K. (2002). Metalearning and neuromodulation. *Neural Netw*, 15(4-6):495–506.

[58] Driessen, E. and Hollon, S. D. (2010). Cognitive behavioral therapy for mood disorders: efficacy, moderators and mediators. *Psychiatr Clin North Am*, 33(3):537–55.

[59] Ezaki, T., Sakaki, M., Watanabe, T., and Masuda, N. (2018). Age-related changes in the ease of dynamical transitions in human brain activity. *Hum Brain Mapp*, 39(6):2673–2688.

[60] Ezaki, T., Watanabe, T., Ohzeki, M., and Masuda, N. (2017). Energy landscape analysis of neuroimaging data. *Philos Trans A Math Phys Eng Sci*, 375(2096).

[61] Faulkner, P. and Deakin, J. F. (2014). The role of serotonin in reward, punishment and behavioural inhibition in humans: insights from studies with acute tryptophan depletion. *Neurosci Biobehav Rev*, 46 Pt 3:365–78.

[62] Ferenczi, E. A., Zalocusky, K. A., Liston, C., Grosenick, L., Warden, M. R., Amatya, D., Katovich, K., Mehta, H., Patenaude, B., Ramakrishnan, C., Kalanithi, P., Etkin, A., Knutson, B., Glover, G. H., and Deisseroth, K. (2016). Prefrontal cortical regulation of brainwide circuit dynamics and reward-related behavior. *Science*, 351(6268):aac9698.

[63] Finc, K., Bonna, K., Lewandowska, M., Wolak, T., Nikadon, J., Dreszer, J., Duch, W., and Kuhn, S. (2017). Transition of the functional brain network related to increasing cognitive demands. *Hum Brain Mapp*.

[64] Finn, E. S., Shen, X., Scheinost, D., Rosenberg, M. D., Huang, J., Chun, M. M., Papademetris, X., and Constable, R. T. (2015). Functional connectome fingerprinting: identifying individuals using patterns of brain connectivity. *Nat Neurosci*, 18(11):1664–71.

[65] Fischer, A. G. and Ullsperger, M. (2017). An update on the role of serotonin and its interplay with dopamine for reward. *Front Hum Neurosci*, 11:484.

[66] Fonseca, M. S., Murakami, M., and Mainen, Z. F. (2015). Activation of dorsal raphe serotonergic neurons promotes waiting but is not reinforcing. *Curr Biol*, 25(3):306–315.

[67] Fox, K. C., Spreng, R. N., Ellamil, M., Andrews-Hanna, J. R., and Christoff, K. (2015). The wandering brain: meta-analysis of functional neuroimaging studies of mind-wandering and related spontaneous thought processes. *Neuroimage*, 111:611–21.

[68] Fox, M. D. and Greicius, M. (2010). Clinical applications of resting state functional connectivity. *Front Syst Neurosci*, 4:19.

[69] Fox, M. D., Snyder, A. Z., Vincent, J. L., Corbetta, M., Van Essen, D. C., and Raichle, M. E. (2005). The human brain is intrinsically organized into dynamic, anticorrelated functional networks. *Proc Natl Acad Sci U S A*, 102(27):9673–8.

[70] Gaspar, P. and Lillesaar, C. (2012). Probing the diversity of serotonin neurons. *Philos Trans R Soc Lond B Biol Sci*, 367(1601):2382–94.

[71] Giorgi, A., Migliarini, S., Galbusera, A., Maddaloni, G., Mereu, M., Margiani, G., Gritti, M., Landi, S., Trovato, F., Bertozzi, S. M., Armirotti, A., Ratto, G. M., De Luca, M. A., Tonini, R., Gozzi, A., and Pasqualetti, M. (2017). Brain-wide mapping of endogenous serotonergic transmission via chemogenetic fmri. *Cell Rep*, 21(4):910–918.

[72] Golden, S. A., Covington, H. E., r., Berton, O., and Russo, S. J. (2011). A standardized protocol for repeated social defeat stress in mice. *Nat Protoc*, 6(8):1183–91.

[73] Gordon, J. A. and Hen, R. (2004). The serotonergic system and anxiety. *Neuromolecular Med*, 5(1):27–40.

[74] Gorka, A. X., Torrisi, S., Shackman, A. J., Grillon, C., and Ernst, M. (2018). Intrinsic functional connectivity of the central nucleus of the amygdala and bed nucleus of the stria terminalis. *Neuroimage*, 168:392–402.

[75] Gratton, C., Laumann, T. O., Nielsen, A. N., Greene, D. J., Gordon, E. M., Gilmore, A. W., Nelson, S. M., Coalson, R. S., Snyder, A. Z., Schlaggar, B. L., Dosenbach, N. U. F., and Petersen, S. E. (2018). Functional brain networks are dominated by stable group and individual factors, not cognitive or daily variation. *Neuron*, 98(2):439–452 e5.

[76] Greicius, M. D., Flores, B. H., Menon, V., Glover, G. H., Solvason, H. B., Kenna, H., Reiss, A. L., and Schatzberg, A. F. (2007). Resting-state functional connectivity in major depression: abnormally increased contributions from subgenual cingulate cortex and thalamus. *Biol Psychiatry*, 62(5):429–37.

[77] Greicius, M. D., Krasnow, B., Reiss, A. L., and Menon, V. (2003). Functional connectivity in the resting brain: a network analysis of the default mode hypothesis. *Proc Natl Acad Sci U S A*, 100(1):253–8.

[78] Greicius, M. D., Supekar, K., Menon, V., and Dougherty, R. F. (2009). Resting-state functional connectivity reflects structural connectivity in the default mode network. *Cereb Cortex*, 19(1):72–8.

[79] Gruberger, M., Ben-Simon, E., Levkovitz, Y., Zangen, A., and Hendler, T. (2011). Towards a neuroscience of mind-wandering. *Front Hum Neurosci*, 5:56.

[80] Gu, S., Cieslak, M., Baird, B., Muldoon, S. F., Grafton, S. T., Pasqualetti, F., and Bassett, D. S. (2018). The energy landscape of neurophysiological activity implicit in brain network structure. *Sci Rep*, 8(1):2507.

[81] Hagmann, P., Jonasson, L., Maeder, P., Thiran, J. P., Wedeen, V. J., and Meuli, R. (2006). Understanding diffusion mr imaging techniques: from scalar diffusion-weighted imaging to diffusion tensor imaging and beyond. *Radiographics*, 26 Suppl 1:S205–23.

[82] Hai, A., Cai, L. X., Lee, T., Lelyveld, V. S., and Jasanoff, A. (2016). Molecular fmri of serotonin transport. *Neuron*, 92(4):754–765.

[83] Hansen, E. C., Battaglia, D., Spiegler, A., Deco, G., and Jirsa, V. K. (2015). Functional connectivity dynamics: modeling the switching behavior of the resting state. *Neuroimage*, 105:525–35.

[84] Hanson, N. D., Owens, M. J., and Nemeroff, C. B. (2011). Depression, antidepressants, and neurogenesis: a critical reappraisal. *Neuropsychopharmacology*, 36(13):2589–602.

[85] Hayashi, K., Nakao, K., and Nakamura, K. (2015). Appetitive and aversive information coding in the primate dorsal raphe nucleus. *J Neurosci*, 35(15):6195–208.

[86] Hearne, L. J., Mattingley, J. B., and Cocchi, L. (2016). Functional brain networks related to individual differences in human intelligence at rest. *Sci Rep*, 6:32328.

[87] Hikishima, K., Komaki, Y., Seki, F., Ohnishi, Y., Okano, H. J., and Okano, H. (2017). In vivo microscopic voxel-based morphometry with a brain template to characterize strain-specific structures in the mouse brain. *Sci Rep*, 7(1):85.

[88] Himberg, J., Hyvarinen, A., and Esposito, F. (2004). Validating the independent components of neuroimaging time series via clustering and visualization. *Neuroimage*, 22(3):1214–22.

[89] Hollerman, J. R. and Schultz, W. (1998). Dopamine neurons report an error in the temporal prediction of reward during learning. *Nat Neurosci*, 1(4):304–9.

[90] Honey, C. J., Sporns, O., Cammoun, L., Gigandet, X., Thiran, J. P., Meuli, R., and Hagmann, P. (2009). Predicting human resting-state functional connectivity from structural connectivity. *Proc Natl Acad Sci U S A*, 106(6):2035–40.

[91] Hornung, J. P. (2003). The human raphe nuclei and the serotonergic system. *J Chem Neuroanat*, 26(4):331–43.

[92] Hou, J. M., Zhao, M., Zhang, W., Song, L. H., Wu, W. J., Wang, J., Zhou, D. Q., Xie, B., He, M., Guo, J. W., Qu, W., and Li, H. T. (2014). Resting-state functional connectivity abnormalities in patients with obsessive-compulsive disorder and their healthy first-degree relatives. *J Psychiatry Neurosci*, 39(5):304–11.

[93] Hoyer, C., Gass, N., Weber-Fahr, W., and Sartorius, A. (2014). Advantages and challenges of small animal magnetic resonance imaging as a translational tool. *Neuropsychobiology*, 69(4):187–201.

[94] Hultman, R., Ulrich, K., Sachs, B. D., Blount, C., Carlson, D. E., Ndubuizu, N., Bagot, R. C., Parise, E. M., Vu, M. T., Gallagher, N. M., Wang, J., Silva, A. J., Deisseroth, K., Mague, S. D., Caron, M. G., Nestler, E. J., Carin, L., and Dzirasa, K. (2018). Brain-wide electrical spatiotemporal dynamics encode depression vulnerability. *Cell*.

[95] Hutchison, R. M., Womelsdorf, T., Allen, E. A., Bandettini, P. A., Calhoun, V. D., Corbetta, M., Della Penna, S., Duyn, J. H., Glover, G. H., Gonzalez-Castillo, J., Handwerker, D. A., Keilholz, S., Kiviniemi, V., Leopold, D. A., de Pasquale, F., Sporns, O., Walter, M., and Chang, C. (2013). Dynamic functional connectivity: promise, issues, and interpretations. *Neuroimage*, 80:360–78.

[96] Ichikawa, N, L. G. Y. N. O. G. T. M. Y. M. S. T. H. R. Y. T. Y. Y. T. H. K. K. K. N. Y. S. K. M. M. J. and Okamoto, Y. (2017). Identifying melancholic depression biomarker using whole-brain functional connectivity. *arXiv*.

[97] Iigaya, K., Fonseca, M. S., Murakami, M., Mainen, Z. F., and Dayan, P. (2018). An effect of serotonergic stimulation on learning rates for rewards apparent after long intertrial intervals. *Nat Commun*, 9(1):2477.

[98] Izquierdo, A., Carlos, K., Ostrander, S., Rodriguez, D., McCall-Craddolph, A., Yagnik, G., and Zhou, F. (2012). Impaired reward learning and intact motivation after serotonin depletion in rats. *Behav Brain Res*, 233(2):494–9.

[99] Jacobsen, J. P., Siesser, W. B., Sachs, B. D., Peterson, S., Cools, M. J., Setola, V., Folgering, J. H., Flik, G., and Caron, M. G. (2012). Deficient serotonin neurotransmission and depression-like serotonin biomarker alterations in tryptophan hydroxylase 2 (tph2) loss-of-function mice. *Mol Psychiatry*, 17(7):694–704.

[100] Jahanshad, N., Kochunov, P. V., Sprooten, E., Mandl, R. C., Nichols, T. E., Almasy, L., Blangero, J., Brouwer, R. M., Curran, J. E., de Zubicaray, G. I., Duggirala, R., Fox, P. T., Hong, L. E., Landman, B. A., Martin, N. G., McMahon, K. L., Medland, S. E., Mitchell, B. D., Olvera, R. L., Peterson, C. P., Starr, J. M., Sussmann, J. E., Toga, A. W., Wardlaw, J. M., Wright, M. J., Hulshoff Pol, H. E., Bastin, M. E., McIntosh, A. M., Deary, I. J., Thompson, P. M., and Glahn, D. C. (2013). Multi-site genetic analysis of diffusion images and voxelwise heritability analysis: a pilot project of the enigma-dti working group. *Neuroimage*, 81:455–469.

[101] Jaynes, E. T. (1957). Information theory and statistical mechanics. *Physical Review*, 106(4):620–630.

[102] Jonckers, E., Shah, D., Hamaide, J., Verhoye, M., and Van der Linden, A. (2015). The power of using functional fmri on small rodents to study brain pharmacology and disease. *Frontiers in Pharmacology*, 6.

[103] Kaiser, R. H., Whitfield-Gabrieli, S., Dillon, D. G., Goer, F., Beltzer, M., Minkel, J., Smoski, M., Dichter, G., and Pizzagalli, D. A. (2016). Dynamic resting-state functional connectivity in major depression. *Neuropsychopharmacology*, 41(7):1822–30.

[104] Kawai, S., Takagi, Y., Kaneko, S., and Kurosawa, T. (2011). Effect of three types of mixed anesthetic agents alternate to ketamine in mice. *Exp Anim*, 60(5):481–7.

[105] Klaassens, B. L., van Gorsel, H. C., Khalili-Mahani, N., van der Grond, J., Wyman, B. T., Whitcher, B., Rombouts, S. A., and van Gerven, J. M. (2015). Single-dose serotonergic stimulation shows widespread effects on functional brain connectivity. *Neuroimage*, 122:440–50.

[106] Klomp, A., Tremoleda, J. L., Wylezinska, M., Nederveen, A. J., Feenstra, M., Gsell, W., and Reneman, L. (2012). Lasting effects of chronic fluoxetine treatment on the late developing rat brain: age-dependent changes in the serotonergic neurotransmitter system assessed by pharmacological mri. *Neuroimage*, 59(1):218–26.

[107] Koh, D. M. and Collins, D. J. (2007). Diffusion-weighted mri in the body: applications and challenges in oncology. *AJR Am J Roentgenol*, 188(6):1622–35.

[108] Komada, M., Takao, K., and Miyakawa, T. (2008). Elevated plus maze for mice. *J Vis Exp*, (22).

[109] Kopell, N. J., Gritton, H. J., Whittington, M. A., and Kramer, M. A. (2014). Beyond the connectome: the dynome. *Neuron*, 83(6):1319–28.

[110] Landhuis, E. (2017). Neuroscience: Big brain, big data. *Nature*, 541(7638):559–561.

[111] Lee, H. J., Weitz, A. J., Bernal-Casas, D., Duffy, B. A., Choy, M., Kravitz, A. V., Kreitzer, A. C., and Lee, J. H. (2016). Activation of direct and indirect pathway medium spiny neurons drives distinct brain-wide responses. *Neuron*, 91(2):412–24.

[112] Lee, J. H., Durand, R., Gradinaru, V., Zhang, F., Goshen, I., Kim, D. S., Fenno, L. E., Ramakrishnan, C., and Deisseroth, K. (2010). Global and local fmri signals driven by neurons defined optogenetically by type and wiring. *Nature*, 465(7299):788–92.

[113] Lee, M. H., Smyser, C. D., and Shimony, J. S. (2013). Resting-state fmri: a review of methods and clinical applications. *AJNR Am J Neuroradiol*, 34(10):1866–72.

[114] Li, Y., Zhong, W., Wang, D., Feng, Q., Liu, Z., Zhou, J., Jia, C., Hu, F., Zeng, J., Guo, Q., Fu, L., and Luo, M. (2016). Serotonin neurons in the dorsal raphe nucleus encode reward signals. *Nat Commun*, 7:10503.

[115] Lim, D. H., Ledue, J., Mohajerani, M. H., Vanni, M. P., and Murphy, T. H. (2013). Optogenetic approaches for functional mouse brain mapping. *Front Neurosci*, 7:54.

[116] Liska, A., Galbusera, A., Schwarz, A. J., and Gozzi, A. (2015). Functional connectivity hubs of the mouse brain. *Neuroimage*, 115:281–91.

[117] Logothetis, N. K. (2003). The underpinnings of the bold functional magnetic resonance imaging signal. *J Neurosci*, 23(10):3963–71.

[118] Lohani, S., Poplawsky, A. J., Kim, S. G., and Moghaddam, B. (2017). Unexpected global impact of vta dopamine neuron activation as measured by opto-fmri. *Mol Psychiatry*, 22(4):585–594.

[119] Lohmann, G., Margulies, D. S., Horstmann, A., Pleger, B., Lepsien, J., Goldhahn, D., Schloegl, H., Stumvoll, M., Villringer, A., and Turner, R. (2010). Eigenvector centrality mapping for analyzing connectivity patterns in fmri data of the human brain. *PLoS One*, 5(4):e10232.

[120] Lottem, E., Banerjee, D., Vertechi, P., Sarra, D., Lohuis, M. O., and Mainen, Z. F. (2018). Activation of serotonin neurons promotes active persistence in a probabilistic foraging task. *Nat Commun*, 9(1):1000.

[121] Lowry, C. A., Hale, M. W., Evans, A. K., Heerkens, J., Staub, D. R., Gasser, P. J., and Shekhar, A. (2008). Serotonergic systems, anxiety, and affective disorder: focus on the dorsomedial part of the dorsal raphe nucleus. *Ann N Y Acad Sci*, 1148:86–94.

[122] Lu, H., Zou, Q., Gu, H., Raichle, M. E., Stein, E. A., and Yang, Y. (2012). Rat brains also have a default mode network. *Proc Natl Acad Sci U S A*, 109(10):3979–84.

[123] Luo, M., Li, Y., and Zhong, W. (2016). Do dorsal raphe 5-ht neurons encode "beneficialness"? *Neurobiol Learn Mem*, 135:40–49.

[124] Lyoo, Y. and Yoon, S. (2017). Brain network correlates of emotional aging. *Sci Rep*, 7(1):15576.

[125] Maier, S. F. and Watkins, L. R. (2005). Stressor controllability and learned helplessness: the roles of the dorsal raphe nucleus, serotonin, and corticotropin-releasing factor. *Neurosci Biobehav Rev*, 29(4-5):829–41.

[126] Mandell, D., Siegle, G. J., Shutt, L., Feldmiller, J., and Thase, M. E. (2014). Neural substrates of trait ruminations in depression. *J Abnorm Psychol*, 123(1):35–48.

[127] Mantini, D., Gerits, A., Nelissen, K., Durand, J. B., Joly, O., Simone, L., Sawamura, H., Wardak, C., Orban, G. A., Buckner, R. L., and Vanduffel, W. (2011). Default mode of brain function in monkeys. *J Neurosci*, 31(36):12954–62.

[128] Marchetti, I., Koster, E. H. W., Klinger, E., and Alloy, L. B. (2016). Spontaneous thought and vulnerability to mood disorders: The dark side of the wandering mind. *Clin Psychol Sci*, 4(5):835–857.

[129] Marcinkiewcz, C. A., Mazzone, C. M., D'Agostino, G., Halladay, L. R., Hardaway, J. A., DiBerto, J. F., Navarro, M., Burnham, N., Cristiano, C., Dorrier, C. E., Tipton, G. J., Ramakrishnan, C., Kozicz, T., Deisseroth, K., Thiele, T. E., McElligott, Z. A., Holmes, A., Heisler, L. K., and Kash, T. L. (2016). Serotonin engages an anxiety and fear-promoting circuit in the extended amygdala. *Nature*, 537(7618):97–101.

[130] Matias, S., Lottem, E., Dugue, G. P., and Mainen, Z. F. (2017). Activity patterns of serotonin neurons underlying cognitive flexibility. *Elife*, 6.

[131] McCabe, C., Mishor, Z., Cowen, P. J., and Harmer, C. J. (2010). Diminished neural processing of aversive and rewarding stimuli during selective serotonin reuptake inhibitor treatment. *Biol Psychiatry*, 67(5):439–45.

[132] McCabe, C., Mishor, Z., Filippini, N., Cowen, P. J., Taylor, M. J., and Harmer, C. J. (2011). Ssri administration reduces resting state functional connectivity in dorso-medial prefrontal cortex. *Mol Psychiatry*, 16(6):592–4.

[133] Medaglia, J. D., Pasqualetti, F., Hamilton, R. H., Thompson-Schill, S. L., and Bassett, D. S. (2017). Brain and cognitive reserve: Translation via network control theory. *Neurosci Biobehav Rev*, 75:53–64.

[134] Melozzi, F., Woodman, M. M., Jirsa, V. K., and Bernard, C. (2017). The virtual mouse brain: A computational neuroinformatics platform to study whole mouse brain dynamics. *eNeuro*, 4(3).

[135] Meyniel, F., Goodwin, G. M., Deakin, J. W., Klinge, C., MacFadyen, C., Milligan, H., Mullings, E., Pessiglione, M., and Gaillard, R. (2016). A specific role for serotonin in overcoming effort cost. *Elife*, 5.

[136] Miyazaki, K., Miyazaki, K. W., and Doya, K. (2012a). The role of serotonin in the regulation of patience and impulsivity. *Mol Neurobiol*, 45(2):213–24.

[137] Miyazaki, K., Miyazaki, K. W., Yamanaka, A., Tokuda, T., Tanaka, K. F., and Doya, K. (2018). Reward probability and timing uncertainty alter the effect of dorsal raphe serotonin neurons on patience. *Nat Commun*, 9(1):2048.

[138] Miyazaki, K. W., Miyazaki, K., and Doya, K. (2012b). Activation of dorsal raphe serotonin neurons is necessary for waiting for delayed rewards. *J Neurosci*, 32(31):10451–7.

[139] Miyazaki, K. W., Miyazaki, K., Tanaka, K. F., Yamanaka, A., Takahashi, A., Tabuchi, S., and Doya, K. (2014). Optogenetic activation of dorsal raphe serotonin neurons enhances patience for future rewards. *Curr Biol*, 24(17):2033–40.

[140] Murakami, M., Vicente, M. I., Costa, G. M., and Mainen, Z. F. (2014). Neural antecedents of self-initiated actions in secondary motor cortex. *Nat Neurosci*, 17(11):1574–82.

[141] Nakamura, K., Matsumoto, M., and Hikosaka, O. (2008). Reward-dependent modulation of neuronal activity in the primate dorsal raphe nucleus. *J Neurosci*, 28(20):5331–43.

[142] Nestler, E. J. and Hyman, S. E. (2010). Animal models of neuropsychiatric disorders. *Nat Neurosci*, 13(10):1161–9.

[143] Neubert, F. X., Mars, R. B., Sallet, J., and Rushworth, M. F. (2015). Connectivity reveals relationship of brain areas for reward-guided learning and decision making in human and monkey frontal cortex. *Proc Natl Acad Sci U S A*, 112(20):E2695–704.

[144] Newman, M. E. J. and Girvan, M. (2004). Finding and evaluating community structure in networks. *Physical Review E*, 69(2).

[145] Nichols, D. E. and Nichols, C. D. (2008). Serotonin receptors. *Chem Rev*, 108(5):1614–41.

[146] Nolen-Hoeksema, S. (2000). The role of rumination in depressive disorders and mixed anxiety/depressive symptoms. *J Abnorm Psychol*, 109(3):504–11.

[147] Novak, N. M., Stein, J. L., Medland, S. E., Hibar, D. P., Thompson, P. M., and Toga, A. W. (2012). Enigmavis: online interactive visualization of genome-wide association studies of the enhancing neuroimaging genetics through meta-analysis (enigma) consortium. *Twin Res Hum Genet*, 15(3):414–8.

[148] Ogawa, S. K., Cohen, J. Y., Hwang, D., Uchida, N., and Watabe-Uchida, M. (2014). Organization of monosynaptic inputs to the serotonin and dopamine neuromodulatory systems. *Cell Rep*, 8(4):1105–18.

[149] Penttonen, M. and G., B. (2003). Natural logarithmic relationship between brain oscillators. *Thalamus Related Systems*, 2(2):145–52.

[150] Pollak Dorocic, I., Furth, D., Xuan, Y., Johansson, Y., Pozzi, L., Silberberg, G., Carlen, M., and Meletis, K. (2014). A whole-brain atlas of inputs to serotonergic neurons of the dorsal and median raphe nuclei. *Neuron*, 83(3):663–78.

[151] Porcelli, S., Fabbri, C., and Serretti, A. (2012). Meta-analysis of serotonin transporter gene promoter polymorphism (5-httlpr) association with antidepressant efficacy. *Eur Neuropsychopharmacol*, 22(4):239–58.

[152] Power, J. D., Cohen, A. L., Nelson, S. M., Wig, G. S., Barnes, K. A., Church, J. A., Vogel, A. C., Laumann, T. O., Miezin, F. M., Schlaggar, B. L., and Petersen, S. E. (2011). Functional network organization of the human brain. *Neuron*, 72(4):665–78.

[153] Power, J. D., Schlaggar, B. L., and Petersen, S. E. (2015). Recent progress and outstanding issues in motion correction in resting state fmri. *Neuroimage*, 105:536–51.

[154] Preti, M. G., Bolton, T. A., and Van De Ville, D. (2017). The dynamic functional connectome: State-of-the-art and perspectives. *Neuroimage*, 160:41–54.

[155] Raichle, M. E., MacLeod, A. M., Snyder, A. Z., Powers, W. J., Gusnard, D. A., and Shulman, G. L. (2001). A default mode of brain function. *Proc Natl Acad Sci U S A*, 98(2):676–82.

[156] Rogers, R. D. (2011). The roles of dopamine and serotonin in decision making: evidence from pharmacological experiments in humans. *Neuropsychopharmacology*, 36(1):114–32.

[157] Rubinov, M. and Sporns, O. (2010). Complex network measures of brain connectivity: Uses and interpretations. *Neuroimage*, 52(3):1059–1069.

[158] Rubinov, M. and Sporns, O. (2011). Weight-conserving characterization of complex functional brain networks. *Neuroimage*, 56(4):2068–2079.

[159] Sachs, B. D., Jacobsen, J. P., Thomas, T. L., Siesser, W. B., Roberts, W. L., and Caron, M. G. (2013). The effects of congenital brain serotonin deficiency on responses to chronic fluoxetine. *Transl Psychiatry*, 3:e291.

[160] Sachs, B. D., Rodriguiz, R. M., Tran, H. L., Iyer, A., Wetsel, W. C., and Caron, M. G. (2015). Serotonin deficiency alters susceptibility to the long-term consequences of adverse early life experience. *Psychoneuroendocrinology*, 53:69–81.

[161] Sanders, A. C., Hussain, A. J., Hen, R., and Zhuang, X. (2007). Chronic blockade or constitutive deletion of the serotonin transporter reduces operant responding for food reward. *Neuropsychopharmacology*, 32(11):2321–9.

[162] Sato, J. R., Moll, J., Green, S., Deakin, J. F., Thomaz, C. E., and Zahn, R. (2015). Machine learning algorithm accurately detects fmri signature of vulnerability to major depression. *Psychiatry Res*, 233(2):289–91.

[163] Saxena, P. R. (1995). Serotonin receptors: subtypes, functional responses and therapeutic relevance. *Pharmacol Ther*, 66(2):339–68.

[164] Schaefer, A., Burmann, I., Regenthal, R., Arelin, K., Barth, C., Pampel, A., Villringer, A., Margulies, D. S., and Sacher, J. (2014). Serotonergic modulation of intrinsic functional connectivity. *Curr Biol*, 24(19):2314–8.

[165] Scholl, J., Kolling, N., Nelissen, N., Browning, M., Rushworth, M. F., and Harmer, C. J. (2017). Beyond negative valence: 2-week administration of a serotonergic antidepressant enhances both reward and effort learning signals. *PLoS Biol*, 15(2):e2000756.

[166] Schultz, W., Dayan, P., and Montague, P. R. (1997). A neural substrate of prediction and reward. *Science*, 275(5306):1593–9.

[167] Schwarz, A. J., Gozzi, A., Reese, T., and Bifone, A. (2007). In vivo mapping of functional connectivity in neurotransmitter systems using pharmacological mri. *Neuroimage*, 34(4):1627–36.

[168] Schweighofer, N., Bertin, M., Shishida, K., Okamoto, Y., Tanaka, S. C., Yamawaki, S., and Doya, K. (2008). Low-serotonin levels increase delayed reward discounting in humans. *J Neurosci*, 28(17):4528–32.

[169] Sejnowski, T. J., Churchland, P. S., and Movshon, J. A. (2014). Putting big data to good use in neuroscience. *Nat Neurosci*, 17(11):1440–1.

[170] Seymour, B., Daw, N. D., Roiser, J. P., Dayan, P., and Dolan, R. (2012). Serotonin selectively modulates reward value in human decision-making. *J Neurosci*, 32(17):5833–42.

[171] Sheline, Y. I., Barch, D. M., Price, J. L., Rundle, M. M., Vaishnavi, S. N., Snyder, A. Z., Mintun, M. A., Wang, S., Coalson, R. S., and Raichle, M. E. (2009). The default mode network and self-referential processes in depression. *Proc Natl Acad Sci U S A*, 106(6):1942–7.

[172] Shimizu, Y., Yoshimoto, J., Toki, S., Takamura, M., Yoshimura, S., Okamoto, Y., Yamawaki, S., and Doya, K. (2015). Toward probabilistic diagnosis and understanding of depression based on functional mri data analysis with logistic group lasso. *PLoS One*, 10(5):e0123524.

[173] Soubrié, P. (1986). Reconciling the role of central serotonin neurons in human and animal behavior. *Behavioral and Brain Sciences*, 9(2):319–335.

[174] Sporns, O. (2013). Structure and function of complex brain networks. *Dialogues Clin Neurosci*, 15(3):247–62.

[175] Sporns, O. and Betzel, R. F. (2016). Modular brain networks. *Annu Rev Psychol*, 67:613–40.

[176] Stafford, J. M., Jarrett, B. R., Miranda-Dominguez, O., Mills, B. D., Cain, N., Mihalas, S., Lahvis, G. P., Lattal, K. M., Mitchell, S. H., David, S. V., Fryer, J. D., Nigg, J. T., and Fair, D. A. (2014). Large-scale topology and the default mode network in the mouse connectome. *Proc Natl Acad Sci U S A*, 111(52):18745–50.

[177] Steinbusch, H. W. and Nieuwenhuys, R. (1981). Localization of serotonin-like immunoreactivity in the central nervous system and pituitary of the rat, with special references to the innervation of the hypothalamus. *Adv Exp Med Biol*, 133:7–35.

[178] Storbeck, J. and Clore, G. L. (2007). On the interdependence of cognition and emotion. *Cogn Emot*, 21(6):1212–1237.

[179] Sunkin, S. M., Ng, L., Lau, C., Dolbeare, T., Gilbert, T. L., Thompson, C. L., Hawrylycz, M., and Dang, C. (2013). Allen brain atlas: an integrated spatio-temporal portal for exploring the central nervous system. *Nucleic Acids Res*, 41(Database issue):D996–D1008.

[180] Supekar, K., Uddin, L. Q., Khouzam, A., Phillips, J., Gaillard, W. D., Kenworthy, L. E., Yerys, B. E., Vaidya, C. J., and Menon, V. (2013). Brain hyperconnectivity in children with autism and its links to social deficits. *Cell Rep*, 5(3):738–47.

[181] Takagi, Y., Sakai, Y., Lisi, G., Yahata, N., Abe, Y., Nishida, S., Nakamae, T., Morimoto, J., Kawato, M., Narumoto, J., and Tanaka, S. C. (2017). A neural marker of obsessive-compulsive disorder from whole-brain functional connectivity. *Sci Rep*, 7(1):7538.

[182] Tanaka, S. C., Schweighofer, N., Asahi, S., Shishida, K., Okamoto, Y., Yamawaki, S., and Doya, K. (2007). Serotonin differentially regulates short- and long-term prediction of rewards in the ventral and dorsal striatum. *PLoS One*, 2(12):e1333.

[183] Tanaka, S. C., Shishida, K., Schweighofer, N., Okamoto, Y., Yamawaki, S., and Doya, K. (2009). Serotonin affects association of aversive outcomes to past actions. *J Neurosci*, 29(50):15669–74.

[184] Taylor, M. J., Sen, S., and Bhagwagar, Z. (2010). Antidepressant response and the serotonin transporter gene-linked polymorphic region. *Biol Psychiatry*, 68(6):536–43.

[185] Tomasi, D. and Volkow, N. D. (2012). Aging and functional brain networks. *Mol Psychiatry*, 17(5):471, 549–58.

[186] van den Heuvel, M. P. and Hulshoff Pol, H. E. (2010). Exploring the brain network: a review on resting-state fmri functional connectivity. *Eur Neuropsychopharmacol*, 20(8):519–34.

[187] van den Heuvel, M. P., Sporns, O., Collin, G., Scheewe, T., Mandl, R. C., Cahn, W., Goni, J., Hulshoff Pol, H. E., and Kahn, R. S. (2013). Abnormal rich club organization and functional brain dynamics in schizophrenia. *JAMA Psychiatry*, 70(8):783–92.

[188] Van Essen, D. C., Ugurbil, K., Auerbach, E., Barch, D., Behrens, T. E., Bucholz, R., Chang, A., Chen, L., Corbetta, M., Curtiss, S. W., Della Penna, S., Feinberg, D., Glasser, M. F., Harel, N., Heath, A. C., Larson-Prior, L., Marcus, D., Michalareas, G., Moeller, S., Oostenveld, R., Petersen, S. E., Prior, F., Schlaggar, B. L., Smith, S. M., Snyder, A. Z., Xu, J., Yacoub, E., and Consortium, W. U.-M. H. (2012). The human connectome project: a data acquisition perspective. *Neuroimage*, 62(4):2222–31.

[189] Vasudeva, R. K., Lin, R. C., Simpson, K. L., and Waterhouse, B. D. (2011). Functional organization of the dorsal raphe efferent system with special consideration of nitrergic cell groups. *J Chem Neuroanat*, 41(4):281–93.

[190] Vasudeva, R. K. and Waterhouse, B. D. (2014). Cellular profile of the dorsal raphe lateral wing sub-region: relationship to the lateral dorsal tegmental nucleus. *J Chem Neuroanat*, 57-58:15–23.

[191] Vatansever, D., Manktelow, A. E., Sahakian, B. J., Menon, D. K., and Stamatakis, E. A. (2016). Cognitive flexibility: A default network and basal ganglia connectivity perspective. *Brain Connect*, 6(3):201–7.

[192] Veerakumar, A., Challis, C., Gupta, P., Da, J., Upadhyay, A., Beck, S. G., and Berton, O. (2014). Antidepressant-like effects of cortical deep brain stimulation coincide with pro-neuroplastic adaptations of serotonin systems. *Biol Psychiatry*, 76(3):203–12.

[193] Vertes, R. P. and Linley, S. B. (2008). *Efferent and afferent connections of the dorsal and median raphe nuclei in the rat*, pages 69–102. Birkhäuser Basel, Basel.

[194] Vidaurre, D., Abeysuriya, R., Becker, R., Quinn, A. J., Alfaro-Almagro, F., Smith, S. M., and Woolrich, M. W. (2018). Discovering dynamic brain networks from big data in rest and task. *Neuroimage*, 180(Pt B):646–656.

[195] Vidaurre, D., Quinn, A. J., Baker, A. P., Dupret, D., Tejero-Cantero, A., and Woolrich, M. W. (2016). Spectrally resolved fast transient brain states in electrophysiological data. *Neuroimage*, 126:81–95.

[196] Vidaurre, D., Smith, S. M., and Woolrich, M. W. (2017). Brain network dynamics are hierarchically organized in time. *Proc Natl Acad Sci U S A*, 114(48):12827–12832.

[197] Vincent, J. L., Patel, G. H., Fox, M. D., Snyder, A. Z., Baker, J. T., Van Essen, D. C., Zempel, J. M., Snyder, L. H., Corbetta, M., and Raichle, M. E. (2007). Intrinsic functional architecture in the anaesthetized monkey brain. *Nature*, 447(7140):83–6.

[198] Warden, M. R., Selimbeyoglu, A., Mirzabekov, J. J., Lo, M., Thompson, K. R., Kim, S. Y., Adhikari, A., Tye, K. M., Frank, L. M., and Deisseroth, K. (2012). A prefrontal cortex-brainstem neuronal projection that controls response to behavioural challenge. *Nature*, 492(7429):428–32.

[199] Waselus, M., Valentino, R. J., and Van Bockstaele, E. J. (2011). Collateralized dorsal raphe nucleus projections: a mechanism for the integration of diverse functions during stress. *J Chem Neuroanat*, 41(4):266–80.

[200] Watanabe, T., Hirose, S., Wada, H., Imai, Y., Machida, T., Shirouzu, I., Konishi, S., Miyashita, Y., and Masuda, N. (2013). A pairwise maximum entropy model accurately describes resting-state human brain networks. *Nat Commun*, 4:1370.

[201] Watanabe, T., Hirose, S., Wada, H., Imai, Y., Machida, T., Shirouzu, I., Konishi, S., Miyashita, Y., and Masuda, N. (2014a). Energy landscapes of resting-state brain networks. *Front Neuroinform*, 8:12.

[202] Watanabe, T., Masuda, N., Megumi, F., Kanai, R., and Rees, G. (2014b). Energy landscape and dynamics of brain activity during human bistable perception. *Nat Commun*, 5:4765.

[203] Watanabe, T. and Rees, G. (2017). Brain network dynamics in high-functioning individuals with autism. *Nat Commun*, 8:16048.

[204] Weissbourd, B., Ren, J., DeLoach, K. E., Guenthner, C. J., Miyamichi, K., and Luo, L. (2014). Presynaptic partners of dorsal raphe serotonergic and gabaergic neurons. *Neuron*, 83(3):645–62.

[205] Willner, P. (1984). The validity of animal-models of depression. *Psychopharmacology*, 83(1):1–16.

[206] Wise, T., Marwood, L., Perkins, A. M., Herane-Vives, A., Joules, R., Lythgoe, D. J., Luh, W. M., Williams, S. C. R., Young, A. H., Cleare, A. J., and Arnone, D. (2017). Instability of default mode network connectivity in major depression: a two-sample confirmation study. *Translational Psychiatry*, 7.

[207] Yamamura, T., Okamoto, Y., Okada, G., Takaishi, Y., Takamura, M., Mantani, A., Kurata, A., Otagaki, Y., Yamashita, H., and Yamawaki, S. (2016). Association of thalamic hyperactivity with treatment-resistant depression and poor response in early treatment for major depression: a resting-state fmri study using fractional amplitude of low-frequency fluctuations. *Transl Psychiatry*, 6:e754.

[208] Yohn, C. N., Gergues, M. M., and Samuels, B. A. (2017). The role of 5-ht receptors in depression. *Mol Brain*, 10(1):28.

[209] Yohn, S. E., Collins, S. L., Contreras-Mora, H. M., Errante, E. L., Rowland, M. A., Correa, M., and Salamone, J. D. (2016). Not all antidepressants are created equal: Differential effects of monoamine uptake inhibitors on effort-related choice behavior. *Neuropsychopharmacology*, 41(3):686–94.

[210] Yoshida, K., Mimura, Y., Ishihara, R., Nishida, H., Komaki, Y., Minakuchi, T., Tsurugizawa, T., Mimura, M., Okano, H., Tanaka, K. F., and Takata, N. (2016). Physiological effects of a habituation procedure for functional mri in awake mice using a cryogenic radiofrequency probe. *J Neurosci Methods*, 274:38–48.

[211] Zang, Y. F., He, Y., Zhu, C. Z., Cao, Q. J., Sui, M. Q., Liang, M., Tian, L. X., Jiang, T. Z., and Wang, Y. F. (2007). Altered baseline brain activity in children with adhd revealed by resting-state functional mri. *Brain Dev*, 29(2):83–91.

[212] Zerbi, V., Grandjean, J., Rudin, M., and Wenderoth, N. (2015). Mapping the mouse brain with rs-fmri: An optimized pipeline for functional network identification. *Neuroimage*, 123:11–21.

[213] Zhi, D., Calhoun, V. D., Lv, L., Ma, X., Ke, Q., Fu, Z., Du, Y., Yang, Y., Yang, X., Pan, M., Qi, S., Jiang, R., Yu, Q., and Sui, J. (2018). Aberrant dynamic functional network connectivity and graph properties in major depressive disorder. *Front Psychiatry*, 9:339.

[214] Zou, Q. H., Zhu, C. Z., Yang, Y., Zuo, X. N., Long, X. Y., Cao, Q. J., Wang, Y. F., and Zang, Y. F. (2008). An improved approach to detection of amplitude of low-frequency fluctuation (alff) for resting-state fmri: fractional alff. *J Neurosci Methods*, 172(1):137–41.

[215] Zuo, X. N., Di Martino, A., Kelly, C., Shehzad, Z. E., Gee, D. G., Klein, D. F., Castellanos, F. X., Biswal, B. B., and Milham, M. P. (2010). The oscillating brain: complex and reliable. *Neuroimage*, 49(2):1432–45.